STRUCTURAL CHARACTERIZATION OF 20 KDA LIPID-BINDING FRAGMENTS OF APOLIPOPROTEIN B100

by

Alexandra M. Reda

Submitted in partial fulfilment of the requirements
for the degree of Master of Science

at

Dalhousie University
Halifax, Nova Scotia
January 2015

DEDICATION PAGE

This thesis is dedicated to my two biggest support systems- my father Francesco Reda and my mother Maria Reda. Thank you for giving me the world, I love you both xox!

TABLE OF CONTENTS

LIST OF TABLES

LIST OF FIGURES

ABSTRACT

Apolipoprotein(apo)B100 is a 550 kDa hydrophobic glycoprotein that forms the structural backbone for the assembly of triglyceride(TG)-rich lipoproteins. ApoB100 is predicted to contain 5 domains: an N-terminal globular $\beta\alpha_1$ domain followed by alternating amphipathic β-strand and α-helical regions (N-$\beta\alpha_1$-β_1-α_2-β_2-α_3-C). However, the hydrophobicity and size of apoB100 have prevented experimental verification of this structural prediction. Amino acids 1694-1880 (B1), within the β_1 domain, tightly bind TG *in vitro*. We expressed and purified two 20 kDa fragments, B1 and B2 (amino acids 1881-2070, which lies at the junction between the β_1 and α_2 domains), in bacterial culture in order to collect high resolution structural information. Under conditions ensuring no more than one apoB per micelle, circular dichroism (CD) spectroscopy of B1 and B2 in dodecylphosphocholine (DPC) or micelles formed with three different lysophospholipids indicated predominantly α-helical character. NMR spectroscopy of $^{13}C/^{15}N$-labeled B1 and B2 in DPC micelles also indicated substantial α-helical structure. Our studies provide the first atomic-level evidence for amphipathic α-helical structural elements in the TG-binding regions of apoB100.

LIST OF ABBREVIATIONS and SYMBOLS USED

δ	chemical shift
ε	molar absorptivity
γ	gyromagnetic ratio
ω_0	Larmor frequency
APM	Alberta proteomics and mass spectrometry facility
ApoB	apolipoprotein B100
Apobec-1	apoB editing complex-1
B_0	static magnetic field
B1	apoB1
B1*	C-terminally extended apoB1
B2	apoB2
B3	apoB3
CD	circular dichroism
cDNA	complementary deoxyribonucleic acid
CM	chylomicron
CMC	critical micelle concentration
COSY	correlation spectroscopy
CSI	chemical shift index
DANGLE	dihedral angles from global likelihood estimates
DDM	*n*-dodecyl-ß-D-maltoside
DHPC	1,2-dihexanoyl-*sn*-glycero-3-phosphocholine
DHPC-7	1,2-diheptanoyl-*sn*-glycero-3-phosphocholine
DPC	*n*-dodecylphosphocholine
DMPC	1,2-dimyristoyl-*sn*-glycero-3-phosphocholine
DSS	2,2-dimethyl-2-sila-pentane-5-sulfonate
DTT	dithiothreitol
E.coli	*Escherichia coli*
EDTA	ethylenediaminetetraacetic acid
ER	endoplasmic reticulum

ESI	electrospray ionization
EtBr	ethidium bromide
IPTG	isopropyl β-D-1-thiogalactopyranoside
IR	infrared
FABP	fatty acid binding protein
FHBL	familial hypobetalipoproteinemia
HDL	high density lipoprotein
HSQC	heteronuclear single quantum coherence
LB	Luria-Bertani
LD	lipid droplet
LDL	low density lipoprotein
LMPC	1-myristoyl-2-hydroxy-*sn*-glycero-3-phosphocholine
LPL	lipoprotein lipase
LPPC	1-palmitoyl-2-hydroxy-*sn*-glycero-3-phosphocholine
LPPG	1-palmitoyl-2-hydroxy-*sn*-glycero-3-phospho-(1'-*rac*-glycerol)
MADLI	matrix-assisted laser desorption ionization
MTP	microsomal triglyceride transfer protein
Na-DOC	sodium deoxycholate
NMR	nuclear magnetic resonance
NOE	nuclear Overhauser effect
NOESY	nuclear Overhauser effect spectroscopy
NRC-IMB	National Research Council Institute for Marine Biosciences
PAGE	polyacrylamide gel electrophoresis
PDI	protein disulfide isomerase
PCR	polymerase chain reaction
QANUC	Quebec/eastern Canada high field NMR facility
SDS	sodium dodecyl sulfate
TEV	tobacco etch virus
TG	triglyceride
TOCSY	total correlation spectroscopy
TOF	time of flight

UV	ultraviolet
VLDL	very low density lipoprotein

ACKNOWLEDGEMENTS

First and foremost, the person without whom this would not have been possible, my supervisor Dr. Roger McLeod. Roger has been a great mentor during my two and a half years in his lab. He was always approachable and willing to give me guidance and direction. Roger did everything in his power to send me to scientific conferences, both locally and abroad. He also supported me in my endeavors and motivated me to do my best.

My time in the lab would not have been as amazing as it was without my past and present lab mates- Vanessa, Eric, Brandon ("B"), Debby, Edgar and Liz. Debby, thank you for being our motherly lab figure and keeping us all in line, especially B! My days would have been so bland without him throwing things at me, sticking things to me, vandalizing my desk space, chasing me down hallways and slamming doors in my face. I'm sure everyone else on the ninth floor misses his antics as much as I do. Eric, thank you for sharing your apoB knowledge and allowing me to pick your brain while writing this thesis. My time in the lab would have been less lively and purposeful without each of you.

I have received countless guidance and help from numerous people throughout my time as a grad student. I would like to thank Marie-Laurence Tremblay for teaching me everything I know about NMR, for helping me collect and process most of my NMR data and for being there whenever I had questions. I would also like to thank Aditya Pandey and Muzaddid Sarkar for their help with interpreting my CD data as well as my NMR data when Marie was not available. I received technical advice from Dr. Tara Sprules at the Québec/Eastern Canada High Field NMR Facility and from Dr. Mike Lumsden at the

Nuclear Magnetic Resonance Research Resource center at Dalhousie University while analyzing and acquiring NMR data. I would like to thank Dr. Stephen Bearne for the use of his CD spectropolarimeter, and his graduate students for their help in acquiring and interpreting the CD data. Mass spectrometry was performed by Dr. Alejandro Cohen at the Dalhousie Proteomics Core Facility and by Jack Moore at the Alberta Proteomics and Mass Spectrometry Facility. I would like to thank my committee members, Drs. Jan Rainey and Neale Ridgway, for their advice during my committee meetings and at several other points during my time as a graduate student.

A special thank you to my best friend and Halifax sister, Crystal, especially for our regular Starbucks dates; I don't know how I would have stayed sane otherwise. Inseparable since day one and still going strong 6 years later, I love you girl, you make the thought of having to leave Nova Scotia really hard, but I know we'll be besties until the end! No matter where life takes us. I want to thank my boyfriend, Rylan, who took the brunt of most of my stress and complaints during grad school. Although we have been physically separated for the majority of my time in grad school, he never let me feel that distance. Thank you for being my go to person, motivating me and giving me something to look forward to. To my family, especially my mom and dad, thank you for believing in me all these years and allowing me to follow my dreams. You have helped me to grow as an individual while still managing to parent me from 1400 km away; for 7 years. Thank you for never questioning me and supporting me in all my endeavors. Thank you for sending me care packages to cheer me up or even "just because." I'm sure the biochemistry administrative staff enjoyed lugging those large, sometimes very heavy, packages up to me in the lab as much as I enjoyed opening them! Thank you to my sister

Danielle, who has been a never ending source of entertainment, as well as support. To the rest of my family; Nonna, Nonno, Angie and anyone who called or came to visit me over the years, thank you for your love. Without the emotional and financial support of my family members, none of this would have been possible.

It has been a wonderful 7 years in Halifax and I will be sad when the time comes to say good-bye to this beautiful province. You will always be my home away from home Halifax. Until we meet again, xo.

Chapter 1 INTRODUCTION

The focus of this thesis is on the structural characterization of 20 kDa fragments originating from the lipid-binding domain of human apolipoprotein (apo) B100. I have worked mostly on the first two fragments, apoB1 (B1) and apoB2 (B2), with some preliminary work on apoB3 (B3). In chapter one, I introduce apoB, its role in hepatic lipoprotein assembly, secretion, structure and function. I review the work that has led to our current understanding of apoB secondary structure and function. I also provide the reader with some of the background knowledge on nuclear magnetic resonance (NMR) spectroscopy and circular dichroism (CD) spectroscopy that is needed to understand my experimental data. Chapter two outlines the experimental details of my studies. In chapter three, I describe the cloning, expression and purification of the 20 kDa fragments B1, B2 and B3. Chapter four describes the structure of B1, B2 and B3 in the presence and absence of micelles as revealed by CD spectroscopy. In chapter five, I discuss the steps taken toward a solution structure of B2 based on my NMR spectra. Finally, I conclude with a discussion of my data and how it contributes to and furthers our knowledge on the experimentally derived structure of apoB.

1.1 APOLIPOPROTEIN B- CONTAINING LIPOPROTEINS

Lipoproteins are soluble spherical particles composed of an outer monolayer of phospholipids (PL), embedded cholesterol and apolipoproteins surrounding a neutral lipid core. The neutral lipid core consists of predominantly triglycerides (TG) and cholesteryl

esters (CE). Although all lipoproteins share a common structural organization, the lipid-to-protein ratio of each lipoprotein varies and results in differences in particle size and density. Four major lipoprotein species are classified according to density. The most dense particles, having the least amount of lipid, are the high density lipoproteins (HDL), d= 1.063-1.21 g/mL; followed by low density lipoproteins (LDL), d= 1.006-1.063 g/mL; very low density lipoproteins (VLDL), d< 1.006 g/mL; and chylomicrons (CM), d< 0.990 g/mL; in order of decreasing density (1). All apoB-containing lipoproteins contain one molecule of apolipoprotein (apo) B per particle, and serve to deliver endogenous hepatic and exogenous intestinal TG to tissues for use or storage (2). The major apoB-containing lipoproteins are outlined in Figure 1.1.

ApoB is a very large (4536 amino acids) and hydrophobic glycoprotein. Its polypeptide molecular mass is approximately 512 kDa, increasing to approximately 550 kDa when glycosylated (1) (Figure 1.2). It serves as the structural backbone for the assembly of TG-rich lipoproteins in the intestine (CM) and the liver (VLDL; Figure 1.3) [reviewed in (3-10)]. In humans, each apoB-containing lipoprotein particle contains a single molecule of apoB, either apoB100 in the liver, or apoB48 [amino-terminal 48%, or 2152 residues, of full-length apoB100 (3)] in the intestine. ApoB100 is synthesized on endoplasmic reticulum (ER) bound ribosomes and the polypeptide is co-translationally translocated into the ER lumen, where it is assembled into a primordial lipoprotein particle (2). In the intestinal enterocyte, apoB100 mRNA editing generates apoB48. ApoB editing complex-1 (Apobec-1), a cytidine deaminase, is required for apoB mRNA editing and converts cytidine 6666 to a uridine (2). This changes codon 2153 from a

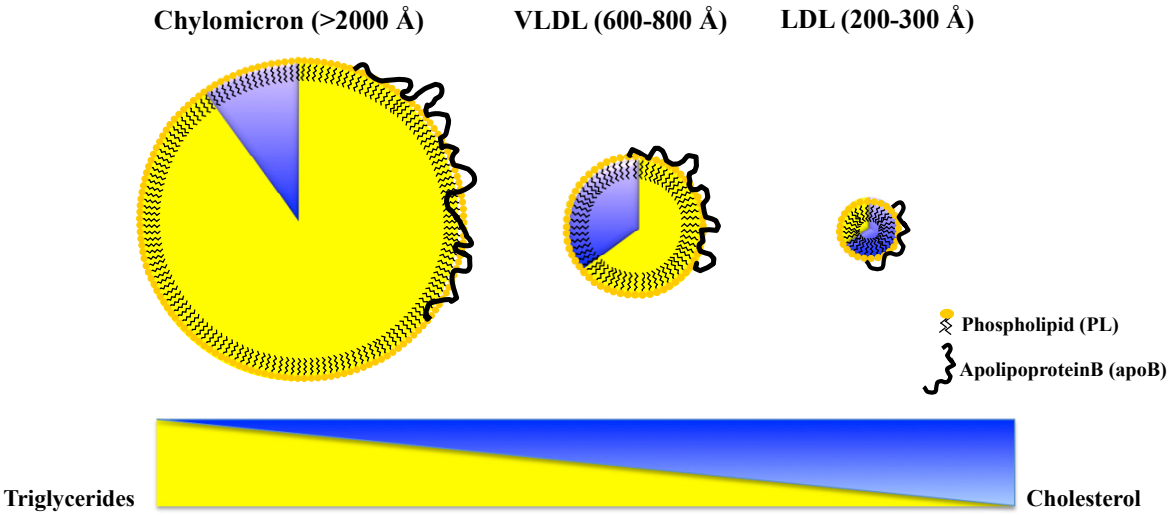

Figure 1.1 Major human apolipoprotein B-containing lipoproteins. The major apolipoproteinB- containing lipoproteins range in diameter from about 6000 Å for CM to about 200 Å for LDL. All lipoproteins contain an outer phospholipid monolayer, with embedded cholesterol, and a neutral lipid core of trigylcerides and cholesteryl esters. A single molecule of apoB encircles the lipoprotein.

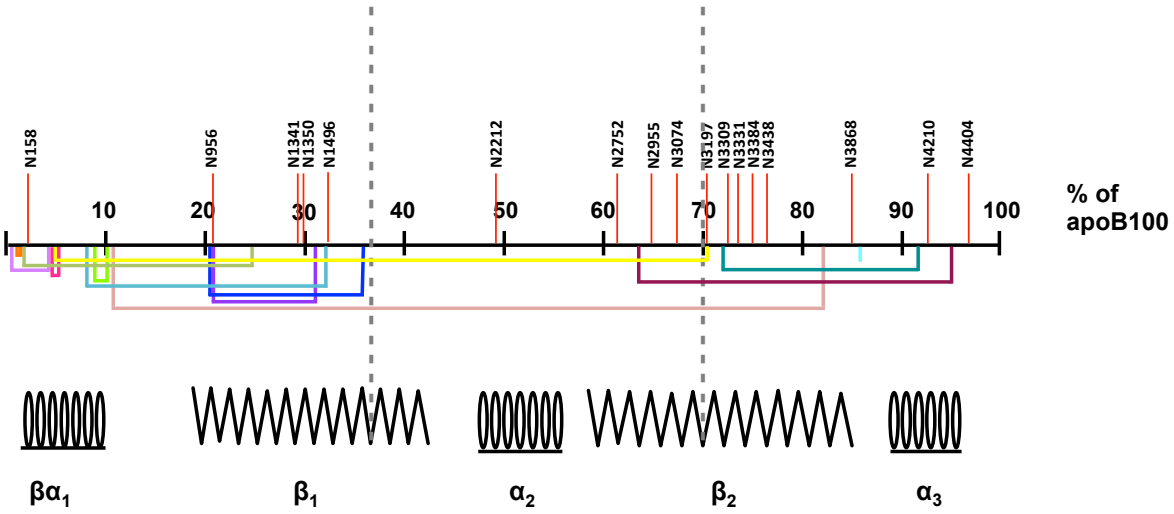

Figure 1.2 Post-translational modifications of apoB100. Locations of the 19 cysteine residues and disulfide bonds (square brackets) are shown on the centile scale map of apoB100. Positions of the asparagine-linked glycosylation sites and corresponding amino acid number are indicated. The dashed lines outline the region of apoB from which the 20 kDa apoB fragments are derived and the pentapartite model is shown for reference.

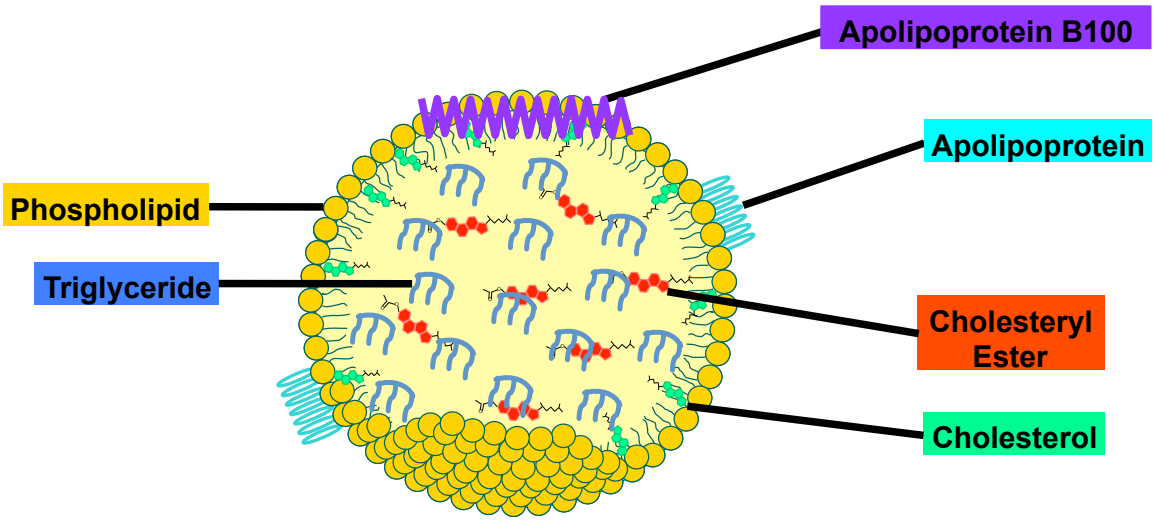

Figure 1.3 Schematic diagram of VLDL structure. The phospholipid monolayer is shown in yellow, cholesteryl esters are shown in red, unesterified cholesterol is shown in green, triglycerides are shown in blue, exchangeable apolipoproteins are shown in aqua and apolipoprotein B100 in purple.

Glutamine to a stop codon, truncating the mRNA and generating apoB48. Unlike the other apolipoproteins, which can transfer between lipoprotein particles and are termed "exchangeable", apoB remains associated with the same lipoprotein on which it is synthesized until that lipoprotein is removed from circulation. Hence, apoB is termed "non-exchangeable."

1.1.1 Hepatic Lipoprotein Metabolism

The liver secretes VLDL for the transport of endogenous TG, which are assembled in the liver from fatty acids that are delivered there from adipose tissue, or made from carbohydrate precursors in the liver itself during *de novo* lipogenesis. Each VLDL contains varying amounts of TG, CE and cholesterol (3). The assembly of VLDL requires three essential components: apoB100, which is constitutively synthesized in hepatocytes, microsomal triglyceride transfer protein (MTP), and an adequate supply of lipids (4-6). MTP is a 97 kDa protein present in a heterodimer with protein disulfide isomerase (PDI) in the lumen of the endoplasmic reticulum. Triglycerides, synthesized by the stepwise addition of three fatty acid moieties to a glycerol backbone, are stored in the lipid droplets (LD). ApoB has the ability to associate with these neutral lipids and increased TG biosynthesis can lead to an increase in hepatic VLDL assembly and secretion (7-12). This can be altered under metabolic conditions such as type 2 diabetes and non-alcoholic fatty liver disease, where there is an abundance of TG but no corresponding increase in VLDL secretion.

Hepatic VLDL assembly occurs in two steps (Figure 1.4) (13, 14). The first is the co-translational formation of small nascent lipoprotein particles in the ER and the

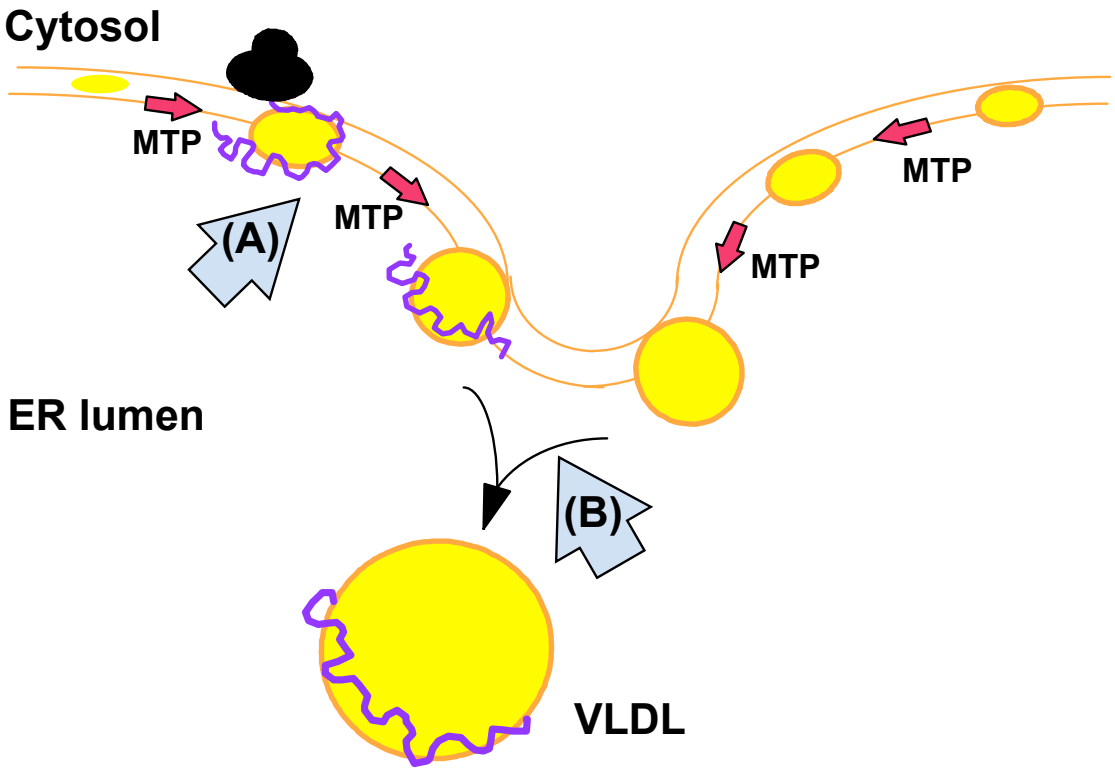

Figure 1.4 Two-step model of hepatic VLDL assembly. (A) As apoB100 is synthesized (solid purple line) and translocated across the ER membrane into the ER lumen, it associates with a small, lipid-poor, particle. Further lipidation occurs co-translationally. Both the initial association of apoB with lipid and the formation of apoB-free luminal lipid droplets appear to require MTP. **(B)** Fully lipidated VLDL is formed post-translationally upon the fusion of the nascent apoB-containing VLDL and a lipid droplet in an MTP-independent manner.

second is the post-translational addition of bulk lipid. MTP lipid binding and transfer activities (15) appear to be essential during the first step of VLDL assembly (16, 17). It is thought that during the second step, bulk lipid is acquired via the fusion of the nascent apoB-containing particle with a luminal LD in the secretory pathway (18, 19). MTP plays a role in the assembly of these apoB-free LD in the lumen of the ER (20, 21). The TG that is incorporated into the LD and added during the second step of VLDL assembly is initially stored in the cytosol in LD and is then mobilized by hydrolysis and re-esterification. MTP transfers TG across the ER membrane to generate a pool of apoB-free TG in the ER lumen. This has been shown in me hepatocytes, where inhibiting MTP decreased the amount of apoB-free TG within the lumen, resulting in a decrease in the number of luminal LD, and in the livers of MTP $^{-/-}$ mice, which have an increased number of cytosolic lipid droplets (20, 21). Thus, MTP is required for both the initiation of VLDL assembly and the formation of apoB-free LD, which subsequently fuse with the nascent apoB-containing particle in an MTP-independent bulk lipidation step to form mature VLDL.

Sufficient lipid must be available at the site of apoB translation in order to initiate VLDL assembly. When the availability of lipids is poor, either the elongation of the apoB polypeptide will be aborted, or if apoB has already been fully translated, the lipid-poor lipoprotein will be degraded intracellularly (22)

1.1.2 Regulation of VLDL Assembly and Secretion

The liver secretes VLDL for the transport of endogenous TG to peripheral sites for energy metabolism or storage. The synthesis of apoB is generally considered to be

constitutive and the rate of secretion of VLDL is a function of assembly (23). In a healthy individual, the liver modulates VLDL secretion according to metabolic and dietary requirements to ensure lipid homeostasis. The assembly of VLDL is affected by the rate of synthesis, cellular and extracellular availability of its lipid components (i.e. TG, cholesterol and CE).

In the plasma, VLDL is metabolized and the TG content is reduced via lipolysis by lipoprotein lipase. The resulting remnant particles may be taken up by the liver, or may be further metabolized to LDL in the plasma. Therefore, VLDL secretion plays an important role in determining the plasma LDL concentration. Overproduction of VLDL can increase circulating LDL concentrations and put one at increased risk for atherosclerosis.

1.1.3 Atherosclerosis and Disorders of Apolipoprotein B Metabolism

Increased hepatic secretion or decreased removal of apoB-containing lipoproteins from circulation can elevate plasma apoB levels and put an individual at an increased risk of atherosclerosis, which can result in myocardial infarction and stroke. Since there is exactly one apoB molecule per lipoprotein, measuring apoB levels in the plasma provides an accurate indication of circulating particle number. As such, plasma apoB level is the target of many dietary and pharmaceutical interventions aimed at lowering risk for cardiovascular disease.

Much of what we understand about apoB structure and function comes from studies of those with apoB mutations. Familial hypobetalipoproteinemia (FHBL) is an autosomal dominant disorder in which patients have negligible plasma levels of LDL-cholesterol or

apoB (24). Although this puts them at a decreased risk of developing cardiovascular diseases, their inability to export hepatic lipids is often associated with fatty livers (25). Studies of FHBL have also revealed that mutations in the amino terminus of apoB100 that prevent the initiation of lipoprotein assembly reduce hepatic VLDL secretion (26, 27). These studies demonstrate that apoB structure is critical in the initiation of VLDL assembly.

1.2 APOLIPOPROTEIN B100 STRUCTURE

1.2.1 Cloning of the apoB cDNA

Several laboratories independently published the initial cloning and expression of partial apoB sequences around the same time. Knott *et al.* cloned the amino terminal 1455 amino acids of human apoB100 and characterized the expression of the 19 kb apoB mRNA in the liver and intestine from this fragment (28). Lusis *et al.* cloned a 20 kb mRNA from a rat liver cDNA library, which predicted a protein of 400 kDa (29). Analysis of the corresponding apoB secondary structure did not predict an abundance of α-helical character, as was characteristic of the other apolipoprotein structures. Law *et al.* cloned a 1.7 kb cDNA fragment of human apoB100, and predicted that the apoB mRNA was 15-18 kb, coding for a 250-387 kDa protein (30). Using computational methods, the investigators predicted that apoB100 contained some helical structure, but that the majority of the protein was composed of beta structure. They postulated that the β-structures participated in lipid interactions and that they were responsible for the insoluble nature of apoB.

Cladaras *et al.* (31) cloned a 5.2 kbp amino terminal segment of apoB coding for

1748 amino acids. Computer-based analyses of the secondary structure potentials for apoB estimated this peptide to be mostly helical in nature and more hydrophilic than hydrophobic. Using overlapping cDNAs, these researchers assembled an almost complete apoB100 cDNA. Evidence predicted the apoB mRNA to be 14.0 kb, encoding a protein of 512 kDa. The authors refined their initial estimates to yield a full-length mRNA of 14,112 nucleotides (including a 128 bp 5'- and 301 bp 3'- untranslated region), coding for 4560 amino acids (513 kDa polypeptide) and a signal peptide of 24 amino acids (32). Several laboratories reported similar findings on the full-length human apoB100 cDNA sequence (33, 34). The apoB100 primary sequence of amino acids has been inferred from cDNA clones and glycosylation sites have been predicted by computer-aided analysis and later verified by chemical methods (72).

1.2.2 Early Studies of Apolipoprotein B Structure

Studying the structure of apoB has been challenging due to its aqueous insolubility and hydrophobicity. Early experimental structural analyses were performed using delipidated, detergent-solubilized apoB, or fragments derived from limited proteolysis of LDL. These studies observed an increase in the α-helical character of apoB on binding to phospholipid or to monomeric detergent (35). After delipidation of LDL and reconstitution of the protein with sodium dodecylsulfate (SDS), the apoB in this study was found to exist as protein fragments that appeared to have an α-helical CD spectrum similar to that of intact LDL. Importantly, the SDS could be replaced by naturally occurring phospholipids (i.e. phosphatidylcholine (PC)), but in the absence of an

amphipathic ligand, the protein was insoluble (35). Thus, it became evident from early on that apoB was a protein with unique properties.

1.2.2.1 Immuno-Characterization of Apolipoprotein B

In the 1980s, the development of monoclonal antibodies to human apoB saw advances in the elucidation of apoB structure. Studies using these antibodies confirmed that each LDL particle had only a single molecule of apoB100 and that apoB100 on LDL was the ligand for the LDL receptor (36-38). Moreover, binding of apoB to the LDL receptor could be inhibited using some of these antibodies that interacted with LDL-bound apoB (37). A different set of monoclonal antibodies was used to assess the expression of apoB epitopes on LDL and VLDL and revealed that differences in particle lipidation caused differential expression of several epitopes (39). Bacterial expression of partial apoB cDNAs generated polypeptides that were used to map apoB monoclonal antibodies and the LDL receptor binding domain (38, 40).

Polyclonal antibodies designed against synthetic peptides corresponding to the apoB100 sequence were used to define the structural relationship between apoB48 and apoB100. Innerarity *et al.* demonstrated that apoB48 represents the amino-terminal 48% of apoB100, and mapped the carboxyl terminus of apoB48 to approximately amino acid residue 2151 of apoBl00 (41). Peptides generated by kallikrein and thrombin proteolysis, and used to map apoB100 on intact LDL, have also shown that apoB48 corresponds to the N-terminal 48% of apoB100, but that apoB48 is not generated from proteolysis of apoB100 (42). Therefore, it is clear that the N-terminal sequences of both apoB48 and apoB100 are identical and that

intestinal apoB48 is the N-terminal 48% of hepatic apoB100. ApoB48 is generated by a mRNA editing process that generates an in-frame stop codon in place of Gln at position 2152 of the apoB mRNA

1.2.2.2 Proteolytic Analysis of Apolipoprotein B

Limited trypsin proteolysis of LDL has shown that approximately 80% of LDL-bound apoB100 remains particle-associated after proteolysis. This suggests that the majority of apoB100 is bound tightly and lipid-associated. Following proteolysis, the CD spectrum revealed a decrease in α-helical character as compared to that of intact LDL (43). This suggests that helices in apoB may be solvent exposed and more readily accessible to proteolytic enzymes. Cardin and Jackson studied the apoB peptides released from LDL as a result of trypsin proteolysis. They showed that the soluble peptides were able to optically clear dimytristoyl phosphatidylcholine (DMPC) micelles. Fluorescence polarization spectroscopy revealed that the apoB-DMPC complexes were approximately 70% α-helix and 5% β-sheet, compared to the parent LDL, which were 42% α-helix and 15% β-sheet (44). Therefore, during the proteolysis, it appears that more of the α-helical regions were released, while the β-structures remained mostly associated with the LDL particle.

Trypsin accessibility has also been used to deduce the regions of apoB100 that are exposed on the surface of an LDL particle. Yang *et al.* used the non-dissociability of tryptic peptides to develop a model in which apoB was divided into five domains: residues 1 to 1000 were trypsin-releasable, residues 1001-1700 were a mixture of releasable and non-releasable peptides, residues 1701-3070 were non-releasable,

residues 3071-4100 were mostly releasable and residues 4101-4536 were non-releasable (45). A multi-domain structure for apoB has also been supported by electron microscopy of LDL following lipid extraction (46), suggesting that apoB structure is retained following delipidation. Some of the peptides released by trypsin could bind to phospholipid emulsions (47), but there was no spectroscopic evidence for β-sheet structures, suggesting that the predicted apoB secondary structures likely did not fit a simple structural model. Proteolytic fragments of apoB were capable of forming LDL-like particles upon addition of lipids, suggesting that the lipid-binding regions of apoB are widely dispersed (48). Proteolytic cleavage, and to a lesser extent CD spectroscopy, of LDL appear to be sensitive to changes in apoB conformation that result from differences in particle density (48, 49). Therefore, apoB100 can be viewed as a flexible molecule that is able to adapt its conformation according to the size of the LDL particle with which it is associated.

1.2.3 Physicochemical Analysis of Apolipoprotein B Structure

CD spectroscopy and electron microscopy have been the principle methods used in studying intact LDL structure. Most of the CD data has suggested that apoB is mainly α-helical in structure, which is in contrast to what the computer algorithms have predicted. Infrared (IR) spectroscopy has estimated the amount of β-sheet structure to be approximately 41% for apoB on LDL; significantly higher than that determined by CD spectroscopy (12%-16%) (50). Fourier transform IR spectroscopy studies have revealed that following proteolysis, the peptides that remained associated with LDL are those rich in β-structure (51). The secondary structure of apoB on LDL was not significantly altered

by chemical modification, as studied using IR and CD spectroscopy. Although there appeared to be slight changes in particle lipid composition, biological activity, as assessed by uptake of the particles into macrophage cell cultures, was retained (52).

Mapping of antibodies onto LDL by electron microscopy has suggested a ribbon and bow conformation for apoB on the surface of spherical LDL (53). According to this model, the N-terminal 89% of apoB, "the ribbon," wraps once around LDL and the C-terminal 11%, "the bow," stretches back and over the "ribbon," like a loop, to bring the C-terminal portion into the vicinity of the LDL receptor-binding site. The authors proposed that the C-terminal "bow" regulates receptor binding by undergoing a conformational change upon lipolysis that exposes the LDL receptor-binding site on apoB (53) [(residues 3,359–3,369 (54)]. Neutron scanning analysis (55) and three-dimensional reconstruction of LDL based on multiple cyro-electron microscopy images (56) have also revealed a spherical structure for LDL. A map of the structure of LDL at 26 Å resolution, generated from cryo-electron microscopy images, implied that apoB is mainly localized along the edge of the particle and that the phospholipid monolayer is on the flat surface (57). This strengthens the notion that apoB adopts a looped topology on the surface of LDL.

Experimental studies of apoB in the absence of lipid have seldom been done since apoB is insoluble. However, Walsh and Atkinson have shown that in the absence of lipids, apoB can be solubilized in sodium deoxycholate (Na-DOC) and that it contained a number of domains consisting of both α and β secondary structures (58, 59). Cryo-electron microscopy images indicated that apoB takes on an extended ribbon-like conformation with a presumed loop at the C-terminal end (60).

Several attempts at modeling the lipid binding regions of apoB have been made using small amphipathic peptides. Lins *et al.* (61) designed amphipathic β-peptides (5-13 residues) with a hydrophobic valine face and a hydrophilic face composed of alternating acidic glutamic acid resides and basic ornithine or lysine residues. These peptides possessed significant β-sheet character (up to 90%), were stable in 6 M guanidine hydrochloride, and self-associated in aqueous solution. Furthermore, synthetic β-sheet peptides corresponding to lipid binding domains of apoB associated with DMPC liposomes in such a manner as to orient with the acyl chains of the phospholipid in Fourier transform IR spectroscopy (62). These observations suggest that amphipathic β-peptides strongly associate with the outer phospholipid monolayer of the LDL particle.

ApoB polypeptides are commonly described using a centile scale (see Figure 1.2), where apoB100 is the full-length gene product, apoB48 is the N-terminal 48% of apoB100 and apoB37-42, for example, represents the polypeptide sequence between the C-termini of apoB37 and apoB42. The interfacial binding properties of two, 12 and 27 residue, amphipathic β-strand peptides from apoB21-41 were studied at triolein/water and dodecane/water interfaces (63). The peptides were elastic and could not be desorbed from the surface upon compression under conditions where α-helical peptides were observed to be desorbed. Similarly, apoB37-41, a 187 amino acid peptide rich in β character, was observed to bind tightly to the interface and exhibit elasticity (64). This suggests that the β-regions of apoB may serve to anchor the protein to the lipoprotein particle and account for its non-exchangeable nature.

1.2.4 Computer Modeling of Apolipoprotein B Structure and The Pentapartite Model

Computational techniques have been important in overcoming the experimental barriers in studying apoB structure. Computer modeling techniques designed to identify internal repeats in apoB, and potential sequence homology to other apolipoproteins, have provided much insight into apoB structure. Initial studies identified repetitive α-helical regions and hydrophobic domains enriched in proline (65). Using a computer program designed to search amino acid primary sequences for potential α and β character, Segrest *et al*. identified 5 consecutive domains in apoB that were enriched in either α or β character. They proposed that apoB had a pentapartite structure (66), wherein the N-terminus forms a compact, globular domain followed by consecutive alternating domains enriched in either β-strand or α-helix. Despite little amino acid sequence homology between species, the pentapartite model has also been applied to apoB100 sequences in nine other vertebrate species: chicken, frog, hamster, monkey, mouse, pig, rat, salmon and rabbit (67).

In 2001, the existing pentapartite model (N-α_1-β_1-α_2-β_2-α_3-C) was updated to reflect the presence of both α- and β- characteristics in the N-terminal domain, which was expanded to encompass residues 1-1000 of apoB100 (68). The originally designated α_1 domain was renamed $\beta\alpha_1$, and the pentapartite model became N-$\beta\alpha_1$-β_1-α_2-β_2-α_3-C (Figure 1.5). In accordance with existing experimental information, the alpha helical domains were postulated to be involved in reversible lipid affinity, while the beta domains represented regions that came into contact with the lipid core.

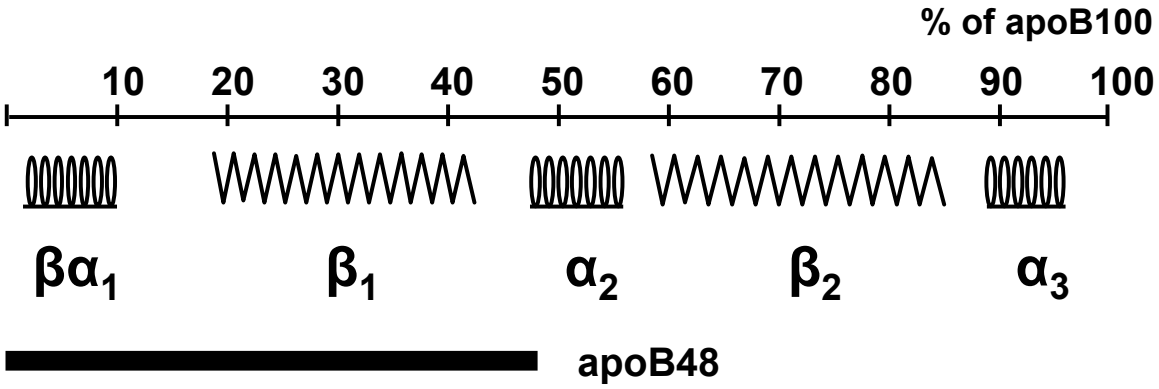

Figure 1.5 Pentapartite model of apoB100 structure. Schematic representation of the pentapartite model of apoB100 secondary structure as described by Segrest *et al*. Positions of the five domains are represented on a centile scale relative to full-length apoB100. The location of apoB48, which is produced in the intestine via mRNA editing, is shown for reference. This figure was originally published in the Journal of Lipid Research. Segrest *et al.* Structure of apolipoprotein B-100 in low density lipoproteins. *J. Lipid Res.* 2001; 42:1346-1367. © The American Society for Biochemistry and Molecular Biology.

Furthermore, it suggested that the β-enriched domains determine lipoprotein particle diameter and that as the size of the particle increased, the α-domains were in more contact with the particle surface. This lent support to a spherical model for LDL. The N-terminal $\beta\alpha_1$ domain has been reported to have sequence and motif homology to lamprey lipovitellin, a globular egg yolk protein whose crystal structure has been solved (69) (Figure 1.6). Based on bioinformatics, similar amphipathic β-strands to those found in apoB were identified in vitellogenin (the lipovitellin precursor protein) from frog, chicken, lamprey and *C. elegans* (70). The investigators also noted sequence homology between the N-terminus of apoB and MTP. This information led them to suggest an assembly model where a lipid pocket is formed by the N-terminus of apoB as a complex with MTP. This intermediate facilitates the initiation of apoB-containing lipoprotein assembly and lipoprotein expansion likely involves the lipidation of β-strand elements from the β1 domain to form progressively larger particles. The apoB-MTP complex has been supported by studies showing that positively charged amino acids located between residues 430-570 of apoB are necessary for MTP binding (71) and by molecular modeling and mutagenesis to show that apoB and MTP contain globular regions that are related to vitellogenin and that structural elements in both could form a stable complex able to transfer lipids during lipoprotein assembly (72).

Phylogenetic analysis of the large lipid transfer protein superfamily reveals the group is composed of three distinct protein families: apoB-like, vitellogenin-like and MTP-like large lipid transfer proteins. While the MTP-like lipid transfer proteins are ubiquitous in nature, the other two families are differentially dispersed among animal

Figure 1.6 Structure of lamprey lipovitellin. This figure was originally published in the Journal of Lipid Research. Segrest *et al.* Structure of apolipoprotein B-100 in low density lipoproteins. *J. Lipid Res.* 2001; 42:1346-1367. © The American Society for Biochemistry and Molecular Biology.

groups. In addition, many of these proteins have functions in addition to lipid uptake and transport (73).

Recently, a three-dimensional model of delipidated apoB was generated using computational algorithms in combination with small angle neutron scattering (74). This model suggests that lipid-free apoB is an expanded, multi-domain, molecule with 5 domains enriched in either α or β character separated by flexible regions (Figure 1.7, top panel). Upon association with lipids, apoB appears to take on a ring-shaped conformation with a central cavity corresponding to the diameter of an average LDL particle (Figure 1.7, bottom panel). However, electron microscopy suggests that despite the difference in global conformation, apoB secondary structural domains are maintained between lipid-free and LDL-associated apoB.

1.2.5 Structure-Function Analysis

The ability to study the assembly of apoB-containing lipoproteins in heterologous systems has provided significant insight into the structure-function relationships within the apoB polypeptide. It has been estimated that the amino terminal 22% of apoB (the first 1,000 amino acids) is necessary for the initiation of a nascent lipoprotein particle (75). Evidence indicates that the N-terminus of apoB does play an important role in lipid recruitment and lipoprotein assembly. Studies with the amino terminal 17% of apoB (apoB17) revealed that this portion of the protein is necessary but not sufficient for secretion, as apoB proteins lacking apoB17 were not secreted, but additional sequences beyond 17% were required for MTP-enhanced secretion (76). ApoB17 has lipid-binding properties and is able to remodel

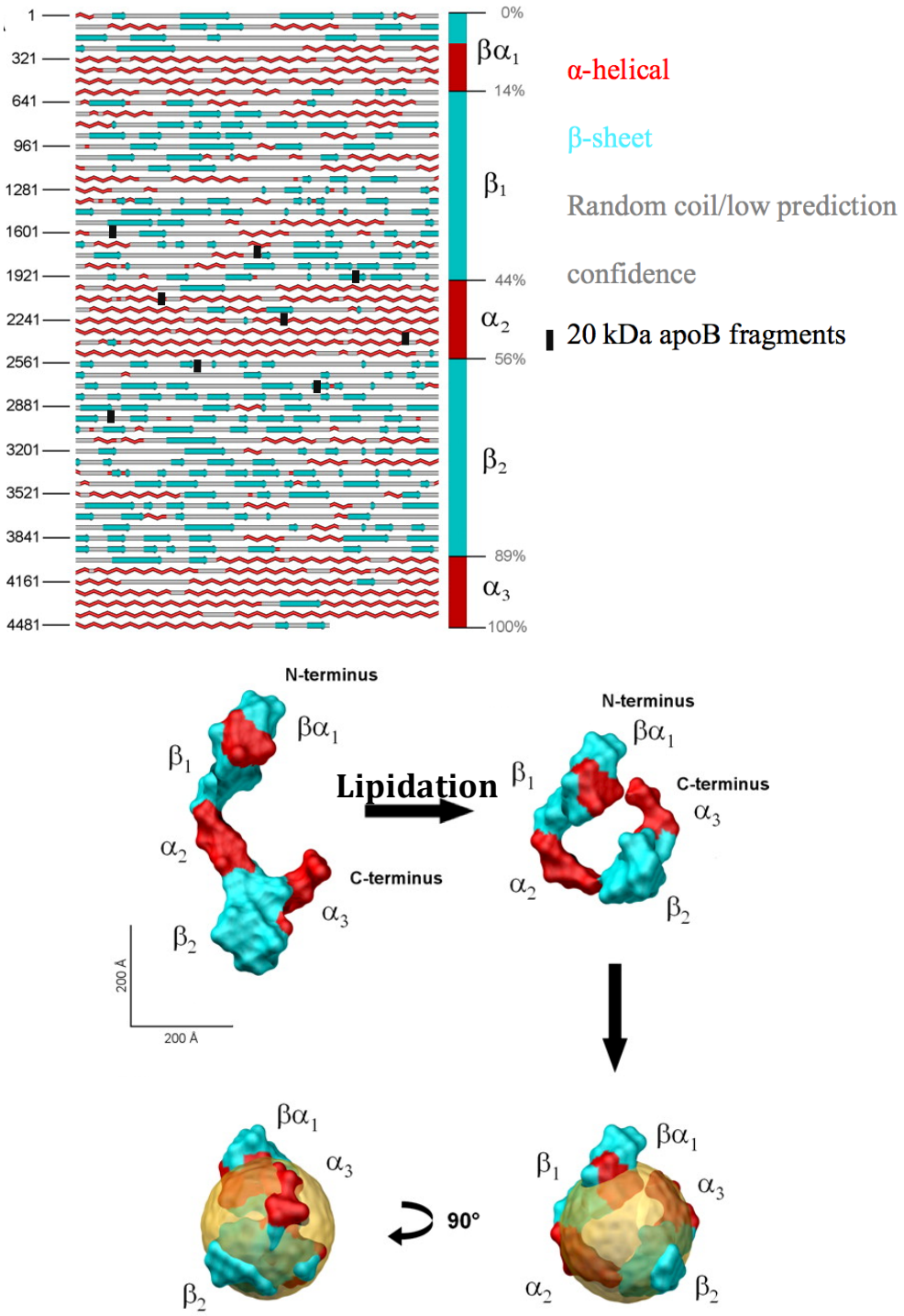

Figure 1.7 Theoretical three-dimensional model of apoB100 domains and their organization on LDL. This figure was originally published in the Journal of Biological Chemistry. Johs *et al.* Modular structure of solubilized human apolipoprotein B-100. Low resolution model revealed by small angle neutron scattering. *J. Biol. Chem.* 2006; 281:19732-19739. © The American Society for Biochemistry and Molecular Biology.

multilamellar DMPC vesicles into smaller discoidal particles, suggesting that this may be sufficient to initiate VLDL assembly (77). Khachfe *et al.* studied the secondary and tertiary structures of apoB17 by CD spectroscopy as a function of temperature and pH. Far ultraviolet (UV) CD spectra revealed the presence of α, β, and random coil structures and under acidic conditions, protonation of histidine residues in apoB17 increased the amount of α-helical and random coil structures but did not affect the content of β-structures (78).

Oil drop tensiometry has been used to study the lipid-binding properties of C-terminally truncated apoB proteins at lipid/water interfaces. Mitsche *et al.* have demonstrated that apoB6-17 is the first lipid-binding portion of apoB100. ApoB6-17 binds to a triolein/water interface and while parts of the protein can be ejected from the surface upon compression, other parts remain irreversibly anchored (79). This implies that apoB6-17 has both α- and β-characteristics. Further dissection of this portion of apoB into apoB6.4-13 an apoB13-17 found that both were surface active and able to bind to neutral lipid. However, apoB6.4-13 exhibited α-helical character, while B13-17 bound more strongly and exhibited β-characteristics (80). Therefore, both phospholipid and neutral lipid recruitment may be initiated very early in the synthesis of apoB100.

While N-terminal fragments of apoB100 as small as apoB6.4 can initiate lipid recruitment, more apoB sequence information is required to stabilize the lipid emulsion to facilitate secretion of a lipoprotein particle (80). The amino terminal 20.1% of apoB100 is capable of initiating lipoprotein assembly. Biophysical studies suggest that apoB20.1 has solvent accessible hydrophobic surfaces that interact with neutral lipid (81). A comparison of apoB20.1 and apoB19, which is unable to initiate lipoprotein

assembly, reveals that the two peptides have similar spectroscopic structures and can both bind lipid, but that apoB20.1 has increased surface activity and interfacial pressure (82). This suggests that the ability of apoB to assemble lipoproteins is not necessarily accompanied by changes in its conformation so much as by increases in its surface activity and elasticity.

It has been proposed that the $\beta\alpha_1$ domain at the N-terminus of apoB forms a lipid-binding pocket associated with MTP that facilitates the initiation of lipoprotein assembly. Evidence of the formation of a pocket capable of lipid-transfer between the first 1000 amino acids of apoB and MTP was demonstrated using C-terminally truncated apoB molecules (83). Dashti *et al.* also demonstrated that the first 1000 amino acids of apoB (B22) are required for the formation of a lipoprotein particle containing both TG and PL in rat hepatoma McA-RH7777 cells (84). However, in COS cells transfected with C-terminally truncated apoB and MTP, B19.5 could form some lipoproteins (85). ApoB17, B19 and B20.1 bind to TG droplets, suggesting that the N-terminus of apoB has lipid-associating regions (82, 86). Therefore, although there are discrepancies regarding the minimal length of apoB100 required, the amino terminus has all the elements required to form nascent lipoprotein particles. It could be that, under certain conditions, apoB proteins of variable length may be able to successfully initiate lipoprotein formation.

1.2.5.1 The Roles of Disulfide Bonds and Glycosylation

The role of disulfide bond formation within the N-terminal 21% of apoB and its effect on the assembly of lipoproteins has been probed by substituting serine residues for cysteine residues involved in disulfide bonds (87). The mutation of cysteine pairs within the first 5% of apoB drastically reduced the assembly and secretion of

lipoproteins, suggesting that the structural conformation of the N-terminus must be intact to foster lipidation. However, these alterations had no impact on the ability of apoB17 to bind to PC vesicles, suggesting that the disulfide bonds in the N-terminal globular domain are not required for phospholipid binding (88). Site-specific asparagine to glutamine mutations of one or several glycosylation sites in the N-terminus revealed their importance in the assembly and secretion of apoB-containing lipoproteins (89), but their specific role is also unclear.

1.2.5.2 Expression and Assembly Studies

The length of the apoB polypeptide dictates the diameter and/or volume of the lipoprotein particle (90, 91). The role of C-terminally truncated apoB proteins in lipoprotein assembly and secretion has been studied in several systems. In HepG2 cells, a human hepatoma cell line, the larger the apoB protein, the greater the core circumference of the lipoprotein. In McA-RH7777 cells secreting full-length apoB100, B94, B88, B80, B72 and B60, the length of the apoB protein was directly related to the size of the lipoprotein particle and inversely related to its density. In C127 mouse mammary-derived carcinoma cells, the diameter and number of TG molecules per particle increased with the length of the apoB protein (92). Transfection of apoB29, B32.5 and B37 revealed that sequence beyond apoB29 accounts for bulk TG recruitment into lipoproteins. Accordingly, McLeod *et al*. showed that recombinant apoB29 lacks the ability to assemble VLDL (93). Further experimental evidence for the structures of these polypeptides at atomic resolution, and the identification and characterization of additional sequences in the β1 and β2 domains, are required.

1.2.6 Characterization of Lipid-Binding Structures

The fatty acid-binding protein (FABP) family is composed of five or six 14-15 kDa proteins that noncovalently bind fatty acids and other hydrophobic ligands (94-96). These lipid-binding proteins have been studied by X-ray crystallography (97) and NMR spectroscopy (98-102). All FABP share a similar secondary structure composed of 10 anti-parallel β-strands that form a flat, barrel-like, structure often referred to as a "β-clam." The ligand-binding cavity is contained within the β-clam and is capped by two short α-helices, which regulates ligand entrance and exit (Figure 1.8). The β-structure and hydrophobic cavity are responsible for the interaction of FABP with their ligands and other lipid-binding proteins utilize similar structural elements to mediate their interactions with hydrophobic ligands.

The exchangeable apolipoproteins are made up of 11 and 22 amino acid homologous repeats, which are predicted to form α-helices that reversibly bind lipids. In contrast, the non-exchangeable apolipoproteins do not have these amino acid repeats. Although apoB could be composed of repeated FABP-like lipid-binding units, this is not evident from its amino acid sequence, which shows no evidence of a repeating unit. The non-exchangeability and expansibility of apoB appears to be a result of its β-strand domains (64, 103). This elasticity may explain how apoB can accommodate a small or large neutral lipid load. However, we still do not have structural information on an apoB polypeptide at atomic resolution.

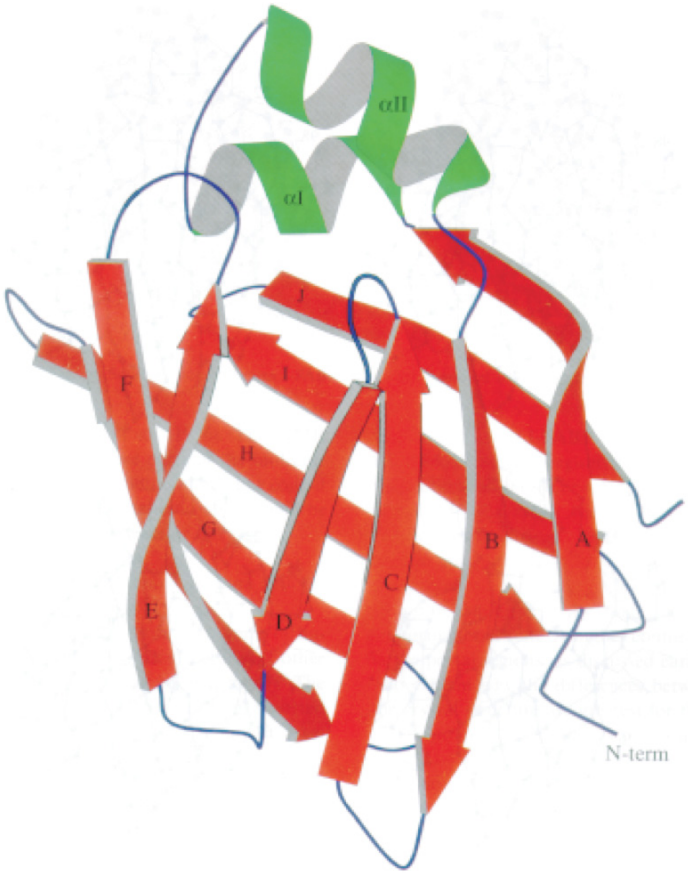

Figure 1.8 A ribbon model of intestinal FABP. All FABP have a similar conformation of 10 antiparallel β-strands (A-J), which form two nearly orthogonal 5-strand β-sheets, and 2 α-helices (αI and αII) that connect the β-sheets and cover the ligand-binding cavity. This figure was originally published in the Journal of Biomolecular NMR. Zhang F, Lücke C, Baier LJ, Sacchettini JC, Hamilton JA. Solution structure of human intestinal fatty acid binding protein: Implications for ligand entry and exit. J. Biomol. NMR. 1997; 9: 213-228.

1.3 CIRCULAR DICHROISM SPECTROSCOPY

Circular dichroism (CD) spectroscopy is a technique allowing estimation of the secondary structural content of a protein (rather quickly) with only microgram (μg) quantities required. It is based on the differences in the absorption of right- vs. left-circularly polarized light as it passes through a chiral sample (104). The CD signal is produced by electronic transitions from a ground state orbital to an excited orbital. The CD spectra of most proteins are collected in the ultraviolet (UV) region, which is further divided into the near UV region (from ~360 nm to ~260 nm), where the contributions of aromatic side chains dominate, and the far UV region (from ~ 260 nm to ~190 nm), where contributions of the polypeptide backbone dominate (105-107). For proteins, the peptide bonds in the polypeptide backbone account for the majority of the electronic transitions, but are modified by additional chirality features arising from protein secondary structures. For example, an α-helix within most proteins spirals in a right-handed manner, adding additional chirality features to the CD spectrum. A typical α-helical structure yields two negative bands at approximately 222 nm and 208 nm as well as a positive band around 190 nm, whereas a β-sheet structure gives rise to a smaller negative band around 215 nm and a smaller positive band around 195 nm (105). Typical CD curves for the major secondary structures are shown in Figure 1.9. Therefore, comparison of the structural features of a CD spectrum to those of reference databases containing spectra of proteins whose structures are known, can allow for either visual or computer algorithm assisted estimation of secondary structure content (104, 105).

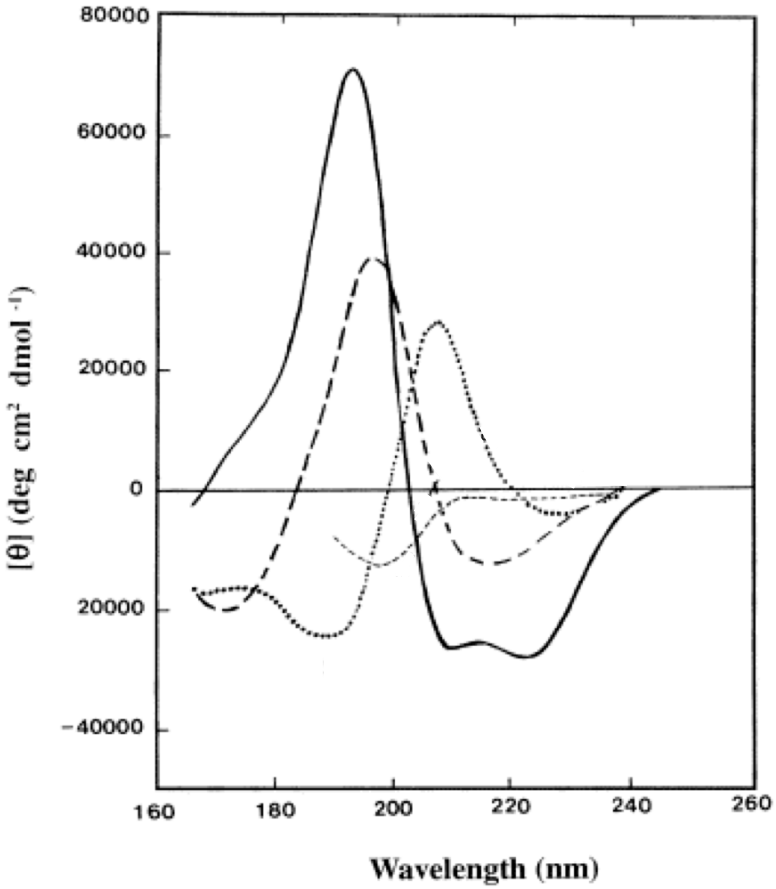

Figure 1.9 CD spectra representing three types of secondary structure. The solid line depicts a protein of mostly α-helical nature, the long dashed line is that of a predominantly β-sheet protein, the dotted line represents β-turns and the short dashed line is that of a protein enriched in random structure. Kelly SM, Jess TJ, Price NC. How to study proteins by circular dichroism. Biochimica et Biophysica Acta (BBA) - Proteins and Proteomics 2005; 1751(2): 119-139.

1.4 USING NUCLEAR MAGNETIC RESONANCE SPECTROSCOPY TO STUDY PROTEINS

1.4.1 The Basics of NMR Spectroscopy

NMR spectroscopy relies on the magnetic properties of certain nuclei to obtain detailed physical, chemical, electronic and three-dimensional structural information about molecules (108). NMR spectroscopy takes advantage of the nuclear spin angular momentum interaction between nuclei when exposed to an external magnetic field. Spin angular momentum is an intrinsic property of a nucleus and can be an integer (0, 1, 2, 3…) for nuclei with an even mass number and odd atomic number or a half-integer (1/2, 3/2, 5/2…) for nuclei with an odd mass number. Nuclei with even mass and atomic numbers have a spin equal to zero and therefore cannot be observed using NMR spectroscopy because a non-zero value of nuclear spin is required. For example, some of the most abundant naturally occurring nuclei in proteins, ^{12}C and ^{16}O, have a nuclear spin of zero and cannot be observed. Although naturally abundant ^{14}N has a spin of 1, it has complex interactions with the magnetic field and produces spectra that are difficult to study. For this reason, almost all NMR experiments are isotope-aided, using the less common isotopes ^{13}C and ^{15}N, which have a spin of ½ (109-111) and almost always also relying on ^{1}H.

A nucleus with spin angular momentum also has a magnetic moment and will behave in a manner analogous to a bar magnet (110). In the absence of an external magnetic field (B_0), the magnetic moments of a sample are distributed such that all directions are represented equally. When an external B_0 is present, the nuclear magnetic moments will align themselves with the magnetic field and become magnetized in the

direction of B_0., eventually reaching an equilibrium magnetization. When this equilibrium is not parallel with B_0, it precesses about B_0 at the Larmor frequency, which is given by:

$$\omega_0 = -\gamma B_0$$

where ω_0 is the nuclear Larmor frequency, γ is the gyromagnetic ratio, which is a constant for a given nucleus, and B_0 is the magnetic field of the NMR spectrometer (110). Although the applied magnetic field is static, the magnetic field around each nucleus is modified by molecular structure (i.e. electrons) and thus slightly different from the applied B_0. This magnetic shielding of the nucleus means that most nuclei will have a unique Larmor frequency and NMR spectroscopy can be used to probe these chemically unique nuclei.

In an NMR experiment, radiofrequency pulses are used to perturb the direction of the equilibrium magnetization so that it is not parallel to B_0. The Larmor frequency of the nuclei are then measured and give rise to unique chemical shift values (δ) (112).

1.4.2 Multi-Dimensional NMR Spectroscopy

With every NMR active nucleus in a sample giving rise to a signal, polypeptides larger than a few residues, as is the case for biological macromolecules, yield one-dimensional spectra with numerous overlapping peaks. One solution to this is to increase the dimensionality of the experiment. For example, in two-dimensional NMR spectroscopy, such as the ^{1}H-^{15}N heteronuclear single quantum coherence (HSQC) experiment, the magnetization is transferred between two nuclei, ^{15}N and ^{1}H, before detection. Only ^{1}H nuclei capable of transferring magnetization to ^{15}N nuclei are

detected, giving rise to a single peak in the spectrum for every amino acid in the protein under study, except for proline. Therefore, plotting each signal with both the ^{15}N and ^{1}H frequencies, along the y and x axes, respectively, yields a less crowded two-dimensional spectrum (109, 111). This can be extended further to three-dimensional spectra. For example, in an HNCA the magnetization is passed from ^{1}H to ^{15}N and then to $^{13}C_{\alpha}$ before being transferred back for detection. Since magnetization is transferred between three nuclei, the resulting signal has ^{1}H, ^{15}N and ^{13}C frequencies and the signal overlap in the resulting three-dimensional spectra is reduced further (113).

1.4.3 Assignment of Protein NMR Spectra

The assignment of chemical shifts in NMR spectra relative to the amino acids in the primary sequence of a protein is the first step in obtaining detailed structural information. The fact that the nuclei in each amino acid have different expected chemical shifts allows one to predict the specific nucleus giving rise to each NMR signal (111). These expected chemical shift patterns can then be used to identify amino acid spin systems. The nuclei of amino acids are designated using Greek nomenclature. The alpha carbon and the nitrogen and carbonyl group attached to it are designated C_{α}, N and (CO), respectively. The first heavy nucleus in the amino acid side chain is labeled as β and you continue going through the Greek alphabet for every subsequent heavy side chain nucleus. The backbone amide proton is designated H^{N} and all other protons are labeled according to which carbon they are attached to, for example the hydrogen attached to C_{α} is denoted H_{α} (111).

The sequential assignment of NMR spectra requires the use of several multi-dimensional resonance experiments. For full, unambiguous protein backbone assignment, a common approach is to assign the protein backbone using a uniformly $^{15}N/^{13}C$ labeled protein. In this method, several complementary heteronuclear triple-resonance experiments are used to correlate the backbone atoms and identify spin system connectivity (111). In the HNCO experiment (113), magnetization is passed from the H^N to ^{15}N of a residue (i) and then to the ^{13}CO of the preceding residue (i-1). In the 3D spectrum, there will be one peak relating the N-H of residue i to the ^{13}CO of the i-1 residue. The complementary spectrum, the HNcaCO (114), produces a correlation between the H^N and ^{15}N of the same residue (i) and the ^{13}CO of both that residue and residue i-1. This results in two carbonyl groups being correlated to the N-H of residue i in the spectrum, one corresponding to $^{13}CO_i$ and the other to $^{13}CO_{i-1}$. Overlaying the HNCO and HNcaCO spectra allows one to distinguish which peak belongs to $^{13}CO_i$ and which to $^{13}CO_{i-1}$. The second set of complementary experiments is the HNCA (113) and HNcoCA (115). In the HNCA, magnetization is transferred from H^N to ^{15}N and then to $^{13}C\alpha$ nuclei. The amide nitrogen and H^N are coupled both to the Cα of residue i and to that of residue i-1, giving rise to two peaks in the spectrum- one for $^{13}C\alpha_i$ and one for $^{13}C\alpha_{i-1}$. Its paired experiment, the HNcoCA, provides solely the inter-residue correlations between the ^NH and ^{15}N of residue i and the $^{13}C\alpha$ of the preceding residue i-1. The spectrum yields one peak corresponding to the $^{13}C\alpha_{i-1}$. Overlaying the HNCA and HNcoCA helps identify the peak belonging to $^{13}C\alpha_i$ and that belonging to $^{13}C\alpha_{i-1}$. Another useful experiment is the HNCACB or CBCANH (116), which produce correlations between the amide of residue i and the $^{13}C\alpha_i/^{13}C\alpha_{i-1}$ and $13C_{\beta i}/^{13}C_{\beta i-1}$, giving rise to four peaks in the spectrum. A

diagram of the correlations observed in the three-dimensional experiments described above is shown in Figure 1.10.

Side chain assignments of the spin systems can then be made using the HCCH-COSY or HCCH-TOCSY experiments, as well as others, which provide connectivities of the aliphatic side chains of individual amino acid residues (108).

After individual spin systems have been identified and amino acid types assigned, nuclear Overhauser effect (NOE) spectroscopy (NOESY) experiments identify residues that neighbour each other or are close in space. In the NOESY, there is direct transfer of magnetization through-space from one nucleus to another (110). Through-space connections are generally seen between the H^N nuclei with the H_α and/or H_β nuclei of the preceding residue. The amount of magnetization that is transferred between nuclei is proportional to the distance between them, with 6 Å considered to be the maximum distance (110).

Once all individual spin systems have been assigned and sequentially connected and distance restraints have been calculated, computer programs are used to generate three-dimensional molecular structures that will undergo iterative modifications to identify the one that best satisfies experimental constraints.

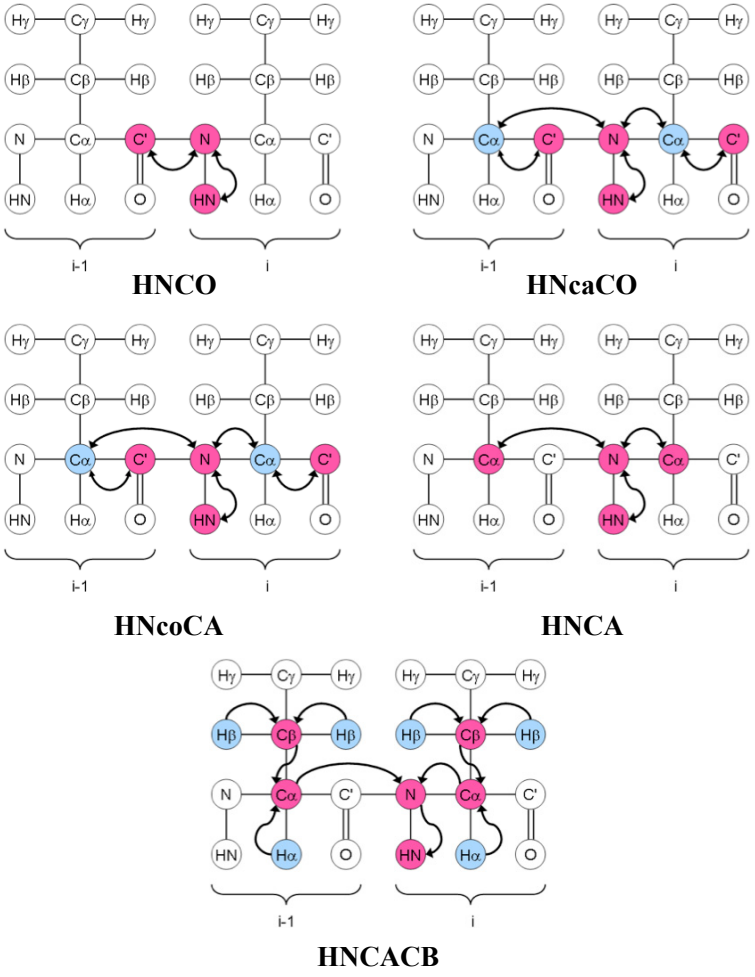

Figure 1.10 Correlations observed in three-dimensional NMR experiments. In each of these experiments, the correlation between the NH group and the inter- or intra- ^{13}C residue is shown. Pink circles denote the residues on which the chemical shift is evolved. These figures were originally published on http://www.protein-nmr.org.uk/

1.5 RATIONALE AND OBJECTIVES

The objective of my work was to perform structural characterization of 20 kDa fragments of apoB100 derived polypeptide sequences at 37-70% of the full-length human apoB100 protein. These fragments were chosen in order to overcome the obstacles associated with the size and insolubility of apoB. At the time this work was conducted, very little was known about the structure of apoB100 and what was known was derived mainly from computational algorithms. My work provides experimental characterization of the structure of fragments of apoB100 at atomic resolution. This information will help better understand how the apoB protein interacts with a lipid monolayer and how the structural features of apoB100 are involved in lipid recruitment, assembly and secretion of VLDL and degradation of apoB100.

Chapter 2 MATERIALS AND METHODS

2.1 APOLIPOPROTEIN B FRAGMENT DESIGN

The lipid binding region of apoB (apoB37.3-70.8) spanning the β_1, α_2 and β_2 regions of the proposed pentapartite model was divided into eight sequential fragments: apoB37.3- 41.4 (B1), apoB41.4-45.6 (B2), apoB45.6-49.8 (B3), apoB18.8-54.0 (B4), apoB54.0-58.2 (B5), apoB58.2- 62.4 (B6), apoB62.4- 66.6 (B7) and apoB66.6-70.8 (B8). Each fragment was approximately 20 kDa. The work presented herein focuses on the characterization of the first three fragments (B1, B2 and B3).

2.2 CLONING OF 20 KDA APOLIPOPROTEIN B100 FRAGMENTS

cDNA fragments encoding amino acids, 1694-1880 (apoB37.3-41.4 or B1), 1881-2070 (apoB41.4-45.6 or B2) and 2071-2260 (apoB45.6-49.8 or B3) from apoB100 were amplified by the polymerase chain reaction (PCR) using full length human apoB100 cDNA as a template and the fragment specific primers listed in Table 1 (Integrated DNA Technologies, Coralville, IA). The PCR conditions were 30 cycles of denaturation at 95°C for 1 min, annealing at 55 °C for 1 min and extension at 72°C for 2 mins followed by a final extension at 72°C for 30 mins for apoB1 and 30 cycles of denaturation at 95°C for 1 min, annealing at 48 °C for 1 min and extension at 72°C for 2 mins followed by a final extension at 72°C for 30 mins for apoB2 and apoB3. PCR products were separated in 1% agarose gels and purified using a QIAEX II Agarose Gel Extraction Kit (Qiagen, Valencia, CA).

PCR products were cloned in the expression vector pET151/D/*lacZI-TOPO* using the Champion™ pET Directional TOPO© Expression Kit (Invitrogen, Carlsbad, CA) and used to transform TOP10 competent *Escherichia coli* (*E. coli*) cells (Invitrogen, Carlsbad, CA). Transformants were selected by ampicillin resistance. Plasmids were purified from *E. coli* using a QIAprep Mini-Prep Kit (Qiagen, Valencia, CA). Cloning was confirmed by digestion of plasmids with *SacI* and *XbaI* restriction enzymes purchased from New England Biolabs (Boston, MA). The orientation of inserted DNA was verified by PCR using T7 forward (T7f) and reverse (T7r) primers (Invitrogen, Carlsbad, CA) and the apoB fragment specific sense and anti-sense primers, followed by DNA sequencing in both the forward and reverse directions (Robarts London Regional Genomics Facility, London, ON).

Initial efforts at cloning apoB1 yielded a C-terminally extended protein (B1*) due to a primer error that went unnoticed. The cloning procedure for B1* was identical to that for the correct apoB1, B2 and B3 fragments described above. The erroneous B1* fragment specific primer is listed in Table 1.

Table 1 Primer sequences used in apoB studies

Primer name	Forward "sense" primer (5'→3')	Reverse "antisense" primer (5'→3')
B1	CACCGTCGACAGCAAAAACATTTTC	TTAGATGGTCATGGTAAACGGG
B1*	CACCGTCGACAGCAAAAACATTTTC	TTAATGGTCATGGTAAACGGG
B2	CACCGATGCACATACAAATGGCA	TTAAAATTGATCAATATTGATG
B3	CACCAACCTGAAGCACATCAAT	TTAATCAATAGCCTCAATGTGTTG
T7	TAATACGACTCACTATGGG	TAGTTATTGCTCAGCGGTGG

2.3 EXPRESSION OF 20 KDA APOLIPOPROTEIN B100 FRAGMENTS

Expression of apoB1, B2 and B3, as well as the apoB1* peptide, were carried out in *E. coli* BL21(DE3) expression strain. For test expression of each construct, a single colony was grown in 250 mL Luria-Bartani (LB) medium with ampicillin (100 μg/mL) to an optical density at 600 nm (OD_{600}) of 0.6. Fifty mL of this culture was then induced with isopropyl β-D-1-thiogalactopyranoside (IPTG) to a final concentration of 1 mM and grown at 37 °C for 4 h post induction. Cells were then pelleted from and re-solubilized in 2X sample buffer (125 mM Tris-HCl pH 8, 4% (w/v) SDS, 20% (v/v) glycerol, 0.02% (w/v) Bromophenol blue). Samples were heated at 100 °C for 5 min and then resolved by SDS-PAGE on a 10% acrylaminde gel (200 V for approximately 45 min). The gels were stained with Coomassie Brilliant Blue R-250, destained, and imaged using a light box.

For optimization prior to large-scale protein expression, the effect of varying IPTG concentration (10 μM, 25 μM, 50 μM, 100 μM, 200 μM, 350 μM, 500 μM, 650 μM, 800 μM) was tested on B1 protein expression (Figure 2.1). No significant difference was observed with variation of IPTG concentration and 1 mM was chosen going forward.

For large-scale expression of B1, B2 and B3, BL21(DE3) *E. coli* were transformed with the corresponding plasmid and grown overnight at 37 °C in a 10 mL falcon tube containing 5 mL of LB medium with ampicillin (100 μg/mL). This was used as a starter culture to inoculate 250 mL of LB medium with ampicillin (100 μg/mL) the following day. Expression was induced by addition of IPTG to a final concentration of 1 mM to the culture once it reached OD_{600} of 0.6. After induction, the cells were grown for 4 h at 37 °C and then harvested by centrifugation (4000 x *g* at 4 °C for 20 mins).

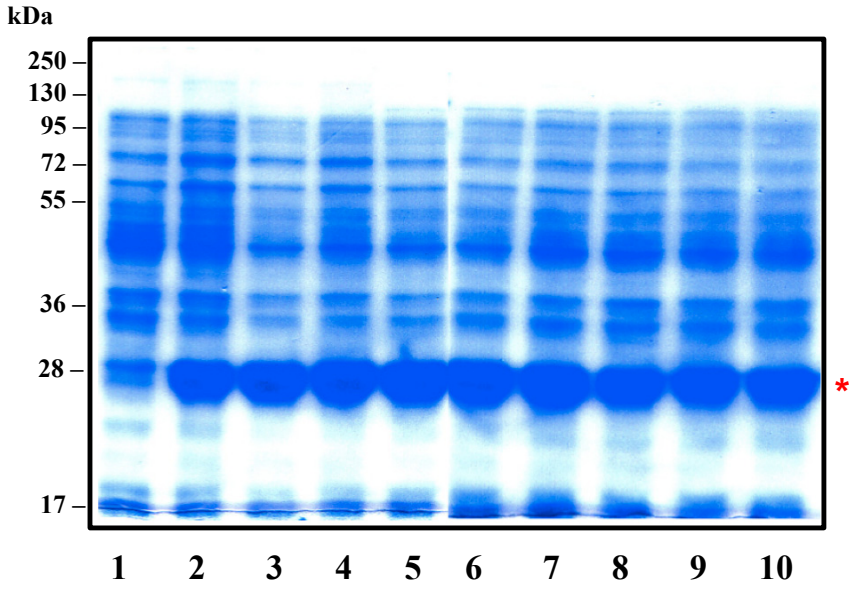

Figure 2.1 IPTG optimization of apoB1 expression. Coomassie blue R250 stained acrylamide gels showing IPTG optimization of apoB1 protein expression in BL21(DE3) *E.coli*. The asterisk indicates the position of the apoB1 bands. Lane 1- non-induced; Lane 2- 10 µM; Lane 3- 25 µM; Lane 4- 50 µM; Lane 5- 100 µM; Lane 6- 200 µM; Lane 7- 350 µM; Lane 8- 500 µM; Lane 9- 650 µM; Lane 10- 800 µM.

2.4 EXPRESSION OF UNIFORMLY LABELED APOLIPOPROTEIN B100 FRAGMENTS

For expression of uniformly ^{15}N- and ^{13}C-enriched apoB1, B2, B3 and B1*, BL21(DE3) *E. coli* were grown in LB medium with ampicillin (100 μg/mL) to OD_{600} of 0.6. Cells were harvested by centrifugation (2500 x *g* for 10 mins) and pelleted cells were re-suspended in an equivalent volume of M9 minimal medium (100 mM NaH_2PO_4, 40 mM K_2HPO_4, 4 mM $MgSO_4$, 1.8 μM $FeSO_4$, 2 g/L $^{13}C_6$ D-glucose, 1 g/L $^{15}NH_4Cl$ and 100 μg/mL ampicillin, titrated with NaOH to pH 7.3) (117). Cultures were grown for 4 h at 37 °C following induction and harvested by centrifugation (4000 x *g* at 4 °C for 20 min).

2.5 PURIFICATION OF APOLIPOPROTEIN B100 FRAGMENTS

ApoB1, B2, B3 and B1*, were purified from inclusion bodies in the presence of 6 M urea. The pellets were re-suspended in 25 mL of sonication buffer (2.6 mM H_2NaPO_4, 47.4 mM Na_2HPO_4, 150 mM NaCl, pH 8), lysed using sonication and then centrifuged at 13,000 x *g* in a benchtop microcentrifuge for 10 minutes at room temperature. The supernatant (supernatant 1) was discarded and the above process repeated once. Again the supernatant (supernatant 2) was discarded and the pellet (inclusion bodies) was re-suspended in 25 mL of binding buffer (2.6 mM H_2NaPO_4, 47.4 mM Na_2HPO_4, 150 mM NaCl, pH 8, 6 M urea) and allowed to solubilize at room temperature for 1 hour. After complete solubilization, 2.5 mL packed Ni-NTA agarose affinity resin (Qiagen, Valencia, CA), equilibrated with binding buffer, was added to the lysate and the suspension was mixed at room temperature for approximately 1.5 h. The suspension was then poured into

a chromatography column (BioRad, Hercules, CA) and the flowthrough (unbound) was collected. The column was then washed sequentially with 25 mL each of binding buffer, wash buffer (45 mM H_2NaPO_4, 5 mM Na_2HPO_4, 150 mM NaCl, pH 5.9, 6 M urea), elution buffer (50 mM H_3PO_4, 150 mM NaCl, pH 4.5, 6 M urea) and strip buffer (2.6 mM H_2NaPO_4, 47.4 mM Na_2HPO_4, 500 mM NaCl, 100 mM EDTA pH 8, 6 M urea). Each fraction was collected and an aliquot was removed and mixed with an equal volume of 2X SDS-PAGE sample buffer and stored for analysis.

Samples from each step of the purification were boiled for 5 min and then resolved by SDS-PAGE on a 10% acrylaminde gel (200 V for approximately 45 min). The gels were stained with Coomassie Brilliant Blue R-250, destained, and images were collected.

The elution buffer fraction, containing the purified protein, was then dialyzed against 5 mM acetic acid (overnight, two changes) using a Spectra/Por® CE dialysis membrane with a 10-12 kDa molecular mass cut off (Spectrum Laboratories Inc., Breda, Netherlands) to remove the urea.

2.6 TEV PROTEASE PRODUCTION AND PURIFICATION

The production and purification of TEV protease containing an N-terminal hexahistidine tag and C-terminal polyarginine tag [His_6-TEV(S219V)-Arg_5] were carried out in a cold room (4-8 °C). One hundred fifty mL of LB broth containing 100 µg/mL ampicillin and 30 µg/ml chloramphenicol was inoculated with a glycerol stock of bacteria containing the expression plasmid for production of the TEV protease [pRK793 transformed *E. coli* BL21(DE3) CodonPlus-RIL cells (ATCC, Manassas, VA)]. The culture was allowed to grow overnight at 250 rpm and 37°C. Twenty-five ml of the

saturated overnight culture was then added to 1 L of LB broth containing 100 μg/ml ampicillin, 30 μg/ml chloramphenicol and 0.2% glucose in a 2 L flask and shaken at 250 rpm and 37°C until the cells reached an OD_{600} of ~0.6. The temperature was reduced to 30°C and 1 mM IPTG was used to induce protein expression. The cells were grown for 4 h with shaking at 250 rpm and then harvested by centrifugation at 5,000 x *g* and 4 °C for 10 min. The cell pellet was stored at −80°C until purification.

Bacterial pellets were thawed on ice and re-suspended in ice-cold cell lysis buffer (50 mM NaH_2PO_4, 300 mM NaCl, 10 mM imidazole, pH to 8.0) at 10 mL/g cell paste. The cells were lysed by sonication (3 x 30 sec) with cooling intervals on ice to prevent excessive elevation in temperature. The lysate was then clarified by centrifugation at 4°C and 15,000 x *g* for 30 min. The supernatant was applied to a 10 ml Ni-NTA agarose resin (Qiagen, Valencia, CA) equilibrated in cell lysis buffer. The column was washed with approximately 5 column volumes wash buffer (50 mM NaH_2PO_4, 300 mM NaCl, 20 mM imidazole, pH to 8.0). The bound TEV protease was eluted using 15 mL of elution buffer (50 mM NaH_2PO_4, 300 mM NaCl, 250 mM imidazole, pH to 8.0). An aliquot of each fraction was mixed with an equal volume of 2X SDS-PAGE sample buffer, heated at 100 °C for 5 min and then resolved by SDS-PAGE on a 10% acrylaminde gel (200 V for approximately 45 min). The gels were stained with Coomassie Brilliant Blue R-250, destained, and images were collected. The buffer was exchanged and the elution fraction was concentrated in an AMICON filter at 4°C. The protease was stored in 10 mL of TEV storage buffer (50 mM Tris-HCl, 1 mM EDTA, 5 mM DTT, 50% glycerol, 0.1% Triton X-100) at −80°C until required.

2.7 TEV CLEAVAGE OF APOLIPOPROTEIN B100 FRAGMENTS B1, B2 AND B3

The dialyzed apoB protein samples were brought to 2 M urea in TEV cleavage buffer [50 mM Tris–HCl (pH 8.0), 0.5 mM EDTA, 1 mM DTT]. One milliliter of purified TEV protease was then added and cleavage was allowed to proceed overnight at 4 °C with rocking. After 24 hours, 1 mL packed Ni-NTA agarose affinity resin (Qiagen, Valencia, CA), equilibrated in binding buffer, was added to the samples. B1 digest sample was made up to 8 M urea after digestion (to maintain solubility) and all samples were allowed to rock at room temperature for approximately 1 h. Each sample was then poured into a chromatography column and the flow through collected. The column was washed with 5 mL each of binding buffer, wash buffer, elution buffer and strip buffer and each was fraction collected. An aliquot of each fraction was mixed with an equal volume of 2X SDS-PAGE sample buffer, heated at 100 °C for 5 min and then resolved by SDS-PAGE on a 10% acrylaminde gel (200 V for approximately 45 min). The gels were stained with Coomassie Brilliant Blue R-250, destained, and images were collected. The elution fraction, containing the cleaved protein, was then dialyzed against 5 mM acetic acid using a Spectra/Por® CE dialysis membrane with a 10-12 kDa molecular mass cut off (Spectrum Laboratories Inc., Breda, Netherlands) to remove the urea. The purified protein was lyophilized and stored at room temperature away from moisture.

2.8 PROTEIN IDENTIFICATION AND ESTIMATION OF LABELING EFFICIENCY BY MASS SPECTROMETRY

Lyophilized unlabeled and $^{13}C/^{15}N$ labeled apoB1 and apoB2 proteins, purified as described in section 2.5, were subjected to electrospray ionization-mass spectrometry (ESI-MS) and matrix assisted laser desorption ionization (MALDI) time of flight (TOF) mass spectrometry, respectively.

ESI-MS on the unlabeled proteins was carried out by Dr. Alejandro Cohen at the Dalhousie Proteomics Core Facility. Proteins were dissolved in 50% acetonitrile/ 50% H_2O with 0.1% formic acid and loaded on coated glass tip emitters (PicoTip Emitter, BG12-94-4-CE-20. New Objective, Woburn, MA, USA) for offline ESI-MS analysis. Data were acquired on a VelosPro Orbitrap (Thermo Scientific, Waltham, MA, USA) mass spectrometer. The raw spectra were collected and analyzed using Xcalibur (Thermo Scientific) and then deconvoluted to yield a single peak, corresponding to the mass of the intact protein, using Bayesian Protein Reconstruct algorithm in BioAnalyst software (AB Sciex, Framingham, MA, USA).

MALDI-TOF mass spectrometry on the $^{13}C/^{15}N$ labeled apoB1 and B2 proteins was carried out by Jack Moore at the Alberta Proteomics and Mass Spectrometry Facility (APS) on an Applied Biosystems Voyager Elite MALDI spectrometer (AB Sciex, Foster City, CA, USA).

2.9 NMR SPECTROSCOPY OF APOLIPOPROTEIN B100 FRAGMENTS B1 AND B2

Lyophilized apoB1 and B2 (9 mg/mL) were re-suspended in 90% deionized water,

10% D_2O containing 20 mM CD_3COO^-, 1 mM 2,2-dimethyl-2-sila-pentane-5-sulfonic acid (DSS) and 1 mM NaN_3 at pH 4. The protein suspension was vortexed for 1 min and protein aggregates were removed by centrifugation at 15, 000 x g for 5 min. The supernatants containing the soluble proteins were sent to the Québec/Eastern Canada High Field NMR Facility (QANUC), supported by the Canada Foundation for Innovation, the Groupe de Recherche Axé sur la Structure des Protéines (GRASP), McGill University Faculty of Science and Department of Chemistry and PROTEO, The Québec Network for Research on Protein Function, Structure, and Engineering, where NMR experiments were collected. The sample was transferred into a 5 mm high quality NMR tube (Bruker Biospin, Fällanden, Switzerland). The final concentration of ApoB1 was approximately 0.7 mM and ApoB2 was approximately 0.8 mM as measured by ultraviolet spectroscopy at 280 nm (estimated ε for B1 and B2 were 11520 M^{-1} cm^{-1} and 19060 M^{-1} cm^{-1}, respectively) in a 0.1 cm path length quartz cuvette (Hellma, Müllheim, Germany). Detailed acquisition parameters for the various NMR experiments are found in Table 2 for B2 and Table 3 for B1.

2.10 NMR SPECTROSCOPY OF APOB1*

Lyophilized B1* (9 mg/mL) was re-suspended in 90% deionized water, 10% D_2O containing 20 mM CD_3COO^-, 1 mM DSS and 1 mM NaN_3 at pH 4. The protein suspension was left to solubilize and any protein aggregates were removed by centrifugation at 15,000 x *g* for 5 min. NMR experiments were collected at the National Research Council Institute for Marine Biosciences (NRC-IMB). The sample was transferred into a 5 mm high quality NMR tube (Bruker Biospin, Fällanden, Switzerland).

The final concentration of B1* was approximately 0.8 mM, as measured by ultraviolet spectroscopy at 280 nm (estimated ε for was 12800 M^{-1} cm^{-1}) in a 0.1 cm path length quartz cuvette (Hellma, Müllheim, Germany). Detailed acquisition parameters for the various NMR experiments are found in Table 4. All experiments were collected at 30 °C.

2.11 ASSIGNMENT OF APOLIPOPROTEIN B100 FRAGMENT B2

All NMR data for B2 were processed using NMRpipe (118) and analyzed using CcpNmr Analysis 2.4 (119). ^{1}H frequencies were referenced to DSS at 0 ppm and ^{13}C and ^{15}N were referenced indirectly to the ^{1}H zero-point DSS frequency (120). ApoB2 backbone resonances were assigned using the following 3D NMR experiments: HNCO, HNcaCO, HNCA, HNcoCA, HNCACB and CCONH. In addition, HCCH-TOCSY, HCCH-COSY, ^{15}N-NOESY-HSQC (mixing time: 100 ms) and ^{15}N-TOCSY-HSQC were collected to help assign side chain chemical shifts.

2.12 ASSIGNMENT OF APOB1*

All NMR data were processed using NMRpipe (118) and analyzed using CcpNmr Analysis 2.4 (119). ^{1}H frequencies were referenced to DSS at 0 ppm and ^{13}C and ^{15}N were referenced indirectly to the ^{1}H zero-point DSS frequency (120). ApoB1 backbone resonances were assigned using the following 3D NMR experiments: HNCO, HNcaCO, HNCA, HNcoCA and HNCACB. In addition, HCCH-TOCSY, ^{15}N-NOESY-HSQC (mixing time: 80 ms), HNHA and HNHB spectra were collected to help assign side chain chemical shifts.

Table 2 Detailed experimental parameters used for data acquisition of TEV cleaved apoB2 solubilized in DPC micelles

Experiment	Recovery delay (s)	# of scans	# of complex points	Sweep width (Hz)	Center position (ppm)	^{1}H frequency (MHz)	Facility
^{1}H-^{15}N HSQC	1.2	4	^{1}H-1666 ^{15}N-200	^{1}H-13008.1 ^{15}N-3241.8	^{1}H-4.67 ^{15}N-119.9	800	QANUC
HNCO	1.15	8	^{1}H-1560 ^{15}N-56 ^{13}C-48	^{1}H-13008.1 ^{15}N-1783 ^{13}C-2010.9	^{1}H-4.67 ^{15}N-115.8 ^{13}C-176.5	800	QANUC
HNcaCO	1.2	32	^{1}H-1666 ^{15}N-56 ^{13}C-48	^{1}H-13008.1 ^{15}N-1783 ^{13}C-2010.9	^{1}H-4.67 ^{15}N-115.8 ^{13}C-58.5	800	QANUC
HNCA	1.2	16	^{1}H-1666 ^{15}N-56 ^{13}C-60	^{1}H-13008.1 ^{15}N-1783 ^{13}C-6032.8	^{1}H-4.67 ^{15}N-115.8 ^{13}C-55.9	800	QANUC
HNcoCA	1.15	16	^{1}H-1560 ^{15}N-56 ^{13}C-60	^{1}H-12019.2 ^{15}N-1783 ^{13}C-6032.8	^{1}H-4.67 ^{15}N-115.8 ^{13}C-55.8	800	QANUC
CCONH	1.0	32	^{1}H-880 ^{15}N-52 ^{13}C-108	^{1}H-8000 ^{15}N-1063.3 ^{13}C-10052.3	^{1}H-4.74 ^{15}N-117.6 ^{13}C-46.0	500	QANUC
HNCACB	1.15	16	^{1}H-1560 ^{15}N-56 ^{13}C-120	^{1}H-13008.1 ^{15}N-1539.7 ^{13}C-14077.1	^{1}H-4.73 ^{15}N-117.1 ^{13}C-45.9	800	QANUC
^{15}N-NOESY-HSQC	1.2	8	^{1}H-1666 ^{15}N-56 ^{1}H-240	^{1}H-13008.1 ^{15}N-1539.7 ^{1}H-9596.8	^{1}H-4.73 ^{15}N-117.1 ^{1}H-4.73	800	QANUC
^{15}N-TOCSY-HSQC	1.2	8	^{1}H-1024 ^{15}N-64 ^{1}H-200	^{1}H-8000 ^{15}N-1063.3 ^{1}H-5997	^{1}H-4.74 ^{15}N-117.6 ^{1}H-4.74	500	QANUC
^{13}C-HSQC	1.2	4	^{1}H-1666 ^{13}C-400	^{1}H-13008.1 ^{13}C-16087.1	^{1}H-4.73 ^{13}C-34.9	800	QANUC
HCCH-TOCSY	1.2	4	^{1}H-1666 ^{15}N-64 ^{1}H-200	^{1}H-13008.1 ^{13}C-6405.1 ^{1}H-7997.3	^{1}H-4.73 ^{15}N-36.2 ^{1}H-4.73	800	QANUC
HCCH-COSY	1.2	4	^{1}H-1666 ^{15}N-64 ^{1}H-200	^{1}H-13008.1 ^{13}C-6405.5 ^{1}H-7997.3	^{1}H-4.73 ^{15}N-36.2 ^{1}H-4.73	800	QANUC

Table 3 Detailed experimental parameters used for data acquisition of TEV cleaved apoB1 solubilized in DPC micelles

Experiment	Recovery delay (s)	# of scans	# of complex points	Sweep width (Hz)	Center position (ppm)	^{1}H frequency (MHz)	Facility
^{1}H-^{15}N HSQC	1.2	8	^{1}H-1666 ^{15}N-200	^{1}H-13008.1 ^{15}N-3241.8	^{1}H-4.73 ^{15}N-119.9	800	QANUC

Table 4 Detailed experimental parameters used for data acquisition of apoB1* solubilized in DPC micelles

Experiment	Recovery delay (s)	# of scans	# of complex points	Sweep width (Hz)	Center position (ppm)	^{1}H frequency (MHz)	Facility
^{1}H-^{15}N HSQC	1.2	4	^{1}H-1666 ^{15}N-128	^{1}H-13008.1 ^{15}N-2107.2	^{1}H-4.67 ^{15}N-116.8	800	QANUC
HNCO	1.0	8	^{1}H-1666 ^{15}N-56 ^{13}C-60	^{1}H-13008.1 ^{15}N-1783 ^{13}C-2010.9	^{1}H-4.67 ^{15}N-115.8 ^{13}C-176.5	800	QANUC
HNcaCO	1.0	32	^{1}H-1666 ^{15}N-64 ^{13}C-60	^{1}H-13008.1 ^{15}N-1783 ^{13}C-2010.9	^{1}H-4.67 ^{15}N-115.8 ^{13}C-58.5	800	QANUC
HNCA	1.0	8	^{1}H-1666 ^{15}N-60 ^{13}C-60	^{1}H-13008.1 ^{15}N-1783 ^{13}C-6032.8	^{1}H-4.67 ^{15}N-115.8 ^{13}C-55.9	800	QANUC
HNcoCA	1.1	16	^{1}H-1538 ^{15}N-60 ^{13}C-60	^{1}H-12019.2 ^{15}N-1783 ^{13}C-6032.8	^{1}H-4.67 ^{15}N-115.8 ^{13}C-55.8	800	QANUC
HNCACB	1.2	16	^{1}H-1666 ^{15}N-60 ^{13}C-128	^{1}H-13008.1 ^{15}N-2107.8 ^{13}C-14077.1	^{1}H-4.67 ^{15}N-119.8 ^{13}C-45.86	800	QANUC
^{15}N-NOESY-HSQC	1.2	16	^{1}H-2048 ^{15}N-56 ^{1}H-128	^{1}H-9803.9 ^{15}N-1561 ^{1}H-6301.2	^{1}H-4.72 ^{15}N-115 ^{1}H-4.72	700	NRC-IMB
HNHA	1.2	16	^{1}H-2048 ^{15}N-36 ^{1}H-106	^{1}H-9803.9 ^{15}N-1631.9 ^{1}H-6161.3	^{1}H-4.72 ^{15}N-115.5 ^{1}H-4.72	700	NRC-IMB
HNHB	1.2	16	^{1}H-2048 ^{15}N-36 ^{1}H-106	^{1}H-9803.9 ^{15}N-6161.3 ^{1}H-6161.3	^{1}H-4.72 ^{15}N-115.5 ^{1}H-4.72	700	NRC-IMB
HCCH-TOCSY	1.2	8	^{1}H-2048 ^{13}C-128 ^{1}H-104	^{1}H-9803.9 ^{13}C-13377.9 ^{1}H-6301.2	^{1}H-4.72 ^{13}C-31.7 ^{1}H-4.72	700	NRC-IMB

2.13 CD SPECTROSCOPY OF APOLIPOPROTEIN B100 FRAGMENTS

Far-UV CD spectra for apoB1, B2 and B3, as well as B1*, were recorded at 25 °C using a Jasco J-810 spectropolarimeter (Easton, MD, USA) at 20 nm/min with a data pitch of 0.1 nm from 260 nm to 190 nm. A cuvette of path length (*l*) 0.1 cm was used for all samples. The apoB1, B2 and B3 samples in the absence of micelles contained 14.8 μM, 3.10 μM and 20.0 μM of protein, respectively. The amount of apoB protein in the micellar B1 and B2 samples is listed in Table 5. The detergent concentrations (Table 5) were calculation using the following equation:

[Detergent] = {CMC+ ([protein]*aggregation number)}

to ensure at least a 1:1 protein to micelle ratio. ApoB1* CD spectra were collected in the presence and absence of DPC. Both samples contained 20 μM of C-terminally extended apoB1* protein.

All sample concentrations (c) were determined using the Beer−Lambert law ($c = A \cdot \varepsilon^{-1} \cdot l^{-1}$) by measuring absorbance (A) at 280 nm using a molar absorptivity (ε; calculated using www.innovagen.se). All data were collected in octuplicate, averaged, and blank subtracted. Data deconvolution was performed using CDSSTR with the set 4 and set 7 dataset as implemented in the DichroWeb server (121).

Table 5 Concentration of apoB1 and apoB2 in micellar CD samples

Micelles	ApoB1 Concentration (μM)	ApoB2 Concentration (μM)
n-dodecyl-ß-D-maltoside (DDM) [112.2 mM]	13.9	1.73
n-dodecylphosphocholine (DPC) [57.1 mM]	20.0	20.0
1,2-dihexanoyl-*sn*-glycero-3-phosphocholine (DHPC) [43.0 mM]	12.7	3.2
1,2-diheptanoyl-*sn*-glycero-3-phosphocholine (DHPC-7) [161.4 mM]	8.00	1.80
1-myristoyl-2-hydroxy-*sn*-glycero-3-phosphocholine (LMPC) [80.1 mM]	28.2	12.2
1-palmitoyl-2-hydroxy-*sn*-glycero-3-phosphocholine (LPPC) [157.1 mM]	12.1	12.5
1-palmitoyl-2-hydroxy-*sn*-glycero-3-phospho-(1'-*rac*-glycerol) (LPPG) [100.6 mM]	1.30	4.98

Chapter 3 CLONING, EXPRESSION AND PURIFICATION OF 20 KDA FRAGMENTS OF APOLIPOPROTEIN B100

3.1 20 KDA FRAGMENTS OF APOLIPOPROTEIN B100

Currently, there is no published atomic resolution experimental structural information for apoB100. In order to gain structural information on the lipid-binding regions of apoB100, we have designed eight 20 kDa fragments (B1-B8) spanning regions of apoB100 from approximately 37-70% (the β_1-β_2 regions of the proposed pentapartite model) of the full-length transcript (Figure 3.1). It has been shown that truncated apoB fragments as small as apoB32.5 can assemble with TG to some extent, while smaller fragments are unable to assemble with TG and form VLDL. The number of TG molecules increases as the length of apoB increases, from 25 in secreted apoB32 particles, to 191 in apoB41 particles (92). Furthermore, the apoB37-41 polypeptide was found to bind tightly to a triolein:water interface, suggesting a role for this region in irreversible TG binding (64). The region between apoB37 and apoB41 also appears to be required for TG recruitment and VLDL assembly (93).

ApoB fragments for the studies described herein were derived from the region of apoB100 known to be important in lipid binding. Fortunately, there are few glycosylation sites and no disulfide bonds in this region and thus it is amenable to expression in *E.* coli, which do not normally perform either of these functions (Figure 1.2, hashed lines). All eight of the fragments, as well as a 40 kDa B1B2 and 60 kDa B1B2B3 composite protein, have been amplified and expressed in *E.* coli. I have focused my analysis on the first three apoB fragments: B1, which corresponds to 37.3- 41.4% of full-length apoB, B2,

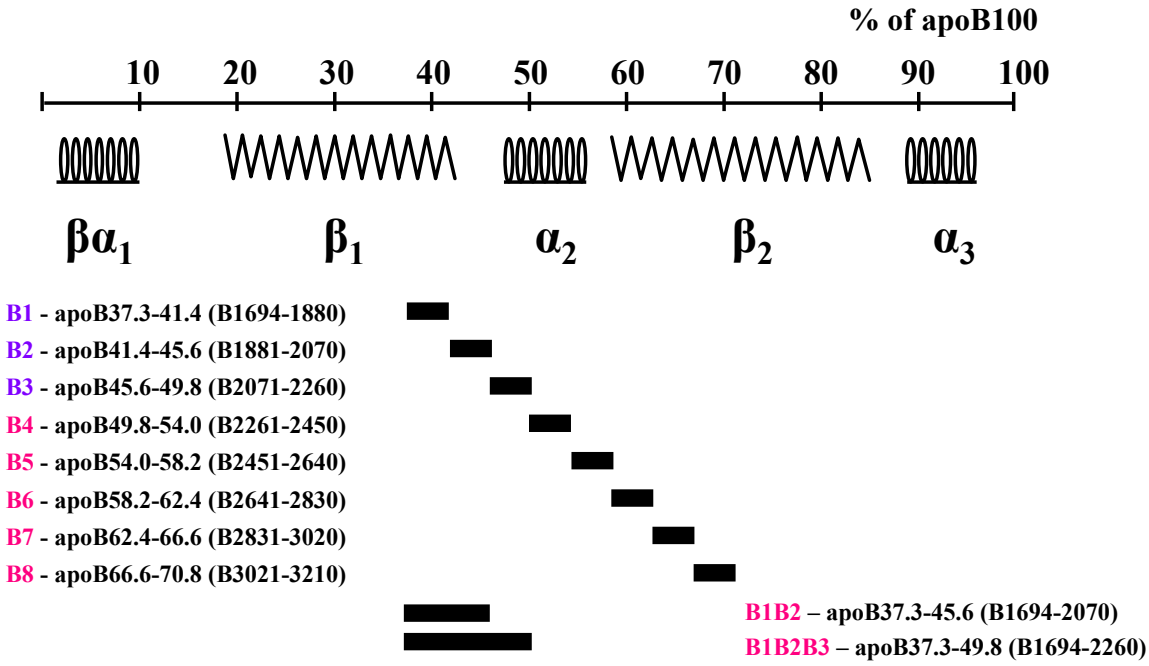

Figure 3.1 ApoB100 fragments. The location of the eight 20 kDa fragments (B1-B8) are shown. They span from approximately 37- 70 % of full-length apoB100, which encompasses the β_1, α_2 and β_2 domains of the proposed pentapartite model shown again here. The 40 kDa B1B2 and 60 kDa B1B2B3 fragments are also outlined.

which corresponds to 41.4-45.6% and B3, which corresponds to 45.6-49.8%.

In this chapter, I present the cloning, expression and purification of hexahistidine-tagged B1, B2 and B3 fusion proteins from *E.coli*, as well as their predicted physiochemical properties.

Also included are the cloning, expression and purification of a C-terminally extended apoB1 fragment, in which a primer error lead to the addition of 25 non-native amino acid residues at the C-terminus. I will refer to this B1 peptide as apoB1* (B1*) from here on in. In lieu of complete structural analysis, these apoB peptides may prove useful as templates for further apoB structural studies.

3.2 CLONING, EXPRESSION AND PURIFICATION OF APOLIPOPROTEIN B100 FRAGMENTS B1, B2 AND B3

In order to gain structural information on the unique lipid-binding regions of apoB100, fragments encompassing codons for apoB1694-1880 (B1), apoB1881-2070 (B2) and apoB2071-2260 (B3) were successfully subcloned from the human apoB100 cDNA. The insertion of B1, B2 and B3 into the pET151 vector using the TOPO© cloning reaction, which is used to directionally clone blunt-end PCR product into vector with high efficiency, was verified with *Xba*I and *Sac*I restriction enzymes. Successful insertions reveal a band of approximately 700 bp on an agarose gel (Figure 3.2). The orientation of the inserts was verified by PCR using the fragment specific sense and anti-sense primers and the T7 forward and reverse primers, which flank the insertion site

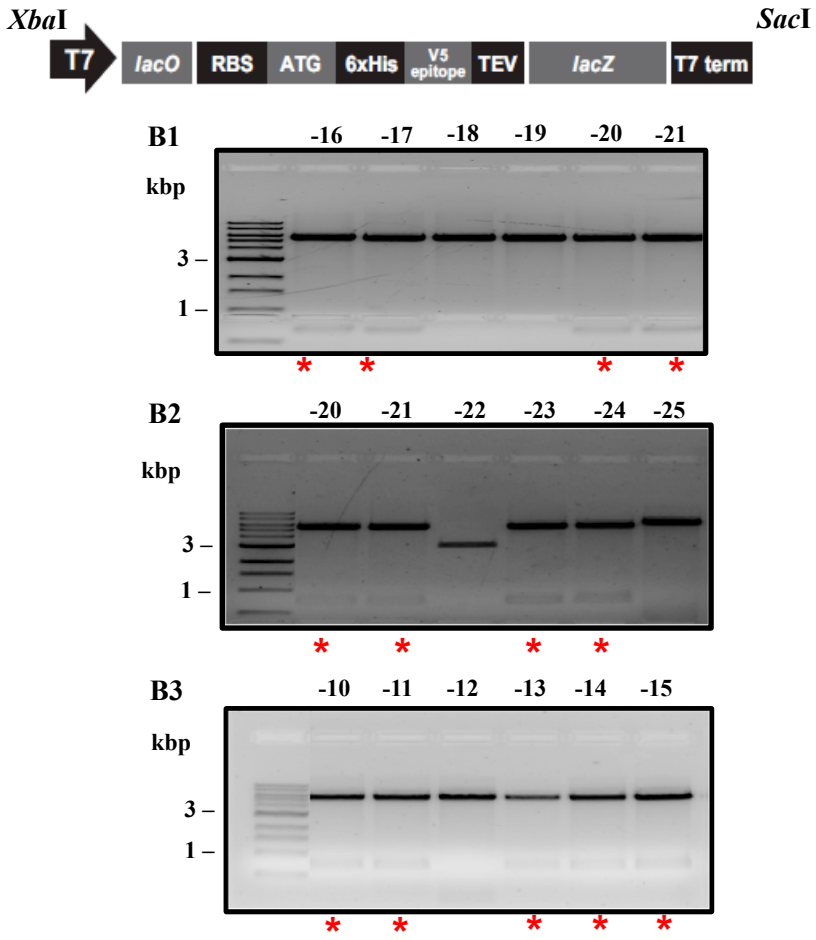

Figure 3.2 Restriction digest of apoB100 fragments B1, B2 and B3. The restriction enzymes *Xba*I and *Sac*I were used to confirm the insertion of the apoB100 fragments B1 (top), B2 (middle) and B3 (bottom) into the pET151 vector following TOPO© cloning. Successful insertions reveal a band around 700 basepairs (red asterisk) on an agarose gel.

upstream and downstream, respectively. The band generated by using the apoB fragment specific forward and reverse primer pair indicates that an insert is present. More importantly, however, use of the T7f and apoB reverse and T7r and apoB forward primer pairs indicates that the inserted fragment is in the correct orientation (Figure 3.3). If the insert were inverted, use of these primer pairs would not yield a band on the agarose gel. This was never observed for any of the apoB fragments. The validity of each apoB fragment was confirmed by complete sequence analysis of the insert.

The C-terminally extended apoB1* fragment, encompassing apoB1694-1880 plus 25 vector encoded amino acids at the C-terminus, was subcloned using the same protocol as described above. The restriction digest confirming the TOPO©-mediated insertion of apoB1* into the pET151 vector is shown in Figure 3.4, panel A. The orientation of the cDNA fragment in the expression vector was confirmed by PCR as described above (Figure 3.4, panel B) and the fragment appears to be in the correct orientation. The sequence of the inserts were verified by DNA sequencing, but it was later discovered that there was an error in the primer design and although the complete apoB1 sequence was present, there was a single amino acid error that caused a frameshift and stop codon read through. This caused the addition of 25 non-native amino acids at the C-terminus.

The pET plasmids containing the apoB fragments were used to transform BL21(DE3) *E.coli*, grown in LB broth and protein expression was induced with 1 mM IPTG (Figure 3.5). B1, B2 and B1* were produced at high levels as indicated by the intensity of the band at approximately 25 kDa on the acrylamide gel. The B3 protein was expressed to a much lesser extent.

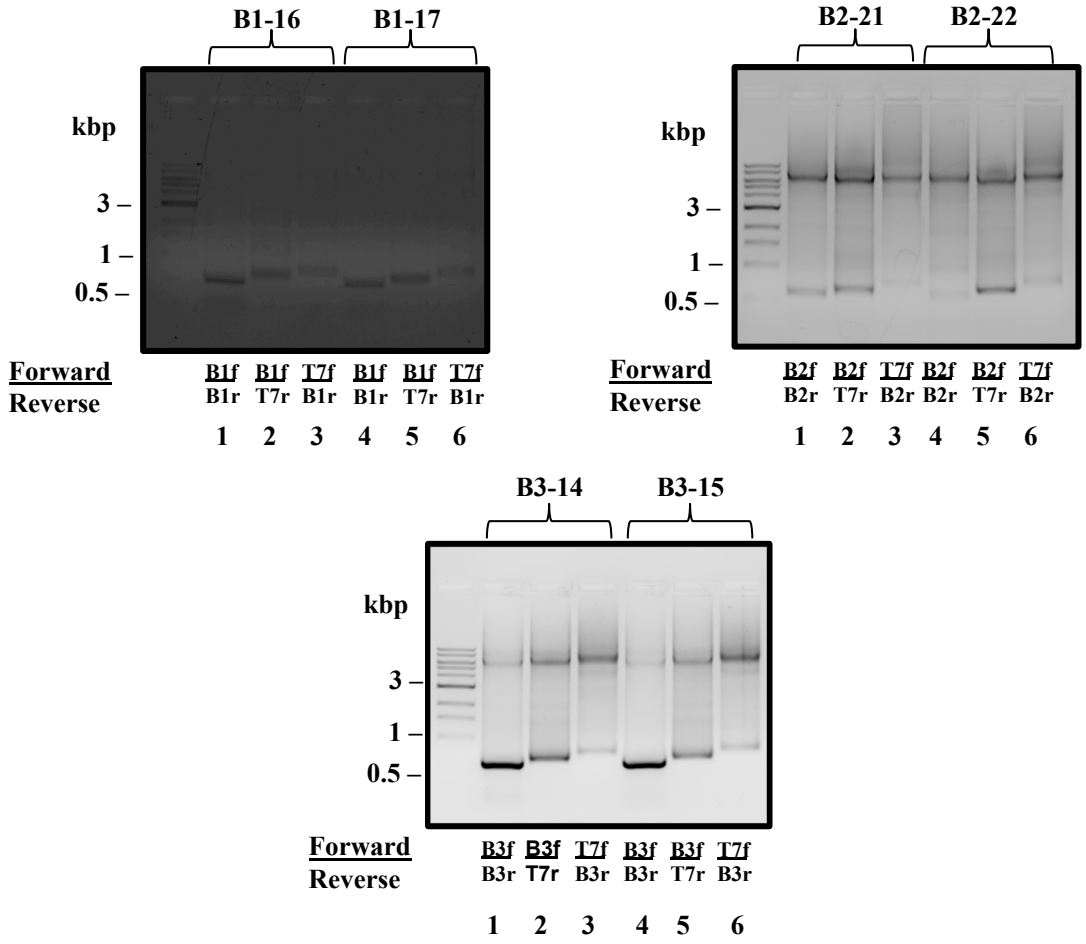

Figure 3.3 PCR orientation check of apoB100 fragments B1, B2 and B3. The orientation of each positive clone was analyzed by PCR using two of the following: T7 forward, T7 reverse, fragment specific forward or fragment specific reverse primers. The presence of an insert is confirmed by the band resulting from the use of the apoB sense and anti-sense fragment specific primers (lane 1 and 4). The correct orientation is exemplified by the bands resulting from the use of the T7r and apoB forward (lanes 2 and 5) and T7f and apoB reverse primer pairs (lanes 3 and 6).

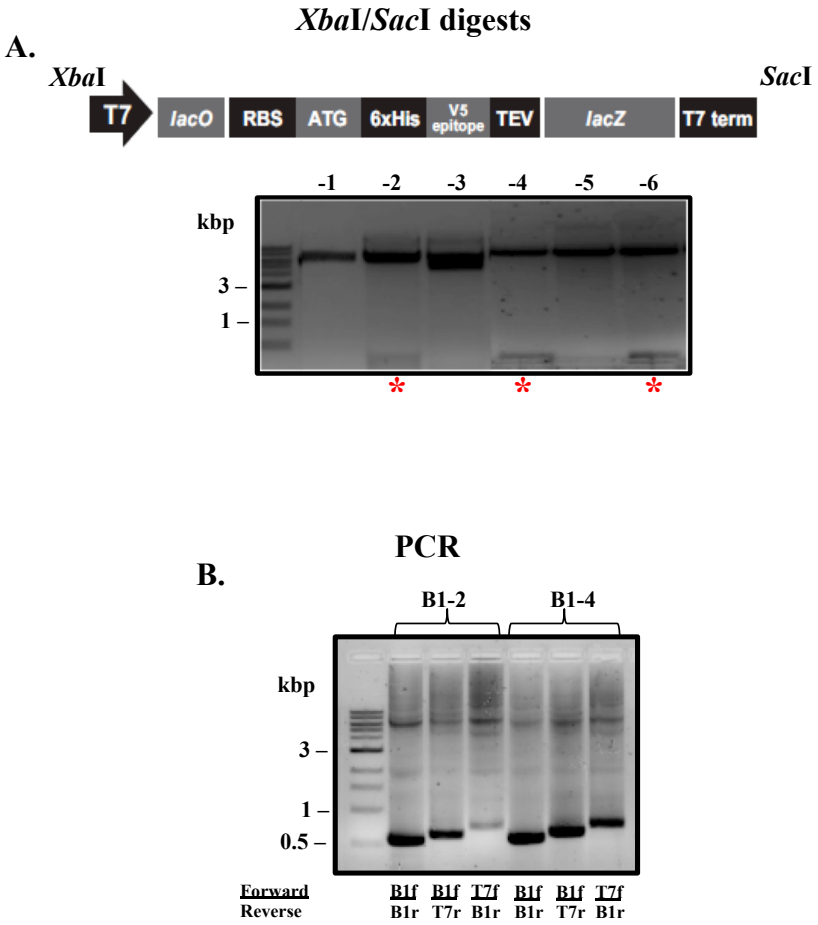

Figure 3.4 Cloning and orientation confirmation of apoB1*. (A) The restriction enzymes *Xba*I and *Sac*I were used to confirm the insertion of the apoB1* into the pET151 vector following TOPO© cloning. Successful insertions reveal a band around 700 basepairs (red asterisk) on an agarose gel. **(B)** PCR was done to verify the orientation of the positive clones using two of the following: T7 forward, T7 reverse, fragment specific forward or fragment specific reverse primers. The presence of a band using the fragment specific forward and reverse primers indicates the presence of an insert while use of the T7 forward and apoB reverse and T7 reverse and apoB forward primer pairs confirms that the insert is in the correct orientation.

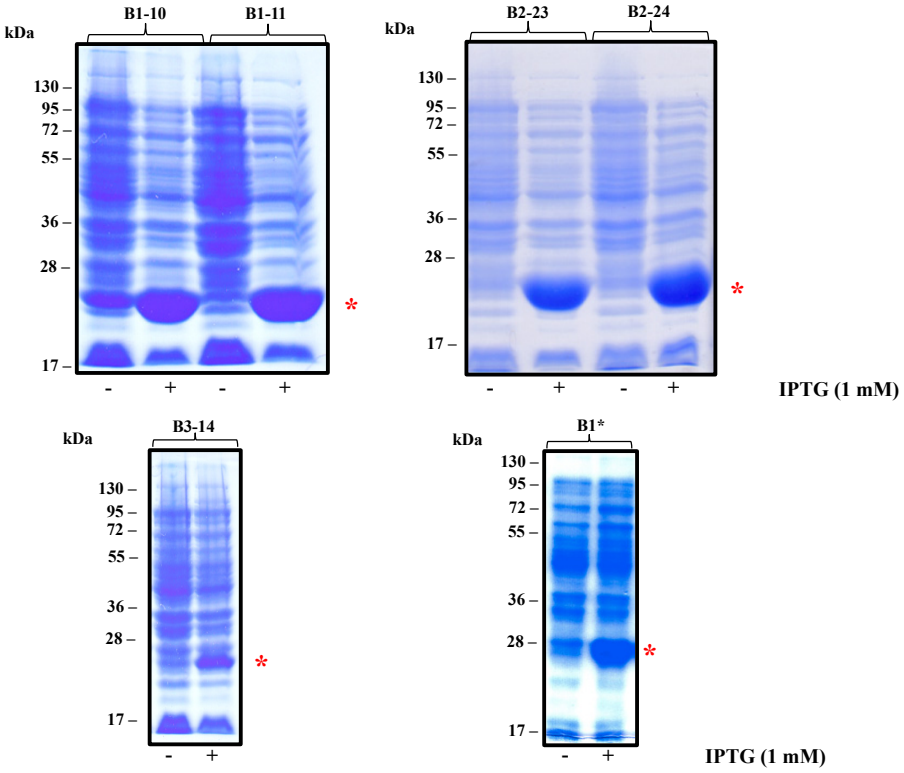

Figure 3.5 Test expression of apoB100 fragments. Coomassie blue R250 stained acrylamide gels showing test expression of apoB1, B2, B3 and apoB1* in BL21(DE3) *E.coli* following IPTG induction. The asterisks indicate the position of the apoB bands corresponding to B1 (top left), B2 (top right), B3 (bottom left) and apoB1* (bottom right).

Expression of the labeled apoB fragments was performed similarly, but after bacterial growth to OD_{600} of approximately 0.6 in complete LB medium, the bacteria were collected and transferred to $^{13}C/^{15}N$ supplemented M9 minimal medium prior to induction. The labeled apoB1, B2, B3 and B1* fragments were purified using a Ni-NTA affinity resin via the hexahistidine tag, encoded by the vector, which was present at the N-terminus. The majority of these proteins are found in inclusion bodies and therefore they were purified in the presence of 6 M urea, which was then removed by dialysis against acetic acid to pH 4. This single-step purification resulted in pure protein and no further purification was required for subsequent experiments (elution lane, Figure 3.6 and Figure 3.7). We were able to purify up to 50 mg/L of these fragments.

3.3 PROPERTIES OF APOLIPOPROTEIN B100 FRAGMENTS B1, B2 AND B3

Innovagen's peptide property calculator (http://www.innovagen.se/custom-peptide-synthesis/peptide-property-calculator/peptide-property-calculator.asp) was used to make calculations and estimations on physiochemical properties, such as water solubility, net charge at neutral pH (pH 7) and extinction coefficient (ε) of the apoB1, B2 and B3 peptides. Purified, unaltered, B1, B2 and B3 were 220, 233 and 223 amino acids in length, respectively. B1 has a net charge at pH 7 of about -1 and was predicted to have poor water solubility, while B2 and B3 had net charges at pH 7 significantly far away enough from zero (negative and positive, respectively) and were predicted to be water-soluble. The full spectrum of properties for apoB1, B2 and B3 are shown in Table 6, top, middle and bottom panels, respectively.

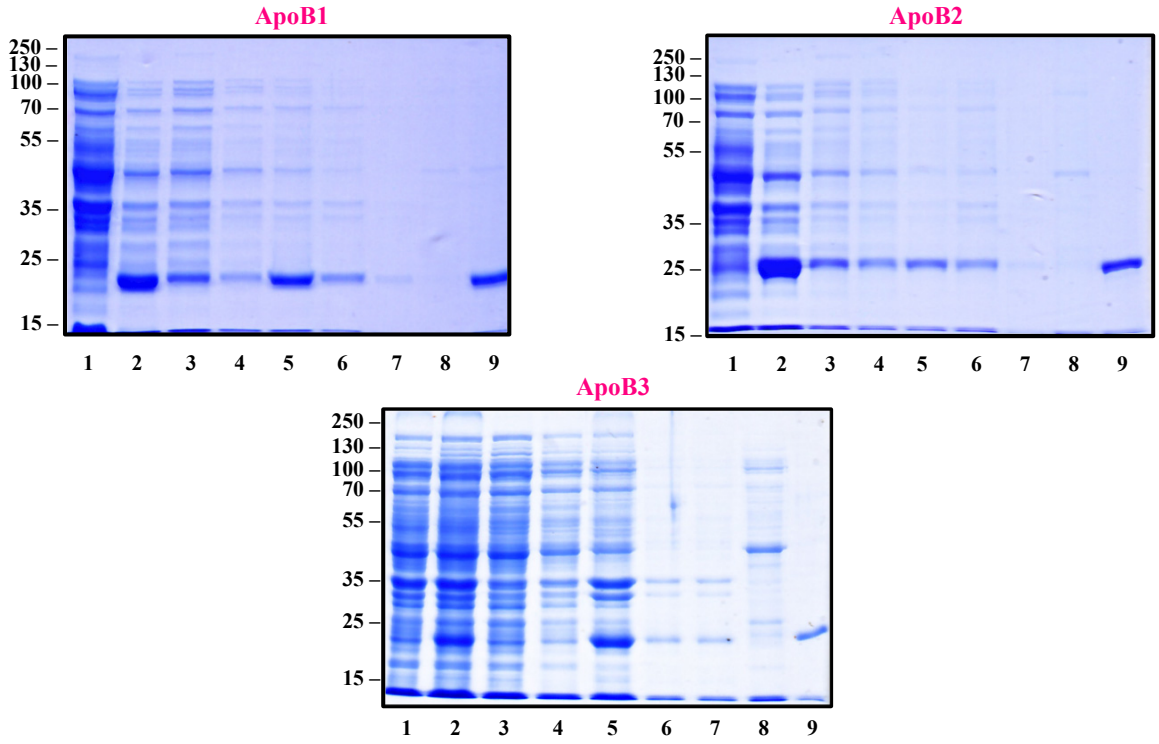

Figure 3.6 Purification of $^{13}C/^{15}N$ apoB100 fragments B1, B2 and B3. Aliquots of each fraction of the purification were resolved on 10% SDS-PAGE gels and revealed by Coomassie blue R250 staining for apoB1 (top left), B2 (top right) and B3 (bottom). Lane 1- non-induced; Lane 2- IPTG induced; Lane 3- sonication supernatant 1; Lane 4- sonication supernatant 2; Lane 5- inclusion bodies; Lane 6- Ni-NTA column flow-through; Lane 7- binding buffer wash (pH 8.0); Lane8- pH 5.9 buffer wash; Lane 9- pH 4.5 elution.

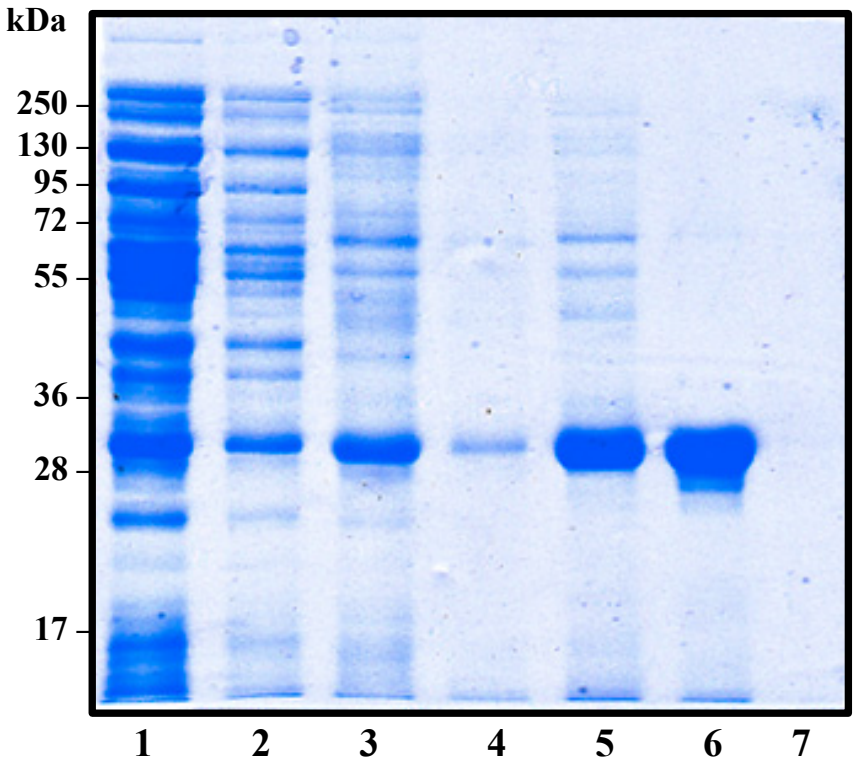

Figure 3.7 Purification of $^{13}C/^{15}N$ apoB1*. Aliquots of each fraction of the purification were resolved on 10% SDS-PAGE gels and revealed by Coomassie blue R250 staining for apoB1. Lane 1 & 2- inclusion bodies; Lane 3- Ni-NTA flow through; Lane 4- pH 8 buffer wash; Lane 5- pH 5.9 buffer wash; Lane 6- pH 4.3 elution buffer; Lane 7- pH 8 stripping buffer wash.

Table 6 Physiochemical properties of apoB100 fragments B1, B2 and B3

	ApoB1	**ApoB2**	**ApoB3**
Number of residues	220	233	223
Molecular weight (g/mol)	24506.73	26551.05	26336.08
Extinction coefficient ($M^{-1}cm^{-1}$)	12800	20340	22900
Iso-electric point	6.66	6.04	9.28
Net charge at pH 7	-1	-5.7	4.4
Estimated solubility	Poor water solubility	Good water solubility	Good water solubility

3.4 TEV PROTEASE PURIFICATION AND CLEAVAGE OF APOLIPOPROTEIN B FRAGMENTS

TEV protease refers to the 27 kDa catalytic domain of a cysteine protease encoded by the tobacco etch virus. The enzyme recognizes a seven amino acid consensus sequence, Glu-Asn-Leu-Tyr-Phe-Gln|Gly (ENLYFQ|G), with high specificity (122) and uses the catalytic triad Cys-Asp-His (C-D-H) to catalyze peptide hydrolysis (123). Commercially available wild-type TEV protease autocatalytically hydrolyses itself to yield a truncated enzyme with diminished activity (124). Several mutants have been constructed with the aim to reduce autocatalysis for use of the enzyme as a reagent for removal of purification and antibody tags from recombinant proteins. The most stable and widely used is the S219V TEV protease mutant, which is resistant to autolysis and more catalytically efficient than the wild-type protease (125).

The TEV protease used in the studies herein is the recombinant S219V mutant with an additional N-terminal maltose-binding protein (MBP) and hexahistidine tag and a C-terminal polyarginine tag (Figure 3.8, panel A). The MBP improves protein solubility during translation and the fusion protein will cleave off the MBP moiety *in vivo* to yield active TEV protease (126). It was produced in high yield from *E.coli* and purified in a single-step purification using a Ni-NTA affinity resin (Figure 3.8, panel B).

The expression of proteins in bacterial culture is often accomplished using an affinity tag to facilitate purification. However, the tag may interfere with structure determination and characterization and is often removed prior to these experiments. ApoB1, B2 and B3 contained an N-terminal hexahistidine tag that was successfully removed using the MBP-TEV protease fusion protein I expressed and purified

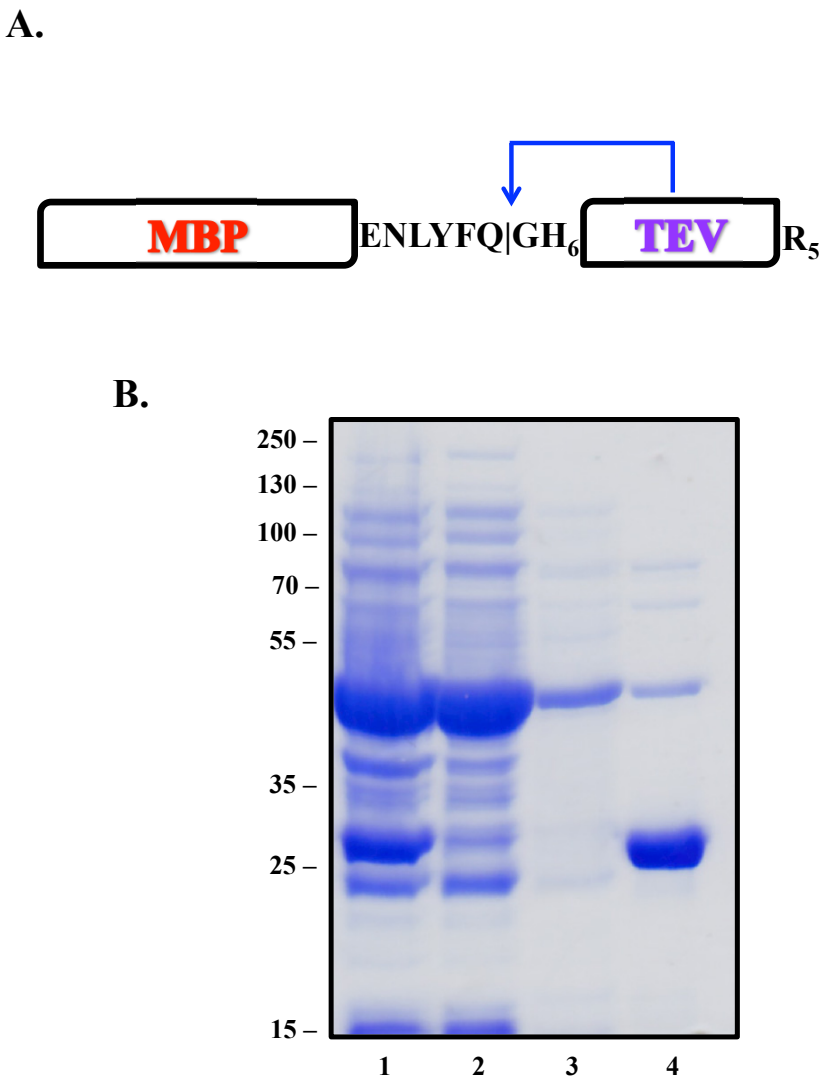

Figure 3.8 TEV protease purification. (A) Schematic of MBP-TEV fusion protein. The arrow indicates the site of autolysis *in* vivo. **(B)** Coomassie blue R250 stained acrylamide gel of each aliquot from the TEV purification. Lane 1- sonication supernatant; Lane 2- Ni-NTA column flow-through; Lane 3- pH 8.0 buffer wash; Lane 4- 250 mM imidazole elution (pH 8).

(Figure 3.9). The majority of apoB1 was cleaved after 24 hr incubation with TEV protease, but 100% hydrolysis was not observed. In contrast, apoB2 and B3 were approximately 100% cleaved after 24 hr incubation with TEV protease. The TEV protease hexahistidine tag also permitted removal of the enzyme from the apoB protein after digestion. Using a Ni-NTA affinity resin, either all (B1 and B3) or the majority (B2) of the protease was removed, leaving only the TEV-cleaved, pure apoB protein.

3.5 PROPERTIES OF TEV-CLEAVED APOLIPOPROTEIN B100 FRAGMENTS B1, B2 AND B3

Innovagen's peptide property calculator was again used to make calculations and estimations on physiochemical properties of the apoB peptides B1, B2 and B3 after TEV cleavage (Table 7) in order to assess any differences that may have resulted from removal of the 27 N-terminal residues. The TEV-cleaved B1, B2 and B3 peptides were 193, 206 and 196 amino acids in length, respectively. Cleavage of the peptides did not appear to significantly affect their predicted physiochemical properties. Both before and after cleavage B1 had a net charge at neutral pH close to 0 and was predicted to have poor water solubility, while B2 and B3 had net charges significantly far away enough from zero (negative and positive, respectively) and they were deemed to be water-soluble.

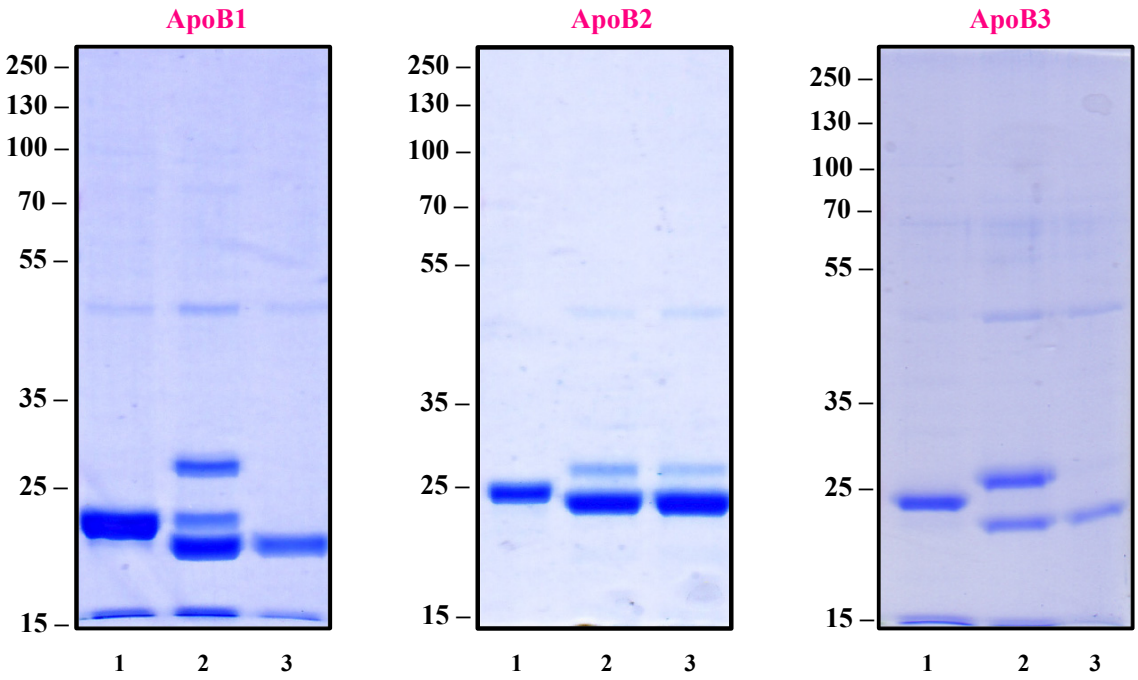

Figure 3.9 TEV cleavage of $^{13}C/^{15}N$ labeled apoB1, B2 and B3. Coomassie blue R250 stained acrylamide gel of TEV cleavage of the apoB100 fragments. The band at approximately 27 kDa is that of TEV protease. The apoB fragments are located at approximately 25 kDa and slightly below that after cleavage. Lane 1: uncleaved apoB; Lane 2: 24 hr post TEV cleavage; Lane 3: Ni-NTA flowthrough containing cleaved apoB

Table 7 Physiochemical properties of TEV cleaved apoB1, B2 and B3

	ApoB1	ApoB2	ApoB3
Number of residues	193	206	196
Molecular weight (g/mol)	21354.17	23398.5	23153.5
Extinction coefficient ($M^{-1}cm^{-1}$)	11520	19060	21620
Iso-electric point	6.62	5.57	9.13
Net charge at pH 7	-0.5	-5.3	2.8
Estimated solubility	Poor water solubility	Good water solubility	Good water solubility

3.6 PROTEIN VERIFICATION AND LABELING EFFICIENCY ESTIMATION BY MASS SPECTROMETRY

Matrix assisted laser desorption ionization (MALDI) time of flight (TOF) and electrospray ionization (ESI) mass spectrometry are often used for protein identification and estimation of isotope incorporation. The identity and estimated molecular masses of the unlabeled apoB1 and B2 fragments were confirmed by ESI-MS. ESI spectra were collected on the VelosPRO Orbitrap (Thermo Scientific, Waltham, MA, USA) system and analyzed with a Bayesian Protein Reconstruct algorithm in the BioAnalyst software to deconvolute the raw spectra (Figure 3.10), yielding a single protein mass. The expected molecular masses for unlabeled TEV cleaved B1 and B2 are 21354.17 Da and 23398.5 Da, respectively. Figure 3.11 top panel, and Figure 3.12, top panel, show the molecular mass determined by ESI analysis for B1 and B2, to be 21354.8 Da and 23415.0 Da, respectively. There is no ambiguity in the B1 data, given that the experimental and estimated masses are almost identical, differing by less than 1 Da. However, the experimental mass for B2 is approximately 17 Da larger than the estimated mass. This discrepancy can likely be attributed to oxidation, which would increase the mass by 16 Da. Oxidation is a common modification seen in mass spectrometry and probably occurred at the one methionine residue present in the B2 sequence. Furthermore, there is a small peak at 23396 Da, representing the non-oxidized B2.

Labeled B1 and B2 spectra were collected on the Applied Biosciences Sciex Voyager Elite MALDI-TOF instrument (AB Sciex, Foster City, CA, USA) at the Alberta Proteomics and Mass Spectroscopy Facility (APM) (University of Alberta, Canada). The

efficiency of incorporation of ^{15}N and ^{13}C stable isotopes were estimated by MALDI-TOF analysis using the equation:

{[(MW observed labeled) – (MW observed unlabeled)] / [(MW expected 100% labeled) – (MW expected unlabeled)]} * 100

The expected molecular masses given 100% isotope enrichment are 22545.23 Da and 24725.57 Da for B1 and B2, respectively. Figure 3.11, bottom panel, and Figure 3.12, bottom panel, show the masses observed by MALDI-TOF to be 22356 Da and 24478 Da for labeled B1 and B2, respectively. Therefore, this is indicative of approximately 84% isotope incorporation for B1 and approximately 80% isotope incorporation for B2. The MALDI spectrum corresponding to labeled B1 has a more abundant peak than that corresponding to labeled B1 at 23427 Da. It is possible that this peak could correspond to labeled B1 that was not cleaved by TEV protease. The expected mass for this fragment is 25517.15 Da. However, according to SDS-PAGE, the Ni-NTA column was able to remove any uncleaved B1 that remained following TEV cleavage (Figure 3.11, insert). In both spectra there are peaks approximately half the mass of the protein peaks, which can likely be attributed to the $[M + 2H]^{2+}$ doubly charged ions. Furthermore, the width of these peaks are about half the width of the $[M + H]^{+}$ singly charged ions, which also supports these peaks belonging the $[M + 2H]^{2+}$ doubly charged ions. Another possibility is that the unexplainable peaks in both the B1 and B2 MALDI spectra are those of contaminants.

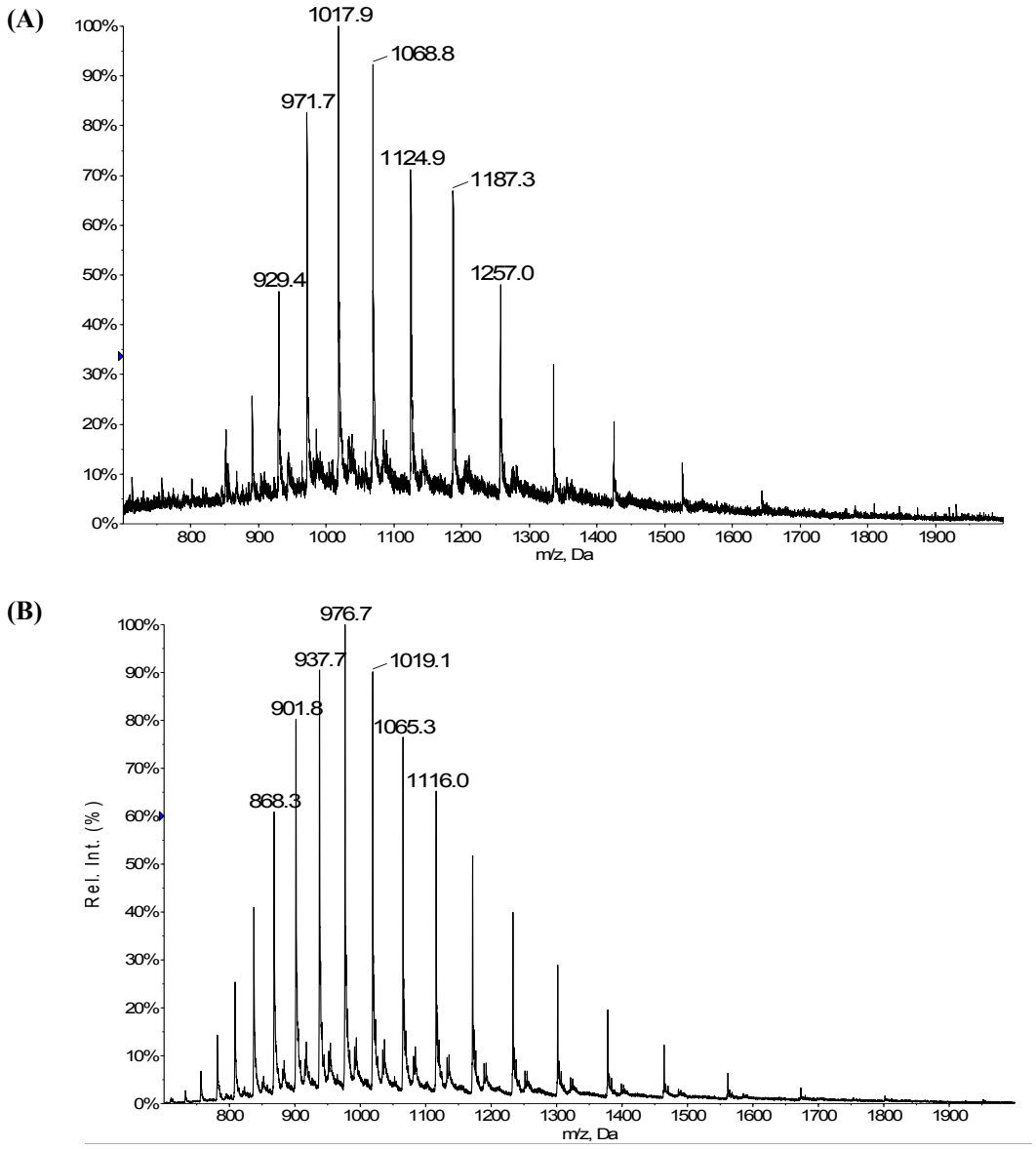

Figure 3.10 ESI mass spectra. Raw ESI spectra of **(A)** apoB1 and **(B)** apoB2 expressed in unlabeled LB medium.

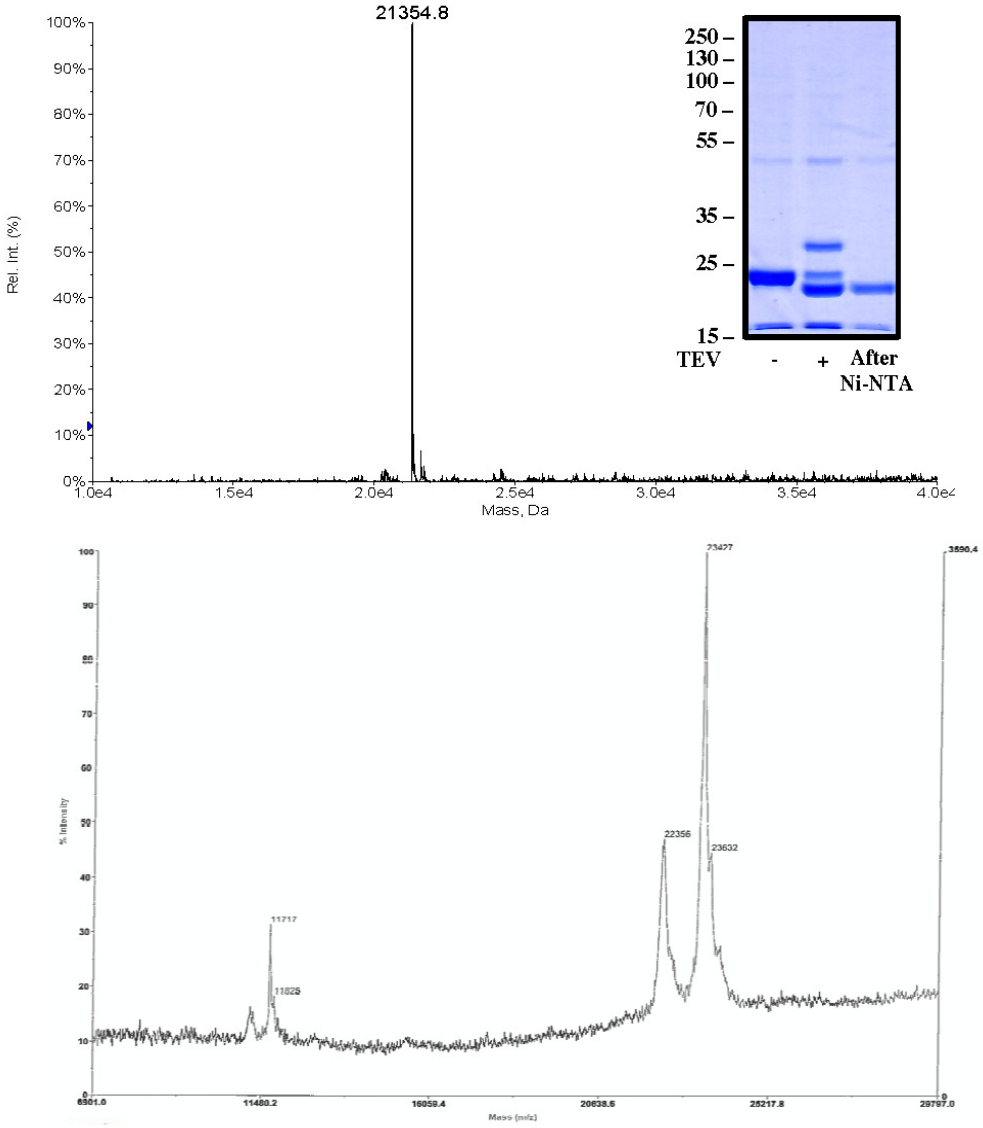

Figure 3.11 Mass Spectra of apoB1 expressed in unlabeled LB medium (expected mass: 21354.17 Da) **(top)** and $^{15}N/^{13}C$ isotope- enriched M9 minimal medium (expected mass with 100% isotope enrichment: 22545.23 Da) **(bottom)**. **Insert-** TEV cleavage of $^{13}C/^{15}N$ labeled apoB1.

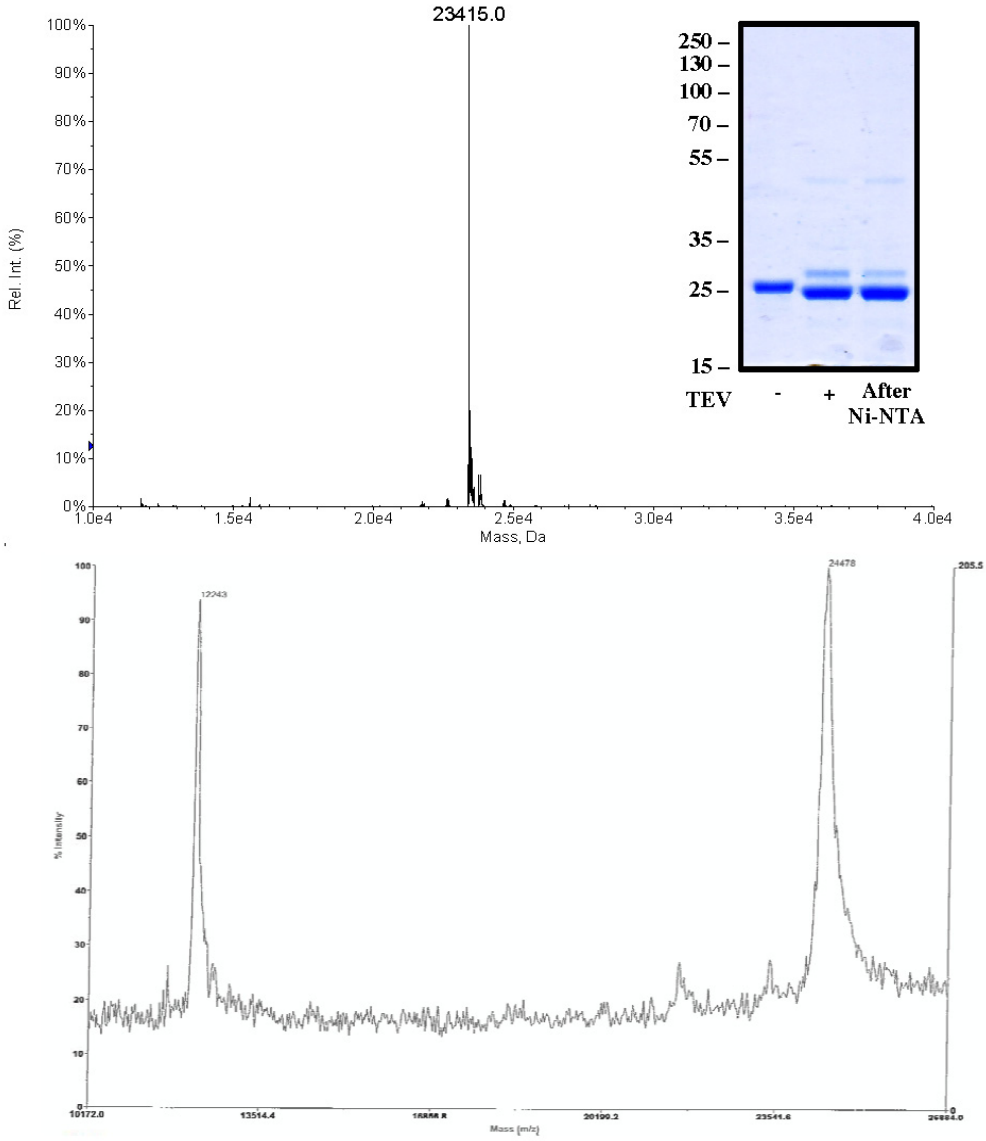

Figure 3.12 Mass Spectra of apoB2 expressed in unlabeled LB medium (expected mass: 23398.5 Da) **(top)** and $^{15}N/^{13}C$ isotope- enriched M9 minimal medium (expected mass with 100% isotope enrichment: 24725.57 Da) **(bottom)**. **Insert-** TEV cleavage of $^{13}C/^{15}N$ labeled apoB2.

Chapter 4 CD SPECTROSCOPY OF APOLIPOPROTEIN B IN MICELLES

4.1 COMMON PHOSPHOLIPID MEMBRANE MIMETICS USED IN PROTEIN STRUCTURAL STUDIES

Biological membranes are a heterogeneous mixture of several noncovalently associated lipid species as building blocks. These building blocks include variations in fatty acyl chains and covalently linked glycans, adding a further layer of complexity. The proteins embedded or tethered to the membrane vary according to the type of membrane and its functions. Accordingly, the secondary structural features of a protein may be highly dependent on its location with respect to the membrane (127).

In light of the complexity of biomembranes, membrane-associated proteins are often studied in a membrane mimetic environment. Membrane mimetic systems have emerged as a common means of studying membrane-associated proteins, and include: micelles, bicelles, liposomes and organic solvents. These model systems are less complex than biological membranes, containing far fewer constituents, but have been demonstrated to be applicable for the study of membrane-associated proteins (128-132).

Structural studies using CD or NMR spectroscopy are often performed in the presence of a membrane mimetic. This is desirable to mimic the native environment of the protein as to maintain structural and functional integrity. Additionally, the protein-micelle complex will tumble fast enough to allow for high-resolution NMR spectra to be obtained (133). In my CD and NMR experiments, I worked with micelles, the structures of their detergent monomers are depicted in Figure 4.1 and their physical properties are presented in Table 8.

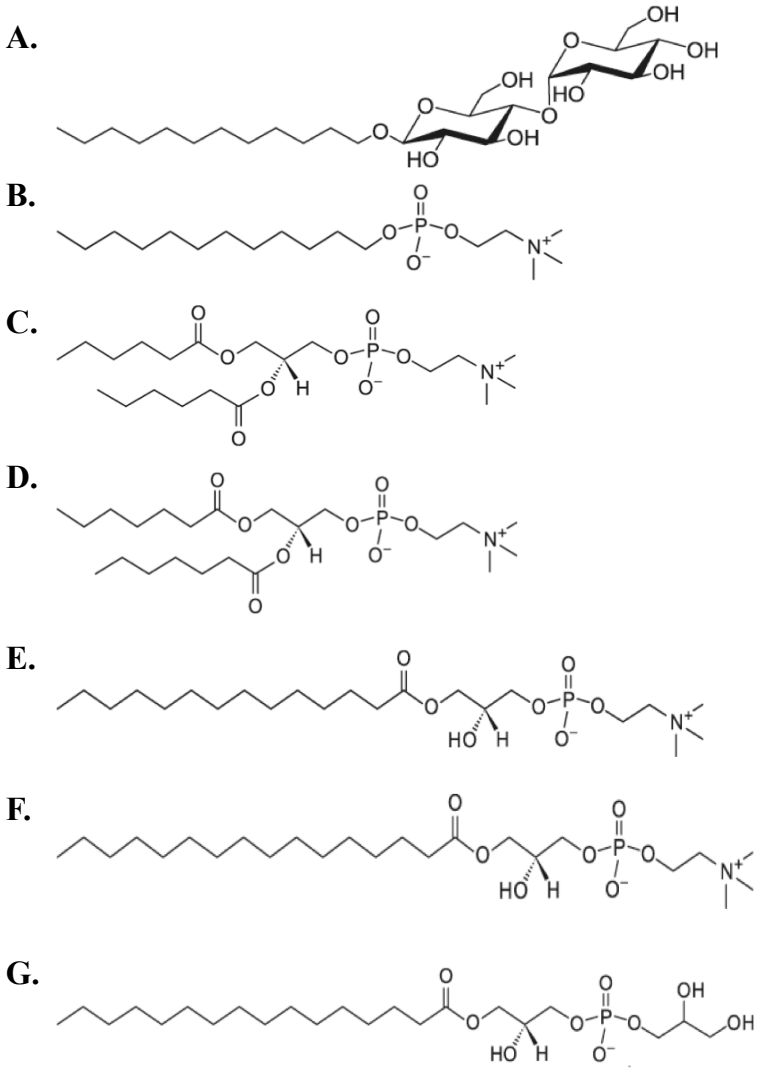

Figure 4.1 The structures of the bilayer mimetics used in apoB CD studies. (A) n-dodecyl-ß-D-maltoside, **(B)** n-dodecylphosphocholine, **(C)** 1,2-dihexanoyl-*sn*-glycero-3-phosphocholine, **(D)** 1,2-diheptanoyl-*sn*-glycero-3-phosphocholine, **(E)** 1-myristoyl-2-hydroxy-*sn*-glycero-3-phosphocholine, **(F)** 1-palmitoyl-2-hydroxy-*sn*-glycero-3-phosphocholine, (**G)** 1-palmitoyl-2-hydroxy-*sn*-glycero-3-phospho-(1'-*rac*-glycerol)

Table 8 Properties of bilayer mimetics used in apoB studies

Bilayer mimetic	Detergent family	CMC (mM)[a]	Chain length	Aggregation number	Micelle MW (kDa)
n-dodecyl-ß-D-maltoside (DDM)	Nonionic	0.2	12	140[c]	72[c]
n-dodecylphosphocholine (DPC)	Monoalkylphosp-hotidylcholine	1.1	12	70[c]	25[c]
1,2-dihexanoyl-*sn*-glycero-3-phosphocholine (DHPC)	Short chain phospholipid	15	6	35[c]	16[c]
1,2-diheptanoyl-*sn*-glycero-3-phosphocholine (DHPC-7)	Short chain phospholipid	1.4	7	25[c]	12[c]
1-myristoyl-2-hydroxy-*sn*-glycero-3-phosphocholine (LMPC)	Lysophosphatid-ylcholine	0.043-0.090	14	122[d]	57[d]
1-palmitoyl-2-hydroxy-*sn*-glycero-3-phosphocholine (LPPC)	Lysophosphatid-ylcholine	0.004-0.0083	16	139[b]	69[*]
1-palmitoyl-2-hydroxy-*sn*-glycero-3-phospho-(1'-*rac*-glycerol) (LPPG)	Lysophosphatid-ylglycerol	0.6	16	160[c]	81[c]

[a]CMC values are Avanti Polar Lipids measurements

[b] Hayashi H, Yamanaka T, Miyajima M and Imae T. Aggregation Numbers and Shapes of Lysophosphatidylcholine and Lysophosphatidylethanolamine Micelles. Chem Lett. 1994. 2407– 2410

[c]Warschawski DE, Arnold AA, Beaugrand M, Gravel A, Chartrand É, and Marcotte I. Choosing Membrane Mimetics for NMR Structural Studies of Transmembrane Proteins. Biochim Biophys Acta. 2011. 1808: 1957-1974.

[d] Sherratt AR, Braganza MV, Nguyen E, Ducat T and Goto NK. Insights into the effect of detergents on the full-length rhomboid protease from Pseudomonas aeruginosa and its cytosolic domain. Biochim Biophys Acta Biomembranes. 2009. 1788: 2444-2453

[*]estimated based on aggregation number and monomer molecular weight

4.2 MICELLE FORMATION

Micelles are (small) well-defined assemblies of detergent molecules. Detergent molecules are amphipathic and will self-assemble into micellar structures at concentrations above their critical micelle concentration (CMC). The CMC is a characteristic property of a detergent and is affected by the length of its alkyl chain. Generally, increasing the alkyl chain by two methylenes results in an approximate 10-fold decrease in the CMC (128, 131, 132). Another characteristic of the detergent is the aggregation number, which is defined as the number of detergent molecules in a micelle. This number can range from as little as three molecules to hundreds (129, 134).

The detergent headgroup has been shown to affect its interaction with proteins (128). Solution NMR studies are frequently done in the presence of detergents with small or charged headgroups, such as DHPC, DPC or the lysophospholipids. However, the optimal choice for a detergent depends on the protein being studied. It should be strong enough to prevent protein aggregation, but mild enough to avoid denaturation (128, 131).

I have employed seven micelle-forming bilayer mimetics in my studies: n-dodecyl-ß-D-maltoside (DDM), n-dodecylphosphocholine (DPC), 1,2-dihexanoyl-*sn*-glycero-3-phosphocholine (DHPC), 1,2-diheptanoyl-*sn*-glycero-3-phosphocholine (DHPC-7), 1-palmitoyl-2-hydroxy-*sn*-glycero-3-phospho-(1'-*rac*-glycerol) (LPPG), 1-palmitoyl-2-hydroxy-*sn*-glycero-3-phosphocholine (LPPC) and 1-myristoyl-2-hydroxy-*sn*-glycero-3-phosphocholine (LMPC). DDM is considered one of the least denaturing detergents. However, it is not often used in structural studies because of the large size of its micelles (128). DPC is one of the most common detergents used in solution NMR experiments due to its low aggregation number that makes it possible to collect high-resolution

spectra. Its structure, although synthetic, is made to resemble that of a phosphatidylcholine. DHPC is a short chain phospholipid with a zwitterionic headgroup and a branched alkyl tail. DHPC-7 is similar in structure to DHPC but has an additional methylene group in its alkyl tail. The lysophospholipids have proven to be some of the best detergents (130). Lysophospholipid implies that one of their hydrophobic tails has been lysed. LPPG, LPPC and LMPC are single-tailed phospholipids with 18 or 16 carbons and either a phosphoglycerol or phosphocholine headgroup, respectively.

Unlike the bilayer of biological membranes, micelles contain a detergent monolayer. This may prove beneficial in studying apoB because lipoproteins are spherical particles that also contain a monolayer. A general rule of thumb in structural studies involving detergent solubilized proteins is that the detergent must be used at a concentration above its CMC to effectively solubilize the protein and ensure at least a 1:1 protein to micelle ratio. I have used CD spectroscopy to probe the interactions of the apoB fragments B1 and B2 with DDM, DPC, DHPC, DHPC-7, LMPC, LPPC and LPPG micelles.

4.3 THE STRUCTURE OF APOLIPOPROTEIN B100 FRAGMENTS IS SIMILAR IN ALL PHOSPHOLIPID MEMBRANE MIMETIC ENVIRONMENTS

Far UV CD spectra (260-190 nm) of B1, B2 and B3 were recorded at 25°C in the presence of DPC micelles as well as in the absence of any membrane mimetic. B1 was relatively insoluble in the absence of amphipathic phospholipid or detergent, whereas B2 and B3 were soluble in their presence or absence. The CD spectra for B1, B2 and B3 in

the absence of any membrane mimetic lack any major contributions from α- or β-structures and are characteristic of disordered proteins (Figure 4.2).

B1 and B2 were also solubilized in DDM, DHPC, DHPC-7, LMPC, LPPC and LPPG. The CD spectra for B1 and B2 solubilized in DDM, DHPC and DHPC micelles are characteristic of disordered proteins. In contrast, in the presence of DPC, LMPC, LPPC and LPPG micelles, B1 and B2 appeared to have significant α-helical character as exemplified by the two negative bands around 222 nm and 208 nm (Figure 4.3).

The secondary structure prediction of B1, B2 and B3 in the presence and absence of DPC micelles was assessed using DichroWeb (104). In the absence of DPC, B1 was 48% α-helical, 33% β-strand and turn and 19% random structure. Upon addition of DPC, B1 was predominantly α-helical (85%), with 8.0% and 7.0% β-strand/turn and random structure, respectively (Figure 4.4, left). This was surprising for B1 because it is located completely within the β_1 region of the proposed pentapartite model. B2, which straddles the end of the β_1 region and the beginning of the α_2 region of the proposed pentapartite model, was predicted to be 70% α-helical, 15% β- strand and turn and 15% random structure in the absence of DPC. In the presence of DPC, the predictions were fairly similar with the α-content increasing slightly to 73% and the β-strand and turn and random structure decreasing to 13% and 14%, respectively (Figure 4.4, middle). Again, this was surprising because having approximately equal amounts located in proposed α and β regions, one would not have expected to see so much α-character.

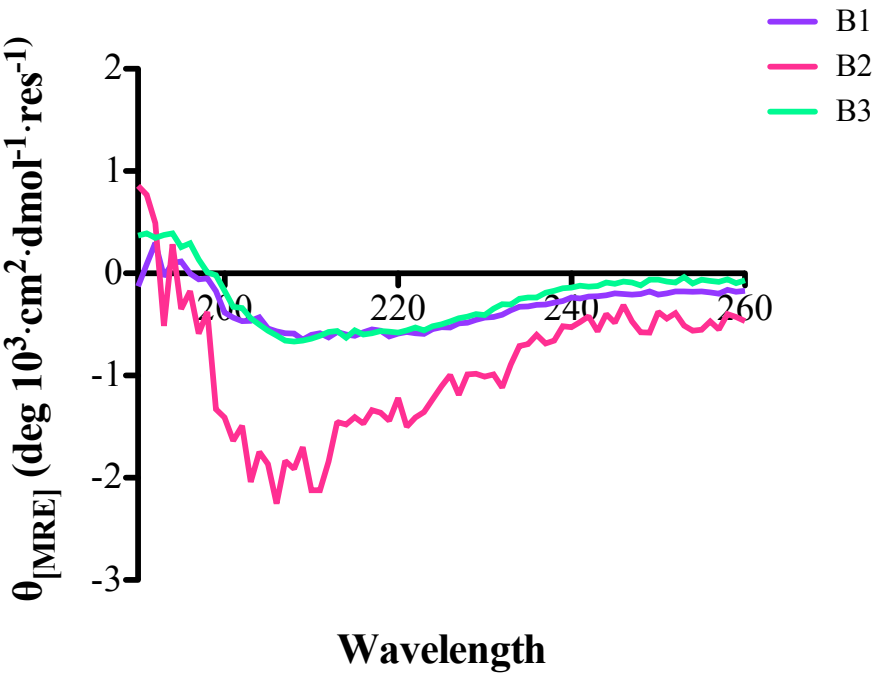

Figure 4.2 CD spectra of apoB1, B2 and B3 in the absence of bilayer mimetics. Far-UV spectra for apoB1, B2 and B3 dissolved in H_2O, in the absence of any amphipathic molecules.

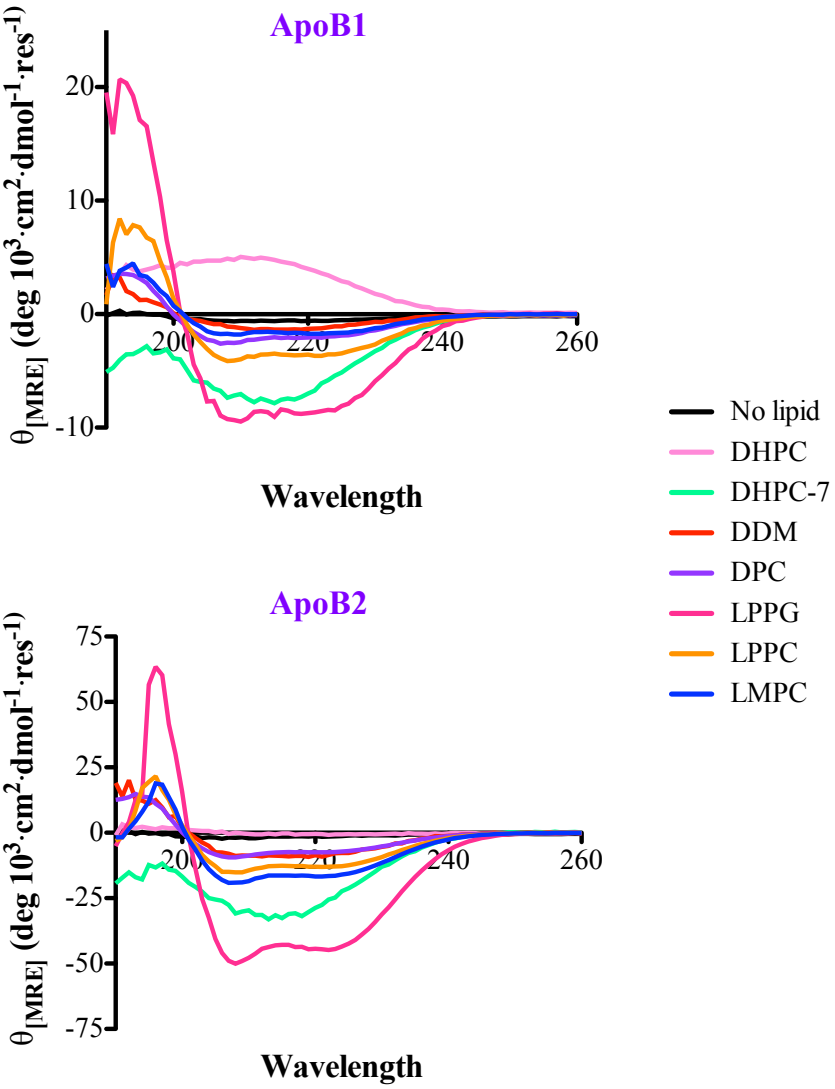

Figure 4.3 CD spectra of apoB1 and B2 in the presence and absence of bilayer mimetics. Far- UV spectra for apoB1 and B2 in the absence and presence of the indicated micellar or solvent environment.

In the absence of DPC, B3 was predicted to be majority random structure (44%), with 21% α-helical and 33% β-strand and turn. Upon addition of DPC, B3 was predicted to be predominantly α-helical (88%), with 7% and 5% β-strand and turn and random structure, respectively (Figure 4.4, right). B3 is contained completely within a proposed α-helical region of the pentapartite model (α_2), so the large amount of helical content was not particularly surprising.

Far UV CD spectra (260-190 nm) of apoB1* were recorded at 25°C in the presence and absence of DPC micelles. Similar to the TEV cleaved B1 fragment, the apoB1* peptide was relatively insoluble in the absence of DPC. The CD spectrum for apoB1* in the absence of any membrane mimetic appears unstructured, or even to contain β-strand/turn character, with the single trough at approximately 218 nm (Figure 4.5, top). However, upon the addition of DPC micelles, apoB1* appeared to adopt significant α-helical character as exemplified by the two characteristic negative peaks around 222 nm and 208 nm (Figure 4.5, top).

The secondary structure propensity of apoB1* in the presence and absence of DPC micelles was assessed using DichroWeb (104). In the absence of DPC, apoB1* was deconvoluted to be 13% α-helical, 55% β-strand and turn and 32% random structure. Upon addition of DPC, the apoB1* fragment was predicted to have approximately the same amount of α-helical (36%) and β-strand/turn (37%) character and 28% random structure (Figure 4.5, bottom). Although the spectra for the TEV-cleaved B1 described above and the uncleaved, C-terminally extended apoB1* described here appear to be visually similar, the DichroWeb deconvolutions in the presence of DPC suggested

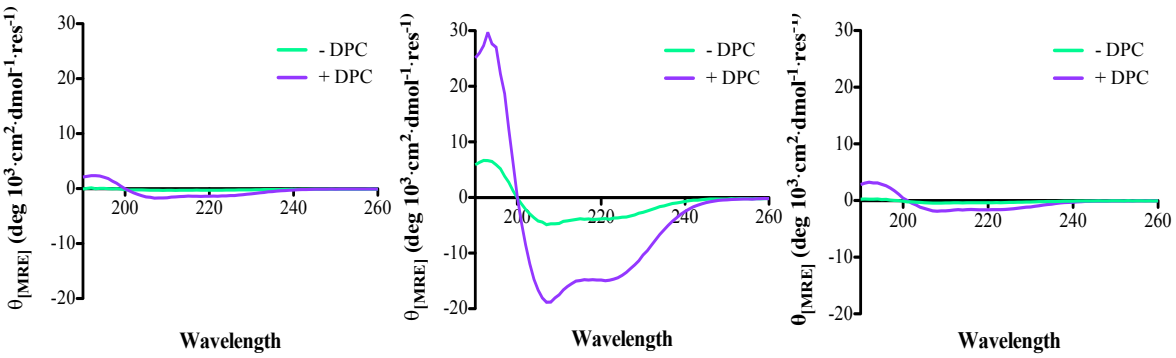

	- DPC	+ DPC
α-helix	48%	85%
β-strand & turn	33%	8%
Unordered	19%	7%

	- DPC	+ DPC
α-helix	70%	73%
β-strand & turn	15%	13%
Unordered	15%	14%

	- DPC	+ DPC
α-helix	21%	88%
β-strand & turn	35%	7%
Unordered	44%	5%

Figure 4.4 CD spectra and DichroWeb analysis in the presence and absence of DPC. Far- UV CD spectra of apoB1, B2 and B3 in the presence and absence of DPC micelles. DichroWeb Deconvolution analysis of apoB1, B2 and B3 using CDSSTR algorithm and reference dataset 4 is presented below each spectrum.

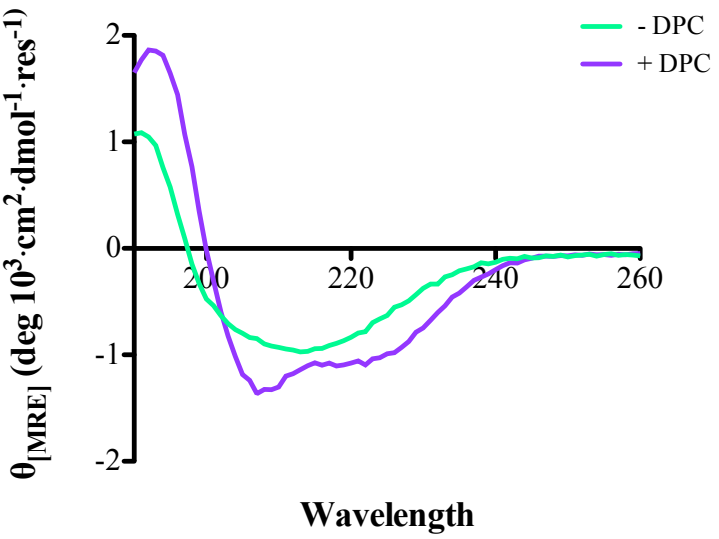

	- DPC	+ DPC
α-helix	13%	36%
β-strand & turn	55%	37%
Unordered	32%	28%

Figure 4.5 CD spectra and DichroWeb analysis of apoB1* in the presence and absence of DPC. Far- UV CD spectra of the un-cleaved apoB1* peptide in the presence and absence of DPC micelles. DichroWeb Deconvolution analysis using the CDSSTR algorithm and reference dataset 4 is presented below the spectrum.

otherwise. While DPC- solubilized, TEV cleaved apoB1 was predicted to be mainly α-helical, the apoB1* peptide was predicted to have equal α- and β- character.

Changes in the structural conformation of DPC-solubilized apoB2 in response to changes in temperature were investigated using CD spectroscopy in order to understand the stability and thermal changes of micelle-associated B2. Temperatures from 25 °C to 75 °C, increasing in increments of 5 °C, and after cooling back to 25 °C were examined. Before heating the apoB2 spectrum was predicted to be 39% α-helical, 34% β-strand and turn and 27% random structure (Figure 4.6). As the temperature increased, there was a decrease in ellipticity at 208 nm and 222 nm, but the essential α-helical features of the spectra were retained (i.e. two negative troughs at approximately 208 nm and 222 nm) (Figure 4.7). The behaviour of apoB2 as a function of temperature, monitored at 208 nm and 222 nm, showed a linear relationship between decreases in ellipticity and increases in temperature (Figure 4.8). After cooling back to 25 °C, the B2 spectrum resembled that at 25 °C prior to heating and was predicted to be 41% α-helical, 35% β-strand and turn and 24% random structure (Figure 4.6). This suggests that the effect of heating was reversible and the structural characteristics of B2 are retained upon heating and cooling.

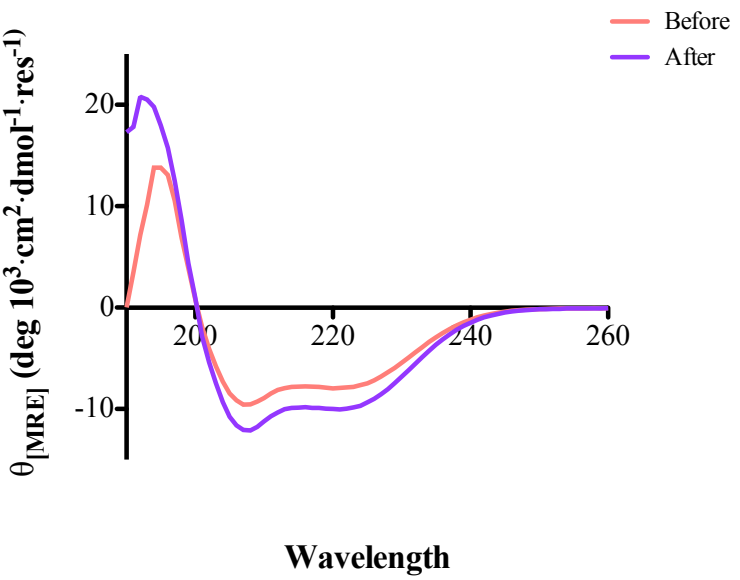

	Before	After
α-helix	39%	41%
β-strand & turn	34%	35%
Unordered	27%	24%

Figure 4.6 CD spectra and DichroWeb analysis of the effects of heating on DPC-solubilized apoB2. Far- UV CD spectra of apoB2 in the presence of DPC micelles at 25 °C prior to and after heating to 75 °C. DichroWeb Deconvolution analysis using the CDSSTR algorithm and reference dataset 4 is presented below the spectrum.

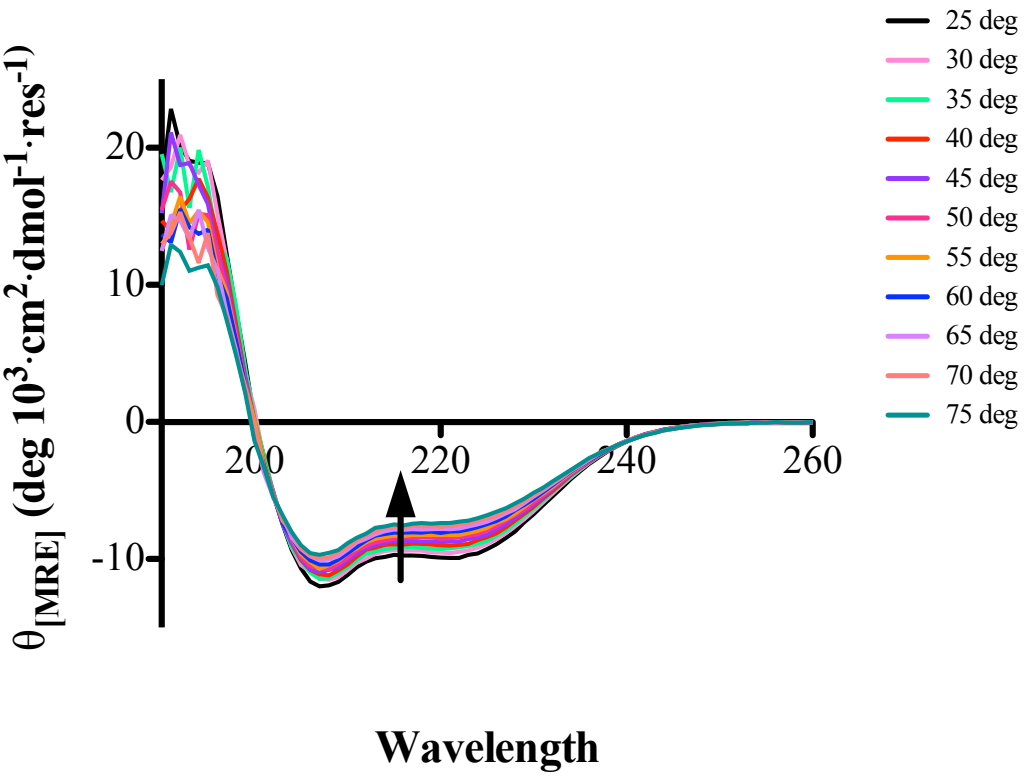

Figure 4.7 The effect of temperature on DPC-solubilized apoB2. Far- UV CD spectra of apoB2 in the presence and absence of DPC micelles from 25 °C to 75 °C, in increments of 5 °C. The arrow indicates the general trend seen in the curves as the temperature is increased.

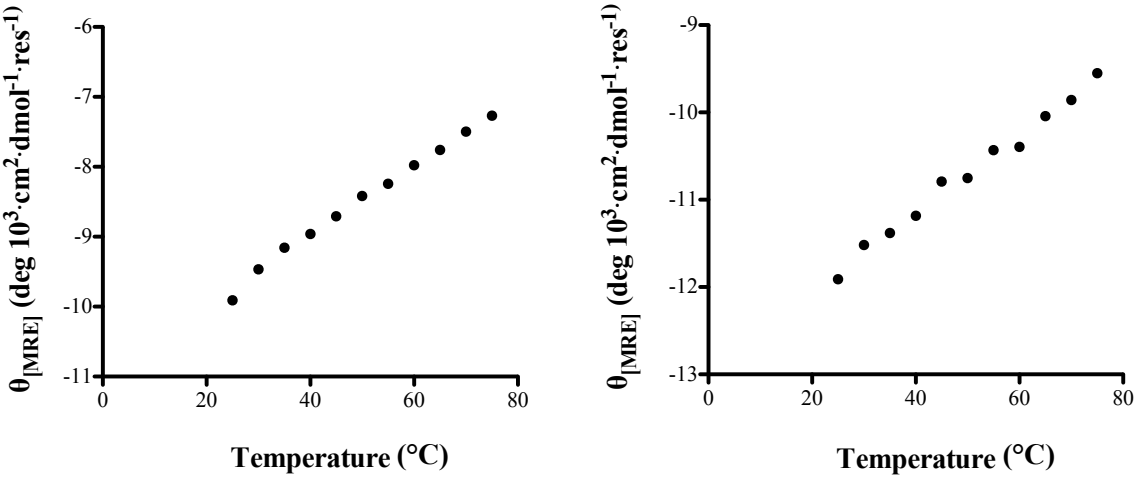

Figure 4.8 The behaviour of DPC-solubilized apoB2 as a function of temperature monitored at 222 nm and 208 nm. DPC-solubilized apoB2 displays a linear relationship between decreased negative ellipticity and increased temperature at 222 nm and 208 nm.

Chapter 5 THE STRUCTURE OF APOLIPOPROTEIN B IN SOLUTION

5.1 THE POTENTIAL FOR APOLIPOPROTEIN B100 STRUCTURE

Currently, no high-resolution structural information of any domain of apoB, nor the intact protein, is available from experimental studies. The imposing size, insolubility and hydrophobicity of apoB100 remain significant barriers to elucidation of atomic resolution structural information. However, improvements in instrumentation, such as the development of higher field spectrometers, advancements in experiments and software available to analyze the data generated, and sample preparation, such as new techniques for macromolecule expression and purification, are allowing researchers to overcome some of the barriers involved in obtaining high quality NMR spectra in a cost-effective way and assigning them with ease.

NMR spectroscopy is a common method for obtaining structural information on proteins. Unfortunately, even with improvements (i.e. in spectrometer hardware) over the years it is still not possible to study intact apoB100. However, NMR is an ideal way to study the structure of small, 20-25 kDa polypeptides derived from apoB100. The secondary structure of these polypeptides can be inferred from chemical shifts of the individual nuclei since chemical shift depends largely on secondary structure (135). Furthermore, these data can then be used in combination with NOESY experiments, which provide through-space structural information on a per-residue basis (136).

High-resolution structure(s) of apoB100 could be of clinical significance given the importance of apoB in lipoprotein metabolism and association with coronary heart disease. Structural knowledge of the apoB100 polypeptide could help us understand the

important sequence elements in the lipidation of apoB and its degradation and thus allow for modulation of VLDL assembly and secretion and also LDL levels as a result. In this chapter, I present NMR data on apoB2 and the C-terminally extended apoB1* at a temperature of 30 °C.

5.2 NMR SPECTROSCOPY OF APOB2 IN DPC MICELLES

ApoB2 was prepared with approximately 0.7 mM polypeptide in 90% deionized water, 10% D_2O containing 20 mM CD_3COO^-, 1 mM NaN_3 and 1 mM DSS as an internal standard. The solution was subjected to NMR analysis at QANUC on either their 800 MHz or 500 MHz spectrometer (Varian, Palo Alto, CA) equipped with a cryogenically cooled probe. All experiments were carried out at 30 °C. The ^{1}H-^{15}N HSQC spectrum of B2 solubilized in DPC micelles has resonance overlap concentrated in its central region (Figure 5.1). However, based on the spectral dispersion of the ^{1}H-^{15}N HSQC, B2 appears to be well folded.

5.3 ASSIGNMENT OF APOLIPOPROTEIN B100 FRAGMENT B2

Sequential backbone assignment (137) of ^{1}H, ^{13}C and ^{15}N resonances for apoB2 were carried out at 30°C using CcpNMR Analysis (Figure 5.2). ApoB2 was only partially assigned. The assignments were complicated because it appeared that several chemical shifts showed deviations from random coil values (120) at 30 °C. Furthermore, although some backbone amide peaks in the B2 spectrum were well dispersed, a significant

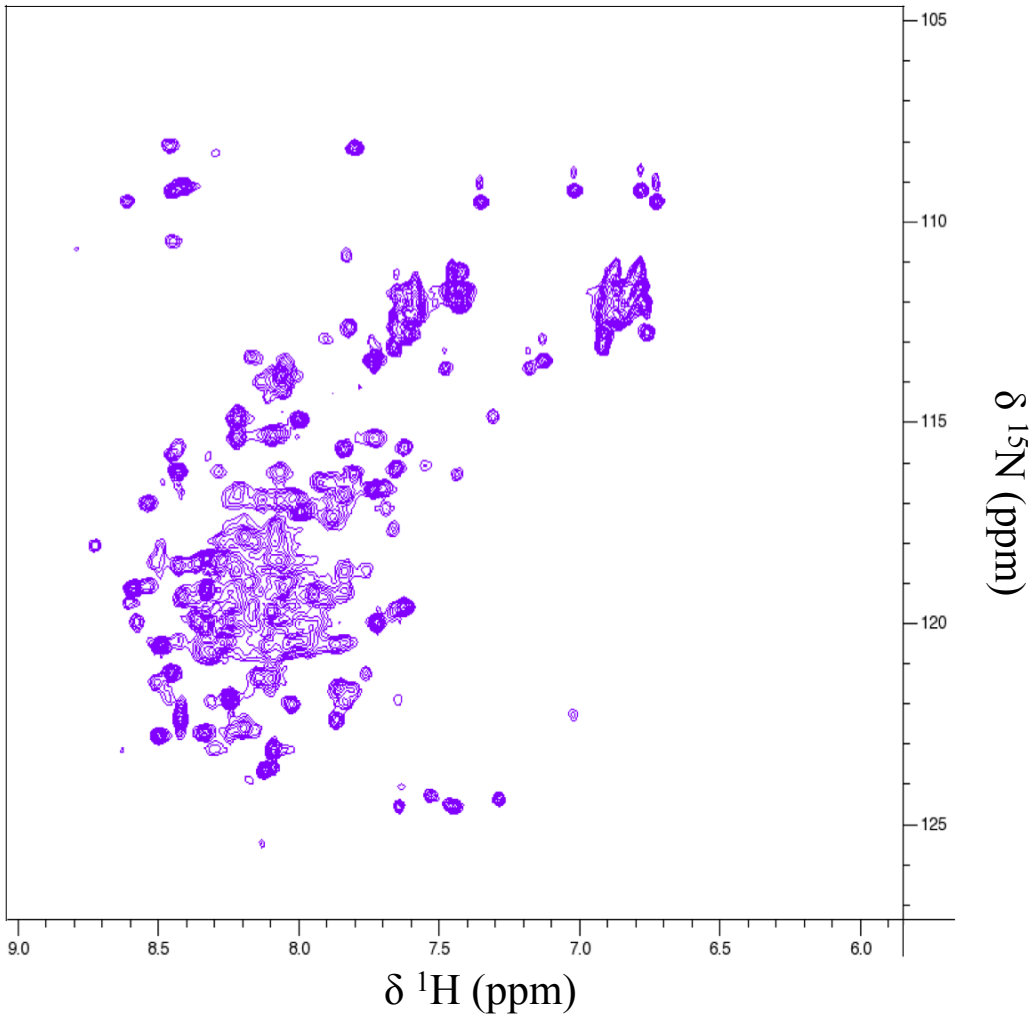

Figure 5.1 ^{1}H-^{15}N HSQC spectrum of apoB2 solubilized in DPC micelles. The ^{1}H-^{15}N HSQC spectrum of apoB2 at 800 MHz (QANUC), collected at 30 °C and in the presence of DPC micelles.

GIDPFT**DAHTNGNGKLALWGEHTGQ**LYSKFLLKAEPLAFTFSH

DYKGSTSHHLVSRKSISAALEHKVSALLTPAEQTGTWKL**KTQFN**

NNEYS**QDLDAYNTK**DKIGVELTGRTLADLTLLDSPIKVPLLLSEP

INIIDALEMRDAVEKPQEFTIVAFVKYDK**NQDVHSINL**PFFETLQ

EYFERNRQTIIVVVENVQRNLKHINIDQF

Figure 5.2 Partial backbone assignments for apoB2 in the presence of DPC micelles. Partial backbone assignments for TEV-cleaved apoB2 (bolded and underlined). The pink residues at the N-terminus correspond to vector sequence remaining after TEV cleavage.

number were clustered in the middle of the spectrum. Due to this spectral overlap and the deviations in chemical shift values for some residues, the majority of the ^{1}H, ^{13}C and ^{15}N resonances in the backbone spectra remain unassigned.

DANGLE and the chemical shift index (CSI) were used to predict B2 secondary structure based solely on the assigned chemical shifts. Secondary chemical shifts were obtained by subtraction of the random coil values in water (120) from the experimental chemical shifts. These were used to determine the CSI (135) at each residue using the consensus value for secondary chemical shift values calculated for C_{α}, H_{α}, C_{β}, and CO. The secondary structure predicted using the algorithm DANGLE, as implemented in CcpNmr Analysis (119, 138), reveals that the assigned regions of B2 are composed of predominantly helical regions (Figure 5.3).

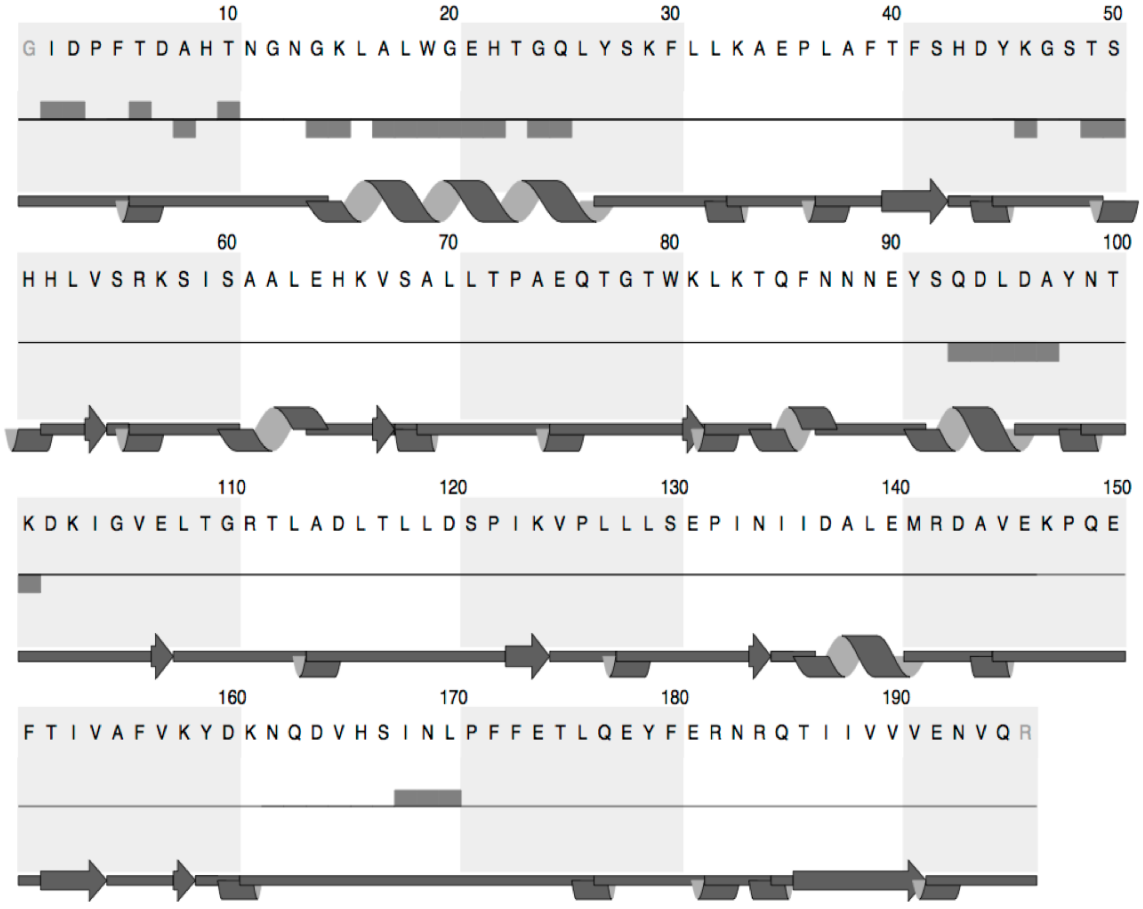

Figure 5.3 DANGLE and CSI prediction of apoB2 secondary structure. Arrows represent β-structure and spirals represent α-structure. The middle line corresponds to the chemical shift index (CSI).

5.4 NMR SPECTROSCOPY OF APOB1* and APOB1 IN DPC MICELLES

A solution of uncleaved, apoB1* prepared with approximately 0.8 mM peptide in 90% deionized water, 10% D_2O containing 20 mM CD_3COO^-, 1 mM NaN_3 and 1 mM DSS as an internal standard, was subjected to NMR analysis at the NRC-IMB on the 700 MHz Bruker Advance III spectrometer (Milton, ON) equipped with a cryogenically cooled probe. A ^1H-^{15}N HSQC was later recollected for the corrected, TEV-cleaved, apoB1 at QANUC on their 800MHz spectrometer (Varian, Palo Alto, CA) equipped with a cryogenically cooled probe. The final concentration of apoB1 was approximately 0.7 mM in 90% deionized water, 10% D_2O containing 20 mM CD_3COO^-, 1 mM NaN_3 and 1 mM DSS. All experiments were carried out at 30°C. The ^1H-^{15}N HSQC spectra of un-cleaved, C-terminally extended apoB1* and TEV- cleaved apoB1 solubilized in DPC micelles are shown on the top and bottom, respectively, of Figure 5.4. Despite the addition 52 residues in apoB1*, the two spectra appear visually similar and both have resonance overlap concentrated in their central regions. Based on the spectral dispersion of the ^1H-^{15}N HSQC, both apoB1 and apoB1* spectra appear to be well folded.

5.5 ASSIGNMENT OF APOB1*

Sequential backbone assignment of ^1H, ^{13}C and ^{15}N resonances for un-cleaved, C-terminally extended apoB1* were partially assigned at 30°C (Figure 5.5). Assignments were complicated due to the fairly large size of this peptide (245 amino acids) and the tendency of the peaks to cluster significantly in the middle of the spectra despite apoB1* being well folded.

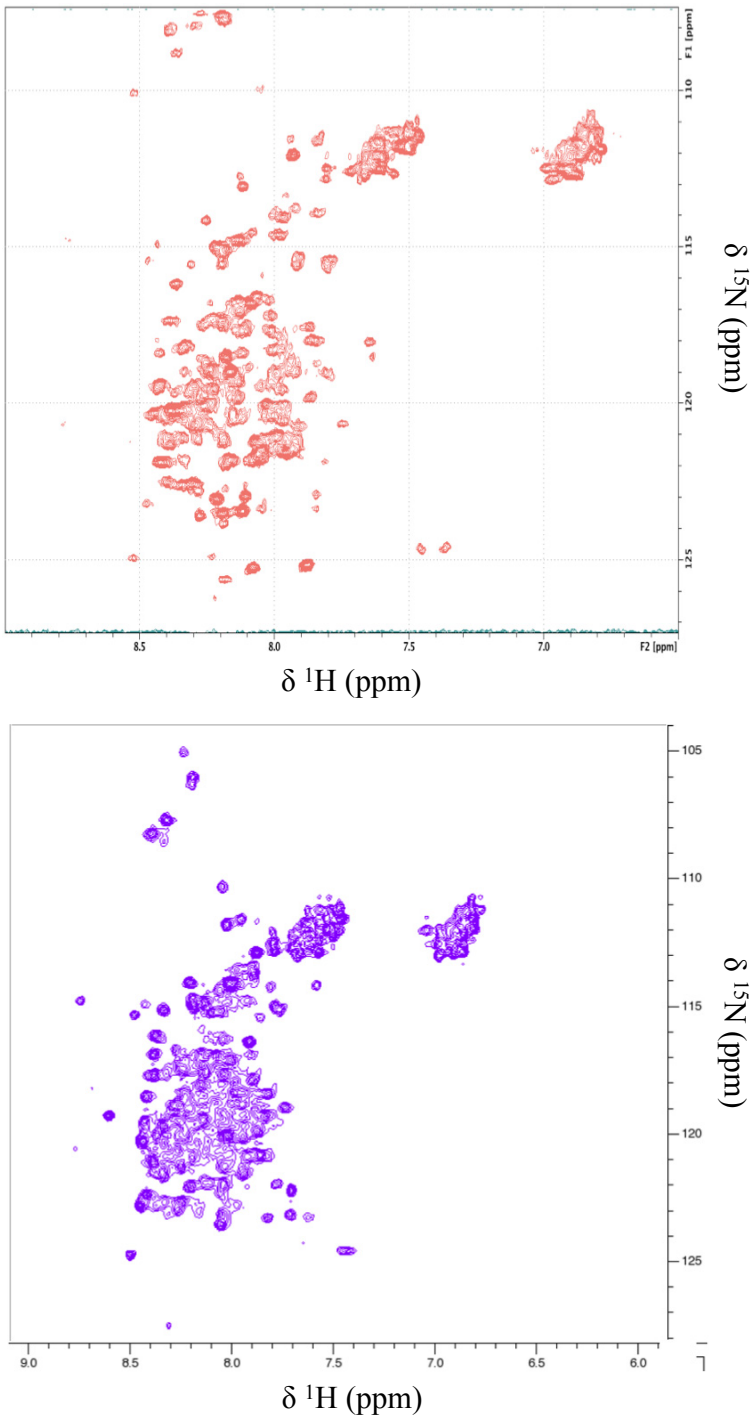

Figure 5.4 ^{1}H-^{15}N HSQC spectra of C-terminally extended and TEV cleaved apoB1 solubilized in DPC micelles. The **^{1}H-^{15}N** HSQC spectrum of the un-cleaved apoB1* collected at 700 MHz (NRC-IMB) is shown on the top and that of TEV-cleaved apoB1 collected at 800 MHz (QANUC) on the bottom. Both spectra were acquired at 30 °C and in the presence of DPC micelles.

MHHHHHH**GK**PIPNPLLGLDSTENLYF**QGID**P**FT****VDSK**

NIFNFKVSQEGLKLSNDMMGSYAEMK**FDHTNSLNIA**

GLSLDFSSKLDNIY**SS**DKFYK**QTV**NLQLQPYSLVTTL

NSDLKYNALDLTNN**GK**LRLEPLKLHVAGNLKGAYQN

NEIKHIYAI**SS**AA**LSASYKADTVA**KV**QGVE**FSHRLNTD

IAGLASAIDMS**TNYNSDSLH**FSNVFRSVMAPFTMTIK

RASSDPAANAKARKEAEKAA**TAEQ**

Figure 5.5 Partial backbone assignments for apoB1* in the presence of DPC micelles. Partial backbone assignments made for C-terminally extended, un-cleaved apoB1* (bolded and underlined). The pink residues at the N-terminus are those corresponding to the hexahistidine tag and vector sequence preceding the cloning site, and the blue residues at the C-terminus to those resulting from the primer error.

Due to this spectral overlap and the error that was eventually discovered in the primary structure, the majority of the ^{1}H, ^{13}C and ^{15}N resonances in the backbone spectra remain unassigned. The newly generated and corrected TEV-cleaved apoB1 will be used to pursue assignment of apoB1 NMR spectra in the future.

DANGLE and the CSI were used to predict the secondary structure for those residues that were assigned for un-cleaved, apoB1* before the error was discovered. The secondary structure was predicted using the algorithm DANGLE, as implemented in CcpNmr Analysis, and revealed that the assigned regions of apoB1* are composed of largely of helical regions (Figure 5.6).

Therefore, in our hands, apoB1*, which has been predicted to contain mostly β structures, is mostly α-helix by CD and NMR spectroscopy thus far.

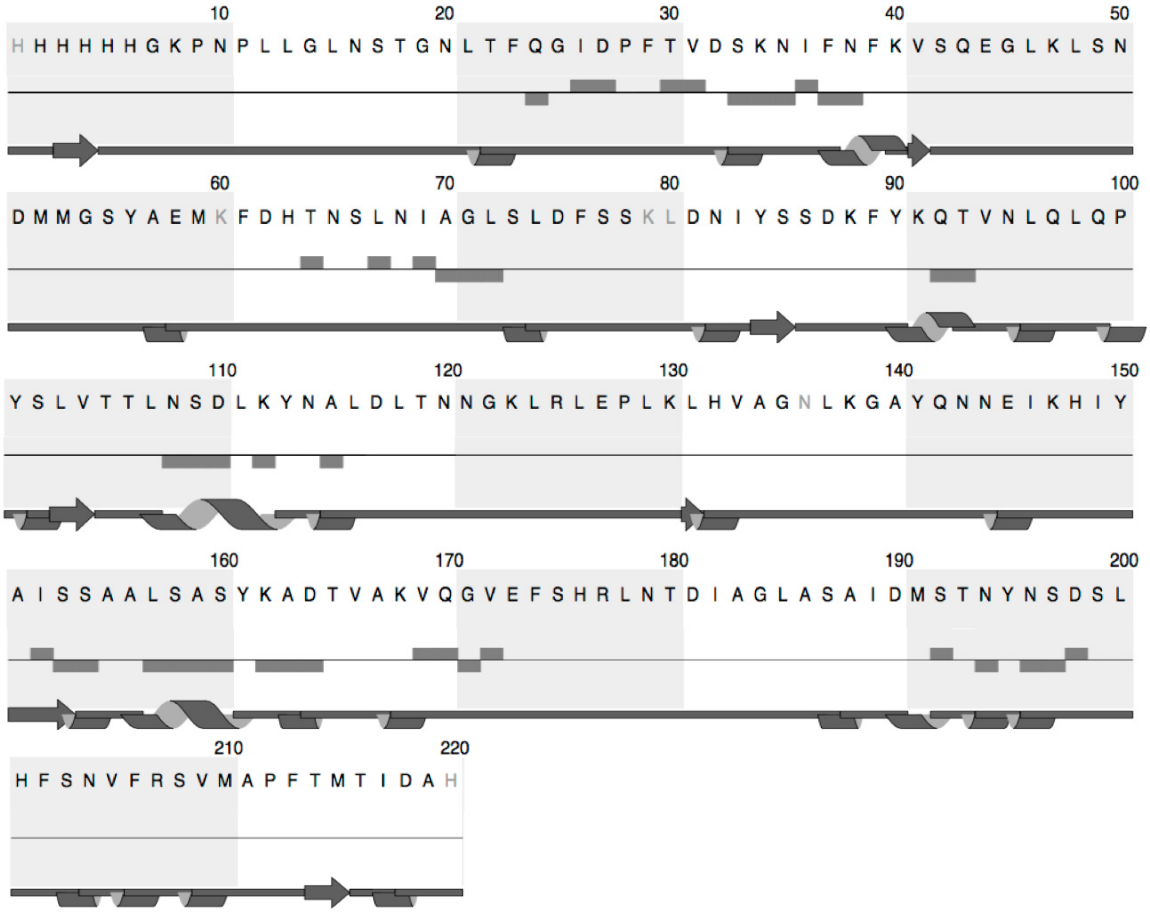

Figure 5.6 DANGLE and CSI prediction of apoB1* secondary structure. Arrows represent β-structure and spirals represent α-structure. The middle line corresponds to the chemical shift index (CSI).

Chapter 6 DISCUSSION

6.1 OVERVIEW

The studies presented herein have focused on the structural characterization of fragments derived from full-length human apoB100. I have studied 20 kDa fragments originating from the lipid-binding region of apoB100 in the presence and absence of several different membrane mimetics using CD spectroscopy and in DPC micelles by NMR spectroscopy. In this discussion, I will present a working model of apoB100 structure derived from experimental information at the atomic resolution.

6.2 APOLIPOPROTEIN B100 STRUCTURE: UPDATE AND PERSPECTIVE

With a protein that exceeds the size limitations of most current experimental structural techniques, a sort of "divide and conquer" method, where we selected a region of apoB and divided it into tractable fragments, is necessary. These fragments were studied individually in membrane mimetic environments and assumed to be structurally representative of the intact apoB100 protein from which they were derived. In support of this approach, numerous studies, many of which are described in the introduction, have probed the functions of apoB100 using smaller fragments derived from the full-length protein to understand the behavior of the protein as a whole. It can be inferred, then, that these smaller apoB fragments fold into functional units that confer behavioural similarity to the full-length apoB100 protein. This lends support to studying smaller pieces of apoB independently of the full-length, intact, protein. Furthermore, although the sizes of protein domains vary, the majority are less than 200 amino acids, conferring an

approximate mass of 20-25 kDa. Accordingly, the apoB fragments in this study were designed to be approximately the size of an average protein domain.

There remains the risk, however, that the fragments described herein will fold differently in the absence of the remainder of the protein, but one has to start somewhere and hope that with improvements in experimental techniques, eventually intact structural information can be acquired. To address the issue of these fragments behaving differently, we have joined two and three consecutive fragments to give 40 kDa (B1B2) and 60 kDa (B1B2B3) peptides, respectively. Although we have not acquired structural information on these peptides yet, we have been able to successfully express them in *E.coli*. The structural information on these peptides by CD spectroscopy, and possibly NMR spectroscopy, will give a better idea as to whether or not the structures of the individual B1, B2 and B3 fragments are representative of intact apoB100.

The NMR structural data on fragments B1, B2 and B1* of apoB100 are the first attempt at atomic resolution structural characterization of apoB100. Although only partially complete, the techniques used will be useful research tools in the characterization of the remaining apoB fragments outlined in Figure 3.1, as well as additional regions of apoB100 outside 37-70% of the full-length protein. The ^{1}H-^{15}N HSQC spectra for all three apoB fragments indicate that the proteins are well folded in the presence of DPC micelles. Three-dimensional spectra have been collected for B2 and B1* and partial backbone assignments have been made for both polypeptides.

ApoB2 was only partially assigned due to resonance overlap and deviations from random coil chemical shifts, which may be representative of the unique secondary structure adopted at those residues. This is not surprising, given that apoB secondary

structure is likely not represented by canonical α-helices and β-sheets. Based on the backbone assignments made, DANGLE predicts that the B2 polypeptide has considerable amounts of alpha helical regions. This is interesting because it is in contrast to what the majority of computer algorithms have predicted for apoB secondary structure. Completion of backbone assignments for B2 will reveal the secondary structures adopted by this fragment experimentally and help better understand the secondary structure of apoB as a whole.

The conformation of a protein solubilized in different membrane mimetics can vary. Initially, the apoB fragments were solubilized in DPC, one of the most common model membrane systems for NMR of biomacromolecules, and we were surprised at the amount of α-helical content in B1, B2 and B3 as revealed by CD spectroscopy. DPC has been reported to encourage α-helical character in proteins (139), so to ensure that this was not the case, B1 and B2 were solubilized in several additional membrane mimetics. The CD spectra of B1 and B2 solubilized in three other biological membrane mimetics (LMPC, LPPC, LPPG) yielded results similar to those of DPC-solubilized B1 and B2. Therefore, it is likely that the α-helical character seen is not an artifact of the presence of DPC micelles.

Although the spectra of B1 and B2 solubilized in DPC micelles have a similar general shape compared to LMPC, LPPC and LPPG, the intensity of the curves vary. These spectral differences could be a result of unequal B1 and B2 concentrations. This α-helical character was not seen in B1 and B2 solubilized in DHPC, DHPC-7 and DDM. Instead, the CD spectra resemble that of an unstructured protein. It is possible that because these detergents less resemble the phospholipid monolayer of a lipoprotein or

because of characteristics of the micelle itself (i.e size), that the apoB fragments were poorly solubilized and did not adopt the appropriate secondary structure in these micelles.

A concern that arises when using servers such as DichroWeb to deconvolute CD data is that predominantly α-helical proteins populate the vast majority of the datasets. Thus, it is difficult to reconcile whether this then "force-fits" or overestimates the protein's helical character. Furthermore, the α and β structures of apoB are likely not typical α-helices and β-sheets, which also questions the reliability of the data sets because proteins with unusual folds are not frequently represented in reference databases. However, a comparison of the results using multiple combinations of algorithms and reference databases yielded similar estimates. As alluded to earlier, the structures of several lipid-binding proteins, such as the FABP family, have been studied by CD spectroscopy and solved by NMR spectroscopy. It is thought that their interactions with lipids are mediated by β-structures. Using a dataset populated with other lipid-binding proteins for the deconvolution of CD spectra might better estimate the secondary structure propensity of the apoB100 fragments. Unfortunately, these databases are extremely difficult to come by and are not available on servers such as DichroWeb. Additionally, although it is difficult to acquire data much below approximately 190 nm, estimates of CD structure may have been more reliable if data was collected further down into the far UV region.

It is interesting that structural analysis of the un-cleaved, C-terminally extended apoB1* fragment was not significantly different from that of the corrected apoB1 fragment. ApoB1* was 245 residues and contained 27 extraneous amino acids at the N-terminus, corresponding to the hexahistidine tag and vector, and 25 extraneous amino

acids at the C-terminus, due to a primer error. Both have the potential to interfere with native structure of the protein, but from our CD and NMR studies, this did not appear to be the case.

In the absence of DPC, both proteins behaved similarly, being rather insoluble. C-terminally extended apoB1* exhibited slightly more β-character than TEV cleaved apoB1, both visually and as predicted by DichroWeb deconvolution analysis. In the presence of DPC, both curves displayed the characteristics of an alpha helical protein, with two negative peaks at approximately 222 nm and 208 nm. However, the DichroWeb deconvolution predicted the TEV cleaved apoB1 to be 85% α-helical compared to 36% for the apoB1* peptide. This may be a reflection of the concerns with using DichroWeb for the analysis of apoB fragments as alluded to above.

Although collected on two different spectrometers (field strength and manufacturer), comparison of the ^{1}H-^{15}N HSQC spectra for the apoB1 and apoB1* peptides revealed similar spectral and peak dispersions and both peptides appeared to be well folded. According to DANGLE, the B1* polypeptide has several alpha helical regions. Again, this is interesting because it is in contrast to what computer algorithms have predicted for apoB secondary structure. Although further assignment of B1* will not be pursued, assignment of TEV cleaved B1 will more accurately reveal the secondary structures adopted by this fragment of apoB experimentally.

One cannot definitively say that the extraneous amino acids at the N- and C-termini are having no effect on the structure of apoB1 without completely solving the three-dimensional structure. Given the data presented herein, it is likely not a profound

effect. Nonetheless, future NMR analysis and structural determination will be done on the corrected, TEV cleaved apoB1 fragment.

6.3 FUTURE WORK

Where to next on the road to an experimentally derived atomic resolution structure of apoB100? It is unlikely that we are going to go from nothing directly to an intact model of apoB100, but continuing with the divide and conquer method is a promising road to follow to gain some much needed apoB structural information. We have expressed eight individual peptide fragments, spanning three domains of the pentapartite model, that can be purified and whose structures can be studied using the same CD and NMR spectroscopy techniques discussed in the preceding chapters. I have started to characterize the first three fragments (B1, B2 and B3), but this is not complete. Further CD studies using addition membrane mimetics and different temperatures and protein or micelle concentrations can be done to get a better idea about how these peptides interact with different micellar monolayers. These CD experiments can then also be applied to the five remaining apoB peptide fragments.

I have acquired NMR spectroscopy data for B2 and partially completed the sequential backbone assignments. These need to be fully completed in order to move on to structural calculations and modeling of the B2 peptide. After this, the next step would be to collect NMR data for the seven other apoB peptide fragments, in hopes of attaining three-dimensional structures for all eight consecutive fragments, beginning with B1. Three-dimensional NMR data have been collected and partially assigned for the C-terminally extended apoB1* and so re-collecting the data for the corrected, TEV cleaved

B1 would be a peptide to start with when collecting new NMR data. The familiarity with the B1 data acquired and the months spent analyzing and assigning the erroneous B1 data may give an advantage in assigning the new data more quickly.

Logically, the next item to address would be whether the structural characterization of these fragments is representative of intact apoB100. Structural characterization of the B1B2 and B1B2B3 peptides would begin to clarify this. If these composite peptides yielded CD spectra that resemble individual B1, B2 and B3 fragments, this lends support to them being representative of apoB100. Furthermore, if the NMR spectra were also similar, this would lend further support to the relevance of these fragments in trying to understand the structure of intact apoB100.

Nonetheless, the work herein presents promising results in the pursuit of the NMR structure of apoB100 in the presence of lipids.

REFERENCES

1. Vance JE, Adeli K. Chapter 18 - assembly and secretion of triacylglycerol-rich lipoproteins. In: Vance DEVE, ed. Biochemistry of Lipids, Lipoproteins and Membranes (Fifth Edition). San Diego: Elsevier; 2008:507-XII.

2. Powell LM, Wallis SC, Pease RJ, Edwards YH, Knott TJ, Scott J. A novel form of tissue-specific RNA processing produces apolipoprotein-B48 in intestine. Cell 1987; 50(6): 831-840.

3. Sniderman AD, Graaf JD, Couture P, Williams K, Kiss RS, Watts GF. Regulation of plasma LDL: The apoB paradigm. Clinical science (London, England : 1979) 2009; 118(5): 333-339.

4. Hussain MM, Shi J, Dreizen P. Microsomal triglyceride transfer protein and its role in apoB-lipoprotein assembly. J Lipid Res 2003; 44(1): 22-32.

5. Gordon DA, Jamil H. Progress towards understanding the role of microsomal triglyceride transfer protein in apolipoprotein-B lipoprotein assembly. Biochim Biophys Acta 2000; 1486(1): 72-83.

6. Wetterau JR, Lin MC, Jamil H. Microsomal triglyceride transfer protein. Biochim Biophys Acta 1997; 1345(2): 136-150.

7. Zhang YL, Hernandez-Ono A, Ko C, Yasunaga K, Huang LS, Ginsberg HN. Regulation of hepatic apolipoprotein B-lipoprotein assembly and secretion by the availability of fatty acids. I. differential response to the delivery of fatty acids via albumin or remnant-like emulsion particles. J Biol Chem 2004; 279(0021-9258; 18): 19362-19374.

8. Sniderman AD, Cianflone K. Substrate delivery as a determinant of hepatic apoB secretion. Arterioscler Thromb 1993; 13(5): 629-636.

9. Taghibiglou C, Carpentier A, Iderstine SCV, Chen B, Rudy D, Aiton A, Lewis GF, et al. Mechanisms of hepatic very low density lipoprotein overproduction in insulin resistance. evidence for enhanced lipoprotein assembly, reduced intracellular apoB degradation, and increased microsomal triglyceride transfer protein in a fructose-fed hamster model. J Biol Chem 2000; 275(12): 8416-8425.

10. Kummrow E, Hussain MM, Pan M, Marsh JB, Fisher EA. Myristic acid increases dense lipoprotein secretion by inhibiting apoB degradation and triglyceride recruitment. J Lipid Res 2002; 43(12): 2155-2163.

11. Zammit VA, Lankester DL. Oleate acutely stimulates the secretion of triacylglycerol by cultured rat hepatocytes by accelerating the emptying of the secretory compartment. Lipids 2001; 36(6): 607-612.

12. Heath RB, Karpe F, Milne RW, Burdge GC, Wootton SA, Frayn KN. Dietary fatty acids make a rapid and substantial contribution to VLDL-triacylglycerol in the fed state. American Journal of Physiology.Endocrinology and Metabolism 2007; 292(0193-1849; 3): E732-E739.

13. Boren J, Rustaeus S, Olofsson SO. Studies on the assembly of apolipoprotein B-100- and B-48-containing very low density lipoproteins in McA-RH7777 cells. J Biol Chem 1994; 269(41): 25879-25888.

14. Innerarity TL, Boren J, Yamanaka S, Olofsson SO. Biosynthesis of apolipoprotein B48-containing lipoproteins. regulation by novel post-transcriptional mechanisms. J Biol Chem 1996; 271(5): 2353-2356.

15. Raabe M, Veniant MM, Sullivan MA, Zlot CH, Bjorkegren J, Nielsen LB, Wong JS, et al. Analysis of the role of microsomal triglyceride transfer protein in the liver of tissue-specific knockout mice. J Clin Invest 1999; 103(9): 1287-1298.

16. Kulinski A, Rustaeus S, Vance JE. Microsomal triacylglycerol transfer protein is required for lumenal accretion of triacylglycerol not associated with ApoB, as well as for ApoB lipidation. J Biol Chem 2002; 277(35): 31516-31525.

17. Jamil H, Jr JKD, Chu CH, Lago MW, Rinehart JK, Biller SA, Gregg RE, et al. Microsomal triglyceride transfer protein. specificity of lipid binding and transport. J Biol Chem 1995; 270(12): 6549-6554.

18. Benoist F, Grand-Perret T. Co-translational degradation of apolipoprotein B100 by the proteasome is prevented by microsomal triglyceride transfer protein. synchronized translation studies on HepG2 cells treated with an inhibitor of microsomal triglyceride transfer protein. J Biol Chem 1997; 272(33): 20435-20442.

19. Wang S, McLeod RS, Gordon DA, Yao Z. The microsomal triglyceride transfer protein facilitates assembly and secretion of apolipoprotein B-containing lipoproteins and decreases cotranslational degradation of apolipoprotein B in transfected COS-7 cells. J Biol Chem 1996; 271(24): 14124-14133.

20. Alexander CA, Hamilton RL, Havel RJ. Subcellular localization of B apoprotein of plasma lipoproteins in rat liver. J Cell Biol 1976; 69(2): 241-263.

21. Hamilton RL, Wong JS, Cham CM, Nielsen LB, Young SG. Chylomicron-sized lipid particles are formed in the setting of apolipoprotein B deficiency. J Lipid Res 1998; 39(8): 1543-1557.

22. Olofsson SO, Boren J. Apolipoprotein B secretory regulation by degradation. Arterioscler Thromb Vasc Biol 2012; 32(6): 1334-1338.

23. Pullinger CR, North JD, Teng BB, Rifici VA, Ronhild dBA, Scott J. The apolipoprotein B gene is constitutively expressed in HepG2 cells: Regulation of secretion by oleic acid, albumin, and insulin, and measurement of the mRNA half-life. J Lipid Res 1989; 30(7): 1065-1077.

24. Schonfeld G, Lin X, Yue P. Familial hypobetalipoproteinemia: Genetics and metabolism. Cellular and molecular life sciences : CMLS 2005; 62(12): 1372-1378.

25. Schonfeld G, Patterson BW, Yablonskiy DA, Tanoli TS, Averna M, Elias N, Yue P, et al. Fatty liver in familial hypobetalipoproteinemia: Triglyceride assembly into VLDL particles is affected by the extent of hepatic steatosis. J Lipid Res 2003; 44(0022-2275; 3): 470-478.

26. Burnett JR, Zhong S, Jiang ZG, Hooper AJ, Fisher EA, McLeod RS, Zhao Y, et al. Missense mutations in APOB within the betaalpha1 domain of human APOB-100 result in impaired secretion of ApoB and ApoB-containing lipoproteins in familial hypobetalipoproteinemia. J Biol Chem 2007; 282(0021-9258; 33): 24270-24283.

27. Chen Z, Fitzgerald RL, Schonfeld G. Hypobetalipoproteinemic mice with a targeted apolipoprotein (apo) B-27.6-specifying mutation: In vivo evidence for an important role of amino acids 1254-1744 of ApoB in lipid transport and metabolism of the apoB-containing lipoprotein. J Biol Chem 2002; 277(16): 14135-14145.

28. Knott TJ, Jr SCR, Innerarity TL, Jacobson SF, Urdea, MS, Levy-Wilson B, et al. Human apolipoprotein B: Structure of carboxyl-terminal domains, sites of gene expression, and chromosomal localization. Science 1985; 230(4721): 37-43.

29. Lusis AJ, West R, Mehrabian M, Reuben MA, LeBoeuf RC, Kaptein JS, Johnson DF, et al. Cloning and expression of apolipoprotein B, the major protein of low and very low density lipoproteins. Proc Natl Acad Sci U S A 1985; 82(14): 4597-4601.

30. Law SW, Lackner KJ, Hospattankar AV, Anchors JM, Sakaguchi AY, Naylor SL, Brewer HB,Jr. Human apolipoprotein B-100: Cloning, analysis of liver mRNA, and assignment of the gene to chromosome 2. Proc Natl Acad Sci U S A 1985; 82(24): 8340-8344.

31. Cladaras C, Hadzopoulou-Cladaras M, Avila, Nussbaum AL, Nicolosi R, Zannis VI. Complementary DNA derived structure of the amino-terminal domain of human apolipoprotein B and size of its messenger RNA transcript. Biochemistry (N Y) 1986; 25(19): 5351-5357.

32. Cladaras C, Hadzopoulou-Cladaras M, Nolte, RT, Atkinson D, Zannis VI. The complete sequence and structural analysis of human apolipoprotein B-100: Relationship between apoB-100 and apoB-48 forms. EMBO J 1986; 5(13): 3495-3507.

33. Chen SH, Yang CY, Chen PF, Setzer D, Tanimura M, Li WH, Jr. AMG, et al. The complete cDNA and amino acid sequence of human apolipoprotein B-100. J Biol Chem 1986; 261(28): 12918-12921.

34. Law SW, Grant SM, Higuchi K, Hospattankar A, Lackner K, Lee N, Brewer HB,Jr. Human liver apolipoprotein B-100 cDNA: Complete nucleic acid and derived amino acid sequence. Proc Natl Acad Sci U S A 1986; 83(21): 8142-8146.

35. Steele JC, Jr, Reynolds JA. Characterization of the apolipoprotein B polypeptide of human plasma low density lipoprotein in detergent and denaturation solutions. J Biol Chem 1979; 254(10): 1633-1680.

36. Marcel YL, Weech PK, Milthorp P, Terce F, Vezina C, Milne RW. Monoclonal antibodies and the characterization of apolipoprotein structure and function. Prog Lipid Res 1984; 23(4): 169-195.

37. Milne RW, Marcel YL. The use of monoclonal antibodies to probe human apolipoprotein B structure and function. Can J Biochem Cell Biol 1985; 63(8): 906-912.

38. Milne R, Jr RT, Maurice R, Pease RJ, Weech PK, Rassart E, Fruchart JC, et al. The use of monoclonal antibodies to localize the low density lipoprotein receptor-binding domain of apolipoprotein B. J Biol Chem 1989; 264(33): 19754-19760.

39. Krul ES, Kleinman Y, Kinoshita M, Pfleger B, Oida K, Law A, Scott J, et al. Regional specificities of monoclonal anti-human apolipoprotein B antibodies. J Lipid Res 1988; 29(7): 937-947.

40. Pease RJ, Milne RW, Jessup WK, Law A, Provost P, Fruchart JC, Dean RT, et al. Use of bacterial expression cloning to localize the epitopes for a series of monoclonal antibodies against apolipoprotein B100. J Biol Chem 1990; 265(1): 553-568.

41. Innerarity TL, Young SG, Poksay KS, Mahley RW, Smith RS, Milne RW, Marcel YL, et al. Structural relationship of human apolipoprotein B48 to apolipoprotein B100. J Clin Invest 1987; 80(6): 1794-1798.

42. Cardin AD, Price CA, Hirose N, Krivanek MA, Blankenship DT, Chao J, Mao SJ. Structural organization of apolipoprotein B-100 of human plasma low density lipoproteins. comparison to B-48 of chylomicrons and very low density lipoproteins. J Biol Chem 1986; 261(35): 16744-16748.

43. Chen GC, Chapman MJ, Kane JP. Secondary structure and thermal behavior of trypsin-treated low-density lipoproteins from human serum, studied by circular dichroism. Biochim Biophys Acta 1983; 754(1): 51-56.

44. Cardin AD, Jackson RL. Interaction of tryptic peptides of apolipoprotein B-100 with dimyristoylphosphatidylcholine. Biochim Biophys Acta 1986; 877(3): 366-371.

45. Yang CY, Gu ZW, Weng SA, Kim TW, Chen SH, Pownall HJ, Sharp PM, et al. Structure of apolipoprotein B-100 of human low density lipoproteins. Arteriosclerosis 1989; 9(1): 96-108.

46. Phillips ML, Schumaker VN. Conformation of apolipoprotein B after lipid extraction of low density lipoproteins attached to an electron microscope grid. J Lipid Res 1989; 30(3): 415-422.

47. Yang CY, Kim TW, Pao Q, Chan L, Knapp RD, Jr. AMG, Pownall HJ. Structure and conformational analysis of lipid-associating peptides of apolipoprotein B-100 produced by trypsinolysis. J Protein Chem 1989; 8(6): 689-699.

48. Chen GC, Hardman DA, Hamilton RL, Mendel CM, Schilling JW, Zhu S, Lau K, et al. Distribution of lipid-binding regions in human apolipoprotein B-100. Biochemistry 1989; 28(6): 2477-2484.

49. Chen GC, Liu W, Duchateau P, Allaart J, Hamilton RL, Mendel CM, Lau K, et al. Conformational differences in human apolipoprotein B-100 among subspecies of low density lipoproteins (LDL). Association of altered proteolytic accessibility with decreased receptor binding of LDL subspecies from hypertriglyceridemic subjects. J Biol Chem 1994; 269(46): 29121-29128.

50. Goormaghtigh E, De Meutter J, Vanloo B, Brasseur R, Rosseneu M, Ruysschaert JM. Evaluation of the secondary structure of apo B-100 in low-density lipoprotein (LDL) by infrared spectroscopy. Biochim Biophys Acta 1989; 1006(1): 147-150.

51. Goormaghtigh E, Cabiaux V, Meutter JD, Rosseneu M, Ruysschaert JM. Secondary structure of the particle associating domain of apolipoprotein B-100 in low-density lipoprotein by attenuated total reflection infrared spectroscopy. Biochemistry (N Y) 1993; 32(23): 6104-6110.

52. Vanderyse L, Devreese AM, Baert J, Vanloo B, Lins L, Ruysschaert JM, Rosseneu M. Structural and functional properties of apolipoprotein B in chemically modified low density lipoproteins. Atherosclerosis 1992; 97(2-3): 187-199.

53. Chatterton JE, Phillips ML, Curtiss LK, Milne R, Fruchart JC, Schumaker VN. Immunoelectron microscopy of low density lipoproteins yields a ribbon and bow model for the conformation of apolipoprotein B on the lipoprotein surface. J Lipid Res 1995; 36(9): 2027-2037.

54. Boren J, Lee I, Zhu W, Arnold K, Taylor S, Innerarity TL. Identification of the low density lipoprotein receptor-binding site in apolipoprotein B100 and the modulation of its binding activity by the carboxyl terminus in familial defective apo-B100. J Clin Invest 1998; 101(5): 1084-1093.

55. Meyer DF, Nealis AS, Bruckdorfer KR, Perkins SJ. Characterization of the structure of polydisperse human low-density lipoprotein by neutron scattering. Biochem J 1995; 310 (Pt 2)(Pt 2): 407-415.

56. Orlova EV, Sherman MB, Chiu W, Mowri H, Smith LC, Jr AMG. Three-dimensional structure of low density lipoproteins by electron cryomicroscopy. Proc Natl Acad Sci U S A 1999; 96(15): 8420-8425.

57. Liu Y, Atkinson D. Immuno-electron cryo-microscopy imaging reveals a looped topology of apoB at the surface of human LDL. J Lipid Res 2011; 52(6): 1111-1116.

58. Walsh MT, Atkinson D. Calorimetric and spectroscopic investigation of the unfolding of human apolipoprotein B. J Lipid Res 1990; 31(6): 1050-1062.

59. Walsh MT, Atkinson D. Physical properties of apoprotein B in mixed micelles with sodium deoxycholate and in a vesicle with dimyristoyl phosphatidylcholine. J Lipid Res 1986; 27(3): 316-325.

60. Gantz DL, Walsh MT, Small DM. Morphology of sodium deoxycholate-solubilized apolipoprotein B-100 using negative stain and vitreous ice electron microscopy. J.Lipid Res 2000.Sep.;41.(9.):1464.-72. 2000; 41(9): 1464-1472.

61. Osterman DG, Kaiser ET. Design and characterization of peptides with amphiphilic beta-strand structures. J Cell Biochem 1985; 29(2): 57-72.

62. Lins L, Brasseur R, Rosseneu M, Yang CY, Sparrow DA, Sparrow JT, Jr AMG, et al. Structure and orientation of apo B-100 peptides into a lipid bilayer. J Protein Chem 1994; 13(1): 77-88.

63. Wang L, Small DM. Interfacial properties of amphipathic beta strand consensus peptides of apolipoprotein B at oil/water interfaces. J Lipid Res 2004; 45(0022-2275; 9): 1704-1715.

64. Wang L, Martin DD, Genter E, Wang J, McLeod RS, Small DM. Surface study of apoB1694-1880, a sequence that can anchor apoB to lipoproteins and make it nonexchangeable. J Lipid Res 2009; 50(7): 1340-1352.

65. De Loof H, Rosseneu M, Yang CY, Li WH, Gotto AM,Jr, Chan L. Human apolipoprotein B: Analysis of internal repeats and homology with other apolipoproteins. J Lipid Res 1987; 28(12): 1455-1465.

66. Segrest JP, Jones MK, Mishra VK, Anantharamaiah GM, Garber DW. apoB-100 has a pentapartite structure composed of three amphipathic alpha-helical domains alternating with two amphipathic beta-strand domains. detection by the computer program LOCATE. Arteriosclerosis & Thrombosis 1994; 14(10): 1674-1685.

67. Segrest JP, Jones MK, Mishra VK, Pierotti V, Young SH, Boren J, Innerarity TL, et al. Apolipoprotein B-100: Conservation of lipid-associating amphipathic secondary structural motifs in nine species of vertebrates. J Lipid Res 1998; 39(1): 85-102.

68. Segrest JP, Jones MK, Loof HD, Dashti N. Structure of apolipoprotein B-100 in low density lipoproteins. J Lipid Res 2001; 42(9): 1346-1367.

69. Raag R, Appelt K, Xuong NH, Banaszak L. Structure of the lamprey yolk lipid-protein complex lipovitellin-phosvitin at 2.8 Å resolution. J Mol Biol 1988; 200(3): 553-569.

70. Segrest JP, Jones MK, Dashti N. N-terminal domain of apolipoprotein B has structural homology to lipovitellin and microsomal triglyceride transfer protein: A lipid pocket model for self-assembly of apob-containing lipoprotein particles. J Lipid Res 1999; 40(8): 1401-1416.

71. Hussain MM, Bakillah A, Nayak N, Shelness GS. Amino acids 430-570 in apolipoprotein B are critical for its binding to microsomal triglyceride transfer protein. J Biol Chem 1998; 273(40): 25612-25615.

72. Mann CJ, Anderson TA, Read J, Chester SA, Harrison GB, Kochl S, Ritchie PJ, et al. The structure of vitellogenin provides a molecular model for the assembly and secretion of atherogenic lipoproteins. J Mol Biol 1999; 285(1): 391-408.

73. Smolenaars MM, Madsen O, Rodenburg KW, Horst DJVd. Molecular diversity and evolution of the large lipid transfer protein superfamily. J Lipid Res 2007; 48(0022-2275; 3): 489-502.

74. Johs A, Hammel M, Waldner I, May RP, Laggner P, Prassl R. Modular structure of solubilized human apolipoprotein B-100. low resolution model revealed by small angle neutron scattering. J Biol Chem 2006; 281(28): 19732-19739.

75. Ingram MF, Shelness GS. Folding of the amino-terminal domain of apolipoprotein B initiates microsomal triglyceride transfer protein-dependent lipid transfer to nascent very low density lipoprotein. J Biol Chem 1997; 272(15): 10279-10286.

76. Gretch DG, Sturley SL, Wang L, Lipton BA, Dunning A, Grunwald KA, Wetterau JR, et al. The amino terminus of apolipoprotein B is necessary but not sufficient for microsomal triglyceride transfer protein responsiveness. J Biol Chem 1996; 271(15): 8682-8691.

77. Jiang ZG, Gantz D, Bullitt E, McKnight CJ. Defining lipid-interacting domains in the N-terminal region of apolipoprotein B. Biochemistry (N Y) 2006; 45(0006-2960; 39): 11799-11808.

78. Khachfe HM, Atkinson D. Conformation and stability properties of B17: I. analytical investigations using circular dichroism. Eur Biophys J 2012; 41(8): 639-646.

79. Mitsche MA, Wang L, Jiang ZG, McKnight CJ, Small DM. Interfacial properties of a complex multi-domain 490 amino acid peptide derived from apolipoprotein B (residues 292-782). Langmuir 2009; 25(4): 2322-2330.

80. Wang L, Jiang ZG, McKnight CJ, Small DM. Interfacial properties of apolipoprotein B292-593 (B6.4-13) and B611-782 (B13-17). insights into the structure of the lipovitellin homology region in apolipoprotein B. Biochemistry (N Y) 2010; 49(18): 3898-3907.

81. Ledford AS, Weinberg RB, Cook VR, Hantgan RR, Shelness GS. Self-association and lipid binding properties of the lipoprotein initiating domain of apolipoprotein B. J Biol Chem 2006; 281(0021-9258; 13): 8871-8876.

82. Ledford AS, Cook VA, Shelness GS, Weinberg RB. Structural and dynamic interfacial properties of the lipoprotein initiating domain of apolipoprotein B. J Lipid Res 2009; 50(1): 108-115.

83. Dashti N, Gandhi M, Liu X, Lin X, Segrest JP. The N-terminal 1000 residues of apolipoprotein B associate with microsomal triglyceride transfer protein to create a lipid transfer pocket required for lipoprotein assembly. Biochemistry 2002.Jun.4;41.(22.):6978.-87. 2002; 41(22): 6978-6987.

84. Dashti N, Manchekar M, Liu Y, Sun Z, Segrest JP. Microsomal triglyceride transfer protein activity is not required for the initiation of apolipoprotein B-containing lipoprotein assembly in McA-RH7777 cells. J Biol Chem 2007; 282(39): 28597-28608.

85. Shelness GS, Hou L, Ledford AS, Parks JS, Weinberg RB. Identification of the lipoprotein initiating domain of apolipoprotein B. J Biol Chem 2003; 278(45): 44702-44707.

86. Weinberg RB, Cook VR, DeLozier JA, Shelness GS. Dynamic interfacial properties of human apolipoproteins A-IV and B-17 at the air/water and oil/water interface. J Lipid Res 2000; 41(0022-2275; 9): 1419-1427.

87. Huang XF, Shelness GS. Identification of cysteine pairs within the amino-terminal 5% of apolipoprotein B essential for hepatic lipoprotein assembly and secretion. J Biol Chem 1997; 272(50): 31872-31876.

88. DeLozier JA, Parks JS, Shelness GS. Vesicle-binding properties of wild-type and cysteine mutant forms of alpha(1) domain of apolipoprotein B. J.Lipid Res 2001 Mar.;42.(3.):399.-406. 2001; 42(3): 399-406.

89. Vukmirica J, Nishimaki-Mogami T, Tran K, Shan J, McLeod RS, Yuan J, Yao Z. The N-linked oligosaccharides at the amino terminus of human apoB are important for the assembly and secretion of VLDL. J Lipid Res 2002; 43(9): 1496-1507.

90. McLeod RS, Zhao Y, Selby SL, Westerlund J, Yao Z. Carboxyl-terminal truncation impairs lipid recruitment by apolipoprotein B100 but does not affect secretion of the truncated apolipoprotein B-containing lipoproteins. J Biol Chem 1994; 269(4): 2852-2862.

91. Spring DJ, Lee SM, Puppione DL, Phillips M, Elovson J, Schumaker VN. Identification of a neutral lipid core in a transiently expressed and secreted lipoprotein containing an apoB-48-like apolipoprotein. J Lipid Res 1992; 33(2): 233-240.

92. Carraway M, Herscovitz H, Zannis V, Small DM. Specificity of lipid incorporation is determined by sequences in the N-terminal 37 of apoB. Biochemistry (N Y) 2000; 39(32): 9737-9745.

93. McLeod RS, Wang Y, Wang S, Rusi+â–Œol A, Links P, Yao Z. Apolipoprotein B sequence requirements for hepatic very low density lipoprotein assembly. J Biol Chem 1996; 271(31): 18445-18455.

94. Coe NR, Bernlohr DA. Physiological properties and functions of intracellular fatty acid-binding proteins. Biochim Biophys Acta 1998; 1391(3): 287-306.

95. Storch J, Thumser AE. The fatty acid transport function of fatty acid-binding proteins. Biochim Biophys Acta 2000; 1486(1): 28-44.

96. Glatz JF, Vusse GJvd. Cellular fatty acid-binding proteins: Their function and physiological significance. Prog Lipid Res 1996; 35(3): 243-282.

97. Thompson J, Winter N, Terwey D, Bratt J, Banaszak L. The crystal structure of the liver fatty acid-binding protein. A complex with two bound oleates. J Biol Chem 1997; 272(11): 7140-7150.

98. Lücke C, Rademacher M, Zimmerman WA, Van Moerkerk, H. T. B., Veerkamp JH, Rüterjans H. Spin-system heterogeneities indicate a selected-fit mechanism in fatty acid binding heart-type fatty acid-binding protein (H-FABP). Biochem J 2001; 354: 259-266.

99. Lücke C, Zhang F, Hamilton JA, Sacchettini JC, Rüterjans H. Solution structure of ileal lipid binding protein in complex with glycocholate. European Journal of Biochemistry 2000; 267(10): 2929-2938.

100. Rademacher M, Zimmerman WA, Rüterjans H, Veerkamp JH, Lücke C. Solution structure of fatty acid-binding protein from human brain. Molecular & Cellular Biochemistry 2002; 239(1-2): 61-68.

101. Zhang F, Lücke C, Baier LJ, Sacchettini JC, Hamilton JA. Solution structure of human intestinal fatty acid binding protein: Implications for ligand entry and exit. J Biomol NMR 1997; 9: 213-228.

102. Gutierrez-Gonzalez LH, Ludwig C, Hohoff C, Rademacher M., Hanhoff T, Rüterjans H, Spener F, Lücke C. Solution structure and backbone dynamics of human epidermal-type fatty acid-binding protein (E-FABP). Biochem J 2002; 364: 725-737.

103. Wang L, Walsh MT, Small DM. Apolipoprotein B is conformationally flexible but anchored at a triolein/water interface: A possible model for lipoprotein surfaces. Proc Natl Acad Sci U S A 2006; 103(18): 6871-6876.

104. Whitmore L, Wallace BA. DICHROWEB, an online server for protein secondary structure analyses from circular dichroism spectroscopic data. Nucleic Acids Research 2004; 32(suppl 2): W668-W673.

105. Wallace BA, Janes RW. Modern Techniques for Circular Dichroism and Synchrotron Radiation Circular Dichroism Spectroscopy. Amsterdamn, Netherlands: IOS Press BV, 2009:231.

106. Sreerama N, Woody RW. Computation and analysis of protein circular dichroism spectra. Meth Enzymol 2004; 383(0): 318-351.

107. Greenfield NJ. Analysis of circular dichroism data. Meth Enzymol 2004; 383(0): 282-317.

108. Lian L, Roberts G. Protein NMR Spectroscopy: Principal Techniques and Applications. Chichester, U.K.: John Wiley and Sons, 2011:351.

109. Keller J. Understanding NMR Spectroscopy. Chichester, U.K.: John Wiley and Sons, 2013:511.

110. Levitt MH. Spin Dynamics: Basics of Nuclear Magnetic Resonance. Chichester, U.K.: John Wiley and Sons, 2008:714.

111. Cavanagh J, Fairbrother WJ, Palmer III AG, Rance M, Skelton NJ. Chapter 1 - classical NMR spectroscopy. In: Cavanagh J, Fairbrother WJ, Palmer AG, Rance M, Skelton NJ, eds. Protein NMR Spectroscopy (Second Edition). Burlington: Academic Press; 2007:1-28.

112. Chary KVR, Govil G. NMR in Biological Systems from Molecules to Humans. Dordrecht, Netherlands: Springer, 2008:521.

113. Kay LE, Ikura M, Tschudin R, Bax A. Three-dimensional triple-resonance NMR spectroscopy of isotopically enriched proteins. J Mag Res 2011; 213(2): 423-441.

114. Clubb RT, Thanabal V, Wagner G. A new 3D HN(CA)HA experiment for obtaining fingerprint H^N-H^α cross peaks in^{15}N- and^{13}C-labeled proteins. J Biomol NMR 1992; 2(2): 203-210.

115. Bax A, Ikura M. An efficient 3D NMR technique for correlating the proton and 15N backbone amide resonances with the alpha-carbon of the preceding residue in uniformly 15N/13C enriched proteins. J Biomol NMR 1991; 1: 99-104.

116. Grzesiek S, and Bax A. Correlating backbone amide and side chain resonances in larger proteins by multiple relayed triple resonance. NMR J Am Chem Soc 1992; 114: 6291-6293.

117. Marley J, Lu M, Bracken C. A method for efficient isotopic labeling of recombinant proteins. J Biomol NMR 2001; 20(1): 71-75.

118. Delaglio F, Grzesiek S, Vuister GW, Zhu G, Pfeifer J, and Bax A. NMRPipe: A multidimensional spectral processing system based on UNIX pipes. J Biomol NMR 1995; 6: 277-293.

119. Vranken WF, Boucher W, Stevens TJ, Fogh RH, Pajon A, Llinas M, Ulrich EL, et al. The CCPN data model for NMR spectroscopy: Development of a software pipeline. Proteins 2005; 59: 687-696.

120. Wishart DS, Bigam CG, Holm A, Hodges RS, and Sykes BD. ^{1}H, 13C and ^{15}N random coil NMR chemical shifts of the common amino acids. I. investigations of nearest-neighbor effects. J Biomol NMR 1995; 5(1): 67-81.

121. Whitmore L, Wallace BA. Protein secondary structure analyses from circular dichroism spectroscopy: Methods and reference databases. Biopolymers 2008; 89(5): 392-400.

122. Tropea JE, Cherry S, Waugh DS. Expression and purification of soluble his_6-tagged TEV protease. Methods in Molecular Biology 2009; 498: 297-307.

123. Phan J, Zdanov A, Evdokimov AG, Tropea JE, Peters HPK, Kapust RB, Li M, et al. Structural basis for the substrate specificity of tobacco etch virus protease. J Biol Chem 2002; 277: 50564-50572.

124. Parks TD, Howard ED, Wolpert TJ, Arp DJ, Dougherty WG. Expression and purification of a recombinant tobacco etch virus NIa proteinase: Biochemical analyses of the full-length and a naturally occurring truncated proteinase form. Virology 1995; 210(1): 194-201.

125. Kapust RB, Tözsér J, Fox JD, Anderson DE, Cherry S, Copeland TD, Waugh DS. Tobacco etch virus protease: Mechanism of autolysis and rational design of stable mutants with wild-type catalytic proficiency. Protein Eng 2001; 14: 993-1000.

126. Kapust RB, Waugh DS. Escherichia coli maltose-binding protein is uncommonly effective at promoting the solubility of polypeptides to which it is fused. Protein Sci 1999; 8: 1668-1674.

127. Lodish H, Berk A, Kaiser C, Krieger M, Scott MP, Bretscher A, Ploegh H, et al. Molecular Cell Biology. New York: W. H. Freeman and Company, 2008:1150.

128. Privé GG. Detergents for the stabilization and crystallization of membrane proteins. Methods 2007; 41: 388-397.

129. Ryan C Oliver, Jan Lipfert, Daniel A Fox, Ryan H Lo, Sebastian Doniach, Linda Columbus. Dependence of micelle size and shape on detergent alkyl chain length and head group. PLoS One 2013; 8: n/a.

130. Krueger-Koplin RD, Sorgen PL, Krueger-Koplin ST, Rivera-Torres IO, Cahill SM, Hicks DB, Grinius L, et al. An evaluation of detergents for NMR structural studies of membrane proteins. J Biomol NMR 2004; 17: 43-57.

131. Seddon AM, Curnow P, Booth PJ. Membrane proteins, lipids and detergents: Not just a soap opera. Biochim Biophys Acta 2004; 1666: 105-117.

132. Garavito RM, Ferguson-Miller S. Detergents as tools in membrane biochemistry. J Biol Chem 2001; 276(35): 32403-32406.

133. Vinogradova O, Sönnichsen F, Sanders II CR. On choosing a detergent for solution NMR studies of membrane proteins. J Biomol NMR 1998; 4: 381-386.

134. le Maire M, Champeil P, Møller JV. Interaction of membrane proteins and lipids with solubilizing detergents. Biochim Biophys Acta - Biomembranes 2000; 1508(1–2): 86-111.

135. Wishart DS, Skyes BD, Richards FM. The chemical shift index: A fast and simple method for the assignment of protein secondary structure through NMR spectroscopy. Biochemistry 1992; 31(6): 1647-1651.

136. Cavanagh J, Fairbrother WJ, Palmer III AG, Rance M, Skelton NJ. Chapter 4 - multidimensional NMR spectroscopy. In: Cavanagh J, Fairbrother WJ, Palmer AG, Rance M, Skelton NJ, eds. Protein NMR Spectroscopy (Second Edition). Burlington: Academic Press; 2007:271-332.

137. Wüthrich K. NMR of Proteins and Nucleic Acids. New York: Wiley, 1986.

138. Cheung M, Maguire ML, Stevens TJ, Broadhurst RW. DANGLE: A bayesian inferential method for predicting protein backbone dihedral angles and secondary structure. J Mag Res2010; 202(2): 223-233.

139. Hornemann S, von Schroetter C, Damberger FF, Wüthrich K. Prion protein-detergent micelle interactions studied by NMR in solution. J Biol Chem 2009; 284: 22713-22721.

APPENDIX A Copyright Permission Letters

SPRINGER LICENSE
TERMS AND CONDITIONS

This is a License Agreement between Alexandra M Reda ("You") and Springer ("Springer") provided by Copyright Clearance Center ("CCC"). The license consists of your order details, the terms and conditions provided by Springer, and the payment terms and conditions.

All payments must be made in full to CCC. For payment instructions, please see information listed at the bottom of this form.

License Number: 3497250753713
License date: Oct 27, 2014
Order Content Publisher: Springer
Order Content Publication: Journal of Biomolecular NMR
Order Content Title: Solution structure of human intestinal fatty acid binding protein: Implications for ligand entry and exit
Order Content Author: Fengli Zhang
Order Content Date: Jan 1, 1997
Volume number: 9
Issue number: 3
Type of Use: Thesis/Dissertation
Portion: Figures
Author of this Springer article: No
Order reference number: None
Original figure numbers: Figure 8
Title of your thesis / dissertation: Structural characterization of 20 kDa lipid-binding fragments of apolipoprotein B100
Expected completion date: May 2015
Estimated size (pages): 200
Total: 0.00 CAD

Terms and Conditions

Introduction

The publisher for this copyrighted material is Springer Science + Business Media. By clicking "accept" in connection with completing this licensing transaction, you agree that the following terms and conditions apply to this transaction (along with the Billing and Payment terms and conditions established by Copyright Clearance Center, Inc. ("CCC"), at the time that you opened your Rightslink account and that are available at any time at http://myaccount.copyright.com).

Limited License

With reference to your request to reprint in your thesis material on which Springer Science and Business Media control the copyright, permission is granted, free of charge, for the use indicated in your enquiry.

Licenses are for one-time use only with a maximum distribution equal to the number that you identified in the licensing process.

This License includes use in an electronic form, provided its password protected or on the university's intranet or repository, including UMI (according to the definition at the Sherpa website: http://www.sherpa.ac.uk/romeo/). For any other electronic use, please contact Springer at (permissions.dordrecht@springer.com or permissions.heidelberg@springer.com).

The material can only be used for the purpose of defending your thesis limited to university-use only. If the thesis is going to be published, permission needs to be re-obtained (selecting "book/textbook" as the type of use).

Although Springer holds copyright to the material and is entitled to negotiate on rights, this license is only valid, subject to a courtesy information to the author (address is given with the article/chapter) and provided it concerns original material which does not carry references to other sources (if material in question appears with credit to another source, authorization from that source is required as well).

Permission free of charge on this occasion does not prejudice any rights we might have to charge for reproduction of our copyrighted material in the future.

Altering/Modifying Material: Not Permitted

You may not alter or modify the material in any manner. Abbreviations, additions, deletions and/or any other alterations shall be made only with prior written authorization of the author(s) and/or Springer Science + Business Media. (Please contact Springer at (permissions.dordrecht@springer.com or permissions.heidelberg@springer.com)

Reservation of Rights

Springer Science + Business Media reserves all rights not specifically granted in the combination of (i) the license details provided by you and accepted in the course of this licensing transaction, (ii) these terms and conditions and (iii) CCC's Billing and Payment terms and conditions.

Copyright Notice: Disclaimer

You must include the following copyright and permission notice in connection with any reproduction of the licensed material: "Springer and the original publisher

/journal title, volume, year of publication, page, chapter/article title, name(s) of author(s), figure number(s), original copyright notice) is given to the publication in which the material was originally published, by adding; with kind permission from Springer Science and Business Media"

Warranties: None

Example 1: Springer Science + Business Media makes no representations or warranties with respect to the licensed material.

Example 2: Springer Science + Business Media makes no representations or warranties with respect to the licensed material and adopts on its own behalf the limitations and disclaimers established by CCC on its behalf in its Billing and Payment terms and conditions for this licensing transaction.

Indemnity

You hereby indemnify and agree to hold harmless Springer Science + Business Media and CCC, and their respective officers, directors, employees and agents, from and against any and all claims arising out of your use of the licensed material other than as specifically authorized pursuant to this license.

No Transfer of License

This license is personal to you and may not be sublicensed, assigned, or transferred by you to any other person without Springer Science + Business Media's written permission.

No Amendment Except in Writing

This license may not be amended except in a writing signed by both parties (or, in the case of Springer Science + Business Media, by CCC on Springer Science + Business Media's behalf).

Objection to Contrary Terms

Springer Science + Business Media hereby objects to any terms contained in any purchase order, acknowledgment, check endorsement or other writing prepared by you, which terms are inconsistent with these terms and conditions or CCC's Billing and Payment terms and conditions. These terms and conditions, together with CCC's Billing and Payment terms and conditions (which are incorporated herein), comprise the entire agreement between you and Springer Science + Business Media (and CCC) concerning this licensing transaction. In the event of any conflict between your obligations established by these terms and conditions and those established by CCC's Billing and Payment terms and conditions, these terms and conditions shall control.

Jurisdiction

All disputes that may arise in connection with this present License, or the breach thereof, shall be settled exclusively by arbitration, to be held in The Netherlands, in accordance with Dutch law, and to be conducted under the Rules of the 'Netherlands Arbitrage Instituut' (Netherlands Institute of Arbitration).***OR:***
All disputes that may arise in connection with this present License, or the breach thereof, shall be settled exclusively by arbitration, to be held in the Federal Republic of Germany, in accordance with German law.

Other terms and conditions:
v1.3

Questions? customercare@copyright.com or +1-855-239-3415 (toll free in the US) or +1-978-646-2777.

Gratis licenses (referencing $0 in the Total field) are free. Please retain this printable license for your reference. No payment is required.

ELSEVIER LICENSE
TERMS AND CONDITIONS

This is a License Agreement between Alexandra M Reda ("You") and Elsevier ("Elsevier") provided by Copyright Clearance Center ("CCC"). The license consists of your order details, the terms and conditions provided by Elsevier, and the payment terms and conditions.

All payments must be made in full to CCC. For payment instructions, please see information listed at the bottom of this form.

Supplier: Elsevier Limited. The Boulevard,Langford Lane, Kidlington, Oxford, OX5 1GB, UK
Registered Company Number: 1982084
Customer name: Alexandra M Reda
Customer address: 5850 college st, Halifax, NS, B3H4R2
License number: 3493290732290
License date: Oct 20, 2014
Licensed content publisher: Elsevier
Licensed content publication: Biochimica et Biophysica Acta (BBA) - Proteins and Proteomics
Licensed content title: How to study proteins by circular dichroism
Licensed content author: Sharon M. Kelly,Thomas J. Jess,Nicholas C. Price
Licensed content date: 10 August 2005
Licensed content volume number: 1751
Licensed content issue number: 2
Number of pages: 21
Start Page: 119
End Page: 139
Type of Use: reuse in a thesis/dissertation
Portion: figures/tables/illustrations
Number of figures/tables/illustrations: 1
Format: electronic
Are you the author of this Elsevier article? No
Will you be translating? No
Title of your thesis/dissertation: Structural characterization of 20 kDa lipid-binding fragments of apolipoprotein B100
Expected completion date: May 2015
Estimated size (number of pages): 200
Elsevier VAT number: GB 494 6272 12
Price: 0.00 CAD
VAT/Local Sales Tax: 0.00 CAD / 0.00 GBP
Total: 0.00 CAD

Terms and Conditions

Introduction

1. The publisher for this copyrighted material is Elsevier. By clicking "accept" in connection with completing this licensing transaction, you agree that the following terms and conditions apply to this transaction (along with the Billing and Payment terms and conditions established by Copyright Clearance Center, Inc. ("CCC"), at the time that you opened your Rightslink account and that are available at any time at http://myaccount.copyright.com).

General terms

2. Elsevier hereby grants you permission to reproduce the aforementioned material subject to the terms and conditions indicated.

3. Acknowledgement: If any part of the material to be used (for example, figures) has appeared in our publication with credit or acknowledgement to another source, permission must also be sought from that source. If such permission is not obtained then that material may not be included in your publication/copies. Suitable acknowledgement to the source must be made, either as a footnote or in a reference list at the end of your publication, as follows:
"Reprinted from Publication title, Vol /edition number, Author(s), Title of article / title of chapter, Pages No., Copyright (Year), with permission from Elsevier [OR APPLICABLE SOCIETY COPYRIGHT OWNER]." Also Lancet special credit - "Reprinted from The Lancet, Vol. number, Author(s), Title of article, Pages No., Copyright (Year), with permission from Elsevier."

4. Reproduction of this material is confined to the purpose and/or media for which permission is hereby given.

5. Altering/Modifying Material: Not Permitted. However figures and illustrations may be altered/adapted minimally to serve your work. Any other abbreviations, additions, deletions and/or any other alterations shall be made only with prior written authorization of Elsevier Ltd. (Please contact Elsevier at permissions@elsevier.com)

6. If the permission fee for the requested use of our material is waived in this instance, please be advised that your future requests for Elsevier materials may attract a fee.

7. Reservation of Rights: Publisher reserves all rights not specifically granted in the combination of (i) the license details provided by you and accepted in the course of this licensing transaction, (ii) these terms and conditions and (iii) CCC's Billing and Payment terms and conditions.

8. License Contingent Upon Payment: While you may exercise the rights licensed immediately upon issuance of the license at the end of the licensing process for the

transaction, provided that you have disclosed complete and accurate details of your proposed use, no license is finally effective unless and until full payment is received from you (either by publisher or by CCC) as provided in CCC's Billing and Payment terms and conditions. If full payment is not received on a timely basis, then any license preliminarily granted shall be deemed automatically revoked and shall be void as if never granted. Further, in the event that you breach any of these terms and conditions or any of CCC's Billing and Payment terms and conditions, the license is automatically revoked and shall be void as if never granted. Use of materials as described in a revoked license, as well as any use of the materials beyond the scope of an unrevoked license, may constitute copyright infringement and publisher reserves the right to take any and all action to protect its copyright in the materials.

9. Warranties: Publisher makes no representations or warranties with respect to the licensed material.

10. Indemnity: You hereby indemnify and agree to hold harmless publisher and CCC, and their respective officers, directors, employees and agents, from and against any and all claims arising out of your use of the licensed material other than as specifically authorized pursuant to this license.

11. No Transfer of License: This license is personal to you and may not be sublicensed, assigned, or transferred by you to any other person without publisher's written permission.

12. No Amendment Except in Writing: This license may not be amended except in a writing signed by both parties (or, in the case of publisher, by CCC on publisher's behalf).

13. Objection to Contrary Terms: Publisher hereby objects to any terms contained in any purchase order, acknowledgment, check endorsement or other writing prepared by you, which terms are inconsistent with these terms and conditions or CCC's Billing and Payment terms and conditions. These terms and conditions, together with CCC's Billing and Payment terms and conditions (which are incorporated herein), comprise the entire agreement between you and publisher (and CCC) concerning this licensing transaction. In the event of any conflict between your obligations established by these terms and conditions and those established by CCC's Billing and Payment terms and conditions, these terms and conditions shall control.

14. Revocation: Elsevier or Copyright Clearance Center may deny the permissions described in this License at their sole discretion, for any reason or no reason, with a full refund payable to you. Notice of such denial will be made using the contact information provided by you. Failure to receive such notice will not alter or invalidate the denial. In no event will Elsevier or Copyright Clearance Center be responsible or liable for any costs, expenses or damage incurred by you as a result of a denial of your permission request, other than a refund of the amount(s) paid by you to Elsevier and/or Copyright Clearance Center for denied permissions.

Limited license

The following terms and conditions apply only to specific license types:

15. **Translation**: This permission is granted for non-exclusive world **English** rights only unless your license was granted for translation rights. If you licensed translation rights you may only translate this content into the languages you requested. A professional translator must perform all translations and reproduce the content word for word preserving the integrity of the article. If this license is to re-use 1 or 2 figures then permission is granted for non-exclusive world rights in all languages.

16. **Posting licensed content on any Website**: The following terms and conditions apply as follows: Licensing material from an Elsevier journal: All content posted to the web site must maintain the copyright information line on the bottom of each image; A hyper-text must be included to the Homepage of the journal from which you are licensing at http://www.sciencedirect.com/science/journal/xxxxx or the Elsevier homepage for books at http://www.elsevier.com; Central Storage: This license does not include permission for a scanned version of the material to be stored in a central repository such as that provided by Heron/XanEdu.

Licensing material from an Elsevier book: A hyper-text link must be included to the Elsevier homepage at http://www.elsevier.com . All content posted to the web site must maintain the copyright information line on the bottom of each image.

Posting licensed content on Electronic reserve: In addition to the above the following clauses are applicable: The web site must be password-protected and made available only to bona fide students registered on a relevant course. This permission is granted for 1 year only. You may obtain a new license for future website posting.

For journal authors: the following clauses are applicable in addition to the above: Permission granted is limited to the author accepted manuscript version* of your paper.

***Accepted Author Manuscript (AAM) Definition:** An accepted author manuscript (AAM) is the author's version of the manuscript of an article that has been accepted for publication and which may include any author-incorporated changes suggested through the processes of submission processing, peer review, and editor-author communications. AAMs do not include other publisher value-added contributions such as copy-editing, formatting, technical enhancements and (if relevant) pagination.

You are not allowed to download and post the published journal article (whether PDF or HTML, proof or final version), nor may you scan the printed edition to create an electronic version. A hyper-text must be included to the Homepage of the journal from which you are licensing at http://www.sciencedirect.com/science/journal/xxxxx. As part of our normal production process, you will receive an e-mail notice when your article appears on Elsevier's online service ScienceDirect (www.sciencedirect.com). That e-mail

will include the article's Digital Object Identifier (DOI). This number provides the electronic link to the published article and should be included in the posting of your personal version. We ask that you wait until you receive this e-mail and have the DOI to do any posting.

Posting to a repository: Authors may post their AAM immediately to their employer's institutional repository for internal use only and may make their manuscript publically available after the journal-specific embargo period has ended. Please also refer to Elsevier's Article Posting Policy for further information.

18. **For book authors** the following clauses are applicable in addition to the above: Authors are permitted to place a brief summary of their work online only.. You are not allowed to download and post the published electronic version of your chapter, nor may you scan the printed edition to create an electronic version. **Posting to a repository:** Authors are permitted to post a summary of their chapter only in their institution's repository.

20. **Thesis/Dissertation**: If your license is for use in a thesis/dissertation your thesis may be submitted to your institution in either print or electronic form. Should your thesis be published commercially, please reapply for permission. These requirements include permission for the Library and Archives of Canada to supply single copies, on demand, of the complete thesis and include permission for Proquest/UMI to supply single copies, on demand, of the complete thesis. Should your thesis be published commercially, please reapply for permission.

Elsevier Open Access Terms and Conditions

Elsevier publishes Open Access articles in both its Open Access journals and via its Open Access articles option in subscription journals.
Authors publishing in an Open Access journal or who choose to make their article Open Access in an Elsevier subscription journal select one of the following Creative Commons user licenses, which define how a reader may reuse their work: Creative Commons Attribution License (CC BY), Creative Commons Attribution – Non Commercial - ShareAlike (CC BY NC SA) and Creative Commons Attribution – Non Commercial – No Derivatives (CC BY NC ND)

Terms & Conditions applicable to all Elsevier Open Access articles:

Any reuse of the article must not represent the author as endorsing the adaptation of the article nor should the article be modified in such a way as to damage the author's honour or reputation.
The author(s) must be appropriately credited.
If any part of the material to be used (for example, figures) has appeared in our publication with credit or acknowledgement to another source it is the responsibility of the user to ensure their reuse complies with the terms and conditions determined by the rights holder.

Additional Terms & Conditions applicable to each Creative Commons user license:

CC BY: You may distribute and copy the article, create extracts, abstracts, and other revised versions, adaptations or derivative works of or from an article (such as a translation), to include in a collective work (such as an anthology), to text or data mine the article, including for commercial purposes without permission from Elsevier

CC BY NC SA: For non-commercial purposes you may distribute and copy the article, create extracts, abstracts and other revised versions, adaptations or derivative works of or from an article (such as a translation), to include in a collective work (such as an anthology), to text and data mine the article and license new adaptations or creations under identical terms without permission from Elsevier

CC BY NC ND: For non-commercial purposes you may distribute and copy the article and include it in a collective work (such as an anthology), provided you do not alter or modify the article, without permission from Elsevier

Any commercial reuse of Open Access articles published with a CC BY NC SA or CC BY NC ND license requires permission from Elsevier and will be subject to a fee.

Commercial reuse includes:
· Promotional purposes (advertising or marketing)
· Commercial exploitation (e.g. a product for sale or loan)
· Systematic distribution (for a fee or free of charge)
Please refer to Elsevier's Open Access Policy for further information.

21. **Other Conditions**:
v1.7
Questions? customercare@copyright.com or +1-855-239-3415 (toll free in the US) or +1-978-646-2777.

Gratis licenses (referencing $0 in the Total field) are free. Please retain this printable license for your reference. No payment is required.